Needleless electrospinning with linear spinnerets

A thesis submitted in fulfilment of requirements for the degree of

Master of Technology

ISRAT JAHAN

B.Sc. in Textile Engineering (Bangladesh University of Textiles)

School of Fashion and Textiles

College of Design and Social Context

RMIT University

March 2019

DECLARATION

I Israt **Jahan,** certify that except where due acknowledgement has been made,

- The work is that of the author alone;
- The work has not been submitted previously, in whole or in part, to qualify for any other academic award;
- The content of the thesis is the result of work which has been carried out in the School of Fashion and Textiles, RMIT University, since the official commencement date 03 July 2017 to 15 March 2019 of the approved research program;
- Any editorial work, paid or unpaid, carried out by a third party is acknowledged, and ethics procedures and guidelines have been followed.

Signature: Israt Jahan

Date: 14 March 2019

DEDICATION

This dissertation is dedicated to my beloved husband Md Saifur Rahman and my generous father Golam Mostafa Feroze for their endless love and support.

ACKNOWLEDGEMENTS

First and foremost, I praise to Allah, the Almighty, the most merciful, who grant me this wonderful opportunity, determination and strength to be on this journey.

I express heartfelt gratitude to my supervisor Dr. Xin Wang, Senior Lecturer, RMIT University who made this thesis possible through his constructive criticism, valuable inputs, caring, patience, guidance, and endless professional support throughout the project. I am really grateful to have such a dynamic supervisor and appreciate all his contributions to knowledge, time, support and ideas. I would also like to thank and offer my sincerest gratitude to my co-supervisor Prof. Lijing Wang whose continuous support and encouragement helped me a lot during the study.

My sincere thanks to the School of Fashion and Textiles, RMIT University, Australia, for all the administrative and laboratory support provided for this dissertation. Dr. Jenny Underwood, Mr. David Castle, and Dr. Sean Ryan always promptly guided and helped me in administration matters. I am grateful to Mr. Martin Gregory, a fine technician, and acknowledge his strong technical support in fabrications of experimental setup. I appreciate the kind help of the Brunswick Laboratory team for experimental support and Microscopy team at RMIT city campus for morphology analysis of nanofibres. Special thanks to Dr. Amit Jadhav for assistance in the experimental work at the early phase of this study.

I am also thankful to my seniors and juniors at RMIT University, especially Dr. Arsheen Moiz who facilitated and encouraged me during the study.

Finally, I would like to take this opportunity to thank my beloved husband, Md Saifur Rahman for his encouraging words, support, and limitless faith in my abilities.

TABLE OF CONTENTS

3. MATERIALS, METHODOLOGY, AND MEASUREMENT

LIST OF TABLES

LIST OF FIGURES

LIST OF PUBLICATIONS

Journals:

1. **Israt Jahan**, Lijing Wang, and Xin Wang. 'Needleless Electrospinning from a Tube with an Embedded Wire Loop' Macromol. Mater. Eng. 2018, 1800588.

   (Impact factor of 2.69), DOI: 10.1002/mame.201800588

2. **Israt Jahan**, Amit Jadhav, Lijing Wang, and Xin Wang. "Electrospinning from a convex needle with multiple jets towards better controlling and enhanced production rate", submitted to Journal of Applied Polymer Science.

   This paper is under review.

3. **Israt Jahan** and Xin Wang. "Evolvement of the spinneret in electrospinning: toward large-scale production of nanofibres", Book chapter.

   This chapter is a book chapter will be included in the book entitled 'Electrospun Polymers and Composites: Ultrafine Materials, High Performance Fibres, and Wearables" proposed to be published by Woodhead Publishing Ltd (the Imprint of Elsevier), Cambridge, UK.

4. **Israt Jahan**, Arsheen Moiz, Xin Wang. " Creating an interconnected PVA nanofibrous membrane on cotton fabrics by dip coating of PDMS-TMS for versatile protection without compromising comfort ", submitted to Cellulose.

   This paper is under review.

LIST OF ABBREVIATIONS AND ACRONYMS

AATCC	American Association of Textile Chemists and Colorists
AS/NZS	Australian/ New Zealand standard
ASTM	American Society for Testing and Materials
DMF	N,N-dimethylformamide
FTIR	Fourier transform infrared spectroscopy
g	Gram
GSM	Fabric weight in gram per square metre
ISO	International organization for standardization
m	Metre
kV	Kilo volt
ml	Mililitre
mm	Millimetre
MMT	Moisture management tester
nm	Nanometre
OMMC	Overall moisture management capacity
OWTC	Cumulative one-way transport capacity
PAN	Poly acrylonitrile
PDMS	Poly dimethylsiloxane
PDEs	Partial differential equations
PTFE	Poly tetrafluoroethylene
PT	Poly dimethylsiloxane- Trimethylated silica
PVA	Polyvinyl alcohol
PEO	Poly ethylene oxide
PLA	Poly lactic acid
PVDF	Poly vinylidene fluoride
PVP	Poly vinyl pyrrolidone
RH	Relative humidity in %
SEM	Scanning electron microscopy
TMS	Trimethylated silica
TPU	Thermoplastic polyurethane
WCA	Water contact angle
WT_t & WT_b	Wetting time for top and bottom surfaces of fabric
μm	Micrometre

ABSTRACT

Electrospinning is the most effective method to produce nanofibres for various applications. The conventional electrospinning technique uses a single needle or multi-needle to produce nanofibres with limited throughput and hassles in controlling and operating. Different methods of needleless electrospinning, such as rotating cylinder, spiral coil, wire, ring, disc, dish and slot, have been established to scale up the production rate of nanofibres. However, stable and trustable, effective needleless electrospinning with the controllable capability to produce high-quality nanofibres is still of great challenge. The aim of this study is to establish new methods of electrospinning from linear spinnerets with lower electricity consumption and higher effectiveness than conventional needle electrospinning.

A literature review was conducted to understand the evolvement of spinneret in electrospinning. As a linear spinneret, a convex needle with a split in its tip was demonstrated to generate multiple polymer jets from a limited free surface in needle-based electrospinning. Another novel spinneret from a single wire loop embedded in a tube was then used as the spinneret for needleless electrospinning with precise controlling. The controllability and efficiency of both spinnerets were compared with needle electrospinning. Furthermore, the linear spinneret from a spiral wire entrenched in a tube was used to perform nanofibrous coating on textiles.

Compared to needle electrospinning, electrospinning from a convex needle showed 2-3 times higher flow rate with multiple jet and finer nanofibres under an applied voltage of 19 kV.

Besides, the wire loop spinneret generated multiple jets with a larger spinnable area due to its special geometrical structure under a high applied voltage of 28 kV. The resultant nanofibres from this spinneret were slightly coarser compared to the needle electrospinning. Nevertheless, it has achieved a higher production rate of 0.48 g/h than needle electrospinning. Both convex needle and wire loop spinnerets generated a stronger electric field compared to needle as per the electric field modelling. The linear spinneret was demonstrated to generate nanofibrous coating on cotton fabrics, and the coated PVA nanofibrous membrane showed versatile protection with comfort after a dip coating of polydimethylsiloxane-trimethylated silica (PDMS-TMS).

The linear spinnerets can be adopted to produce nanofibres with high throughput and controllability. The limited free surface in the spinneret tip allows the generation of strong electric field intensity under a low applied voltage (19-28 kV) with little solvent evaporation. Additionally, the linear spinnerets are also efficient in preforming nanofibrous coating. Overall, the linear spinnerets are stable, effective, and capable of fabricating high quality nanofibres for various practical implications.

CHAPTER 1

INTRODUCTION

1.1 Background

Nanofibres are defined as superfine or ultrathin fibres of one-dimensional nanomaterial with a diameter less than 1µm (Bellan, Coates & Craighead 2006) and fibre length to diameter ratio larger than 100:1. Nanofibres have application potentials due to their extremely high surface area to weight ratio, small fibre diameter and small pore size (Deitzel et al. 2001). Nanofibre has been used in a wide range of applications, such as wound dressing (Yang et al. 2017), drug delivery (Hu et al. 2014), nanosensors (Ahuja & Kumar 2009), tissue engineering (Pham, Sharma & Mikos 2006), filter media (Barhate & Ramakrishna 2007) and protective clothing (Lee & Obendorf 2007). Electrospinning has been considered as a most versatile, convenient, cost-effective method to produce nanofibres as it provides the facility of reproducibility, controllable morphology and scalability.

The basic electrospinning setup consists of a high voltage power supply, a syringe pump, needle nozzle, and a collector. High voltage power supply is applied to nozzle creating a strong electric field where the metal collector is earthed to have zero potential. A viscoelastic polymer solution is supplied through the capillary of nozzle using the syringe pump. Under the electrostatic force, the solution at the needle tip overcomes its surface tension, forms a

cone shape (Taylor cone) and is stretched under a high electric field to form solid filaments. These filaments are elongated in a jet and deposited on the collector forming a randomly oriented nanofibres web (Doshi & Reneker 1995). Four different factors of processing parameters such as polymer solution concentration, applied voltage, the flow rate of polymer solution and the distance between the collector and the spinneret influence the morphology of nanofibres. In conventional needle electrospinning, a needle-like nozzle is used to produce nanofibres. Each needle spinneret produces only one jet which inhibits the production rate of nanofibres. Traditional electrospinning usually produces 0.3-1 g/h depending on the solution and process parameters (Theron, Zussman & Yarin 2004). The low productivity of conventional needle-based process is a barrier for commercial production of nanofibres.

To increase the number of jets in electrospinning, multi-needle, needles with cylindrical electrode, a tube with liner holes had been introduced. However, needle-based nozzles have its potential drawbacks, for instance, under a high electric voltage the multi-needle produces corona discharge, clogging of the needle tip, large operating space requirements, poor fibre quality, lower productivity, etc. Due to these demerits, it is difficult to implement needle-based nozzles commercially. In the recent decade, needleless electrospinning has been introduced to overcome the difficulties associated with needle electrospinning. Needleless electrospinning can be described as electrospinning of nanofibres randomly from a free liquid surface. In needleless electrospinning, spinneret geometry plays important roles in determining the control of electrospinning process, fibre morphology and production rate. Research efforts have contributed to the different types of needleless spinnerets, such as electrospinning from magnetic fluid (Theron et al. 2005), cylinder roller (Jirsak et al. 2004), air bubbles (Liu & He 2007), rotary cone (Lu, B et al. 2010), conical wire coil (Wang et al. 2009), spiral coils (Wang et al. 2012), multiple rings (Wang, Lin & Wang 2014), disk (Niu

& Lin 2012; Niu, Lin & Wang 2009; Yang et al. 2010), slot (Yan et al. 2017), needle-disk (Liu, Ang & He 2017), metal dish (Wei, Yu, et al. 2018), single wire (Forward & Rutledge 2012) and multiple wires (Holopainen et al. 2014).

Even though the development of spinneret has contributed quite a lot in scaling up the production rate of nanofibre from electrospinning, needleless electrospinning still has several drawbacks such as higher electricity consumption (60-70 kV), higher process cost, difficulty in controlling, fibre morphology, wider diameter distributions etc. As a result, stable and trustable, effective needleless electrospinning with the controllable capability to produce high-quality nanofibres is still of great challenge.

1.2 Research Question

Considering the current development and the challenges in large scale production of nanofibres from electrospinning, the research question of this study has been defined as:

How to produce a stable, trustable, effective and controllable needleless electrospinning method for nanofibres fabrication and application?

1.3 Aim and objectives

This study focuses on electrospinning with linear spinnerets to overcome the drawbacks of existing electrospinning methods. The aim of this study is thus to design and realise the linear spinnerets that hold the advantages in generating multiple polymer jet with a low applied voltage and easy controlling.

The objectives of this study are as follows:

- To introduce an economic method of needleless electrospinning which is stable and trustworthy.
- To scale up the production of nanofibres with lower consumption of electricity so that the production cost will be low throughout the process with ensuring high quality.
- To develop a new method of electrospinning from linear spinnerets that will be effective and controllable compared to existing methods.
- To apply the linear spinneret in nanofibrous coating on textiles as a demonstration of the potential of the as-developed electrospinning method.

1.4 Contribution of this research

This research employs different linear spinnerets such as a convex needle, a tube with an embedded wire loop spinneret, a tube with spiral wire loop etc. to generate multiple polymer jet in electrospinning, ensuring better controlling and operating under a low applied voltage.

- It is found that the developed methods are more stable, trustable, effective, and controllable with high quality nanofibres electrospun with these methods. These methods can be implemented to overcome the drawbacks of both needle and needleless electrospinning.

- It is observed that nanofibres from various polymers having the wide range of applications are made easily by these methods with low electricity consumption which lead to lower process cost.

- To justify the effectiveness of the proposed methods, several applications of nanofibres such as nanofibrous coating and versatile protection with electrospun fibres have been demonstrated using the as-developed electrospinning methods.

1.5 Dissertation overview

This dissertation is divided into seven chapters as overviewed below.

Chapter 1 introduces the basic information about nanofibres and electrospinning, research background, the aim and objects, as well as the significance of this study.

Chapter 2 represents an intensive literature review to understand different aspects of the research problems, including the evolvement of electrospinning towards large-scale production of nanofibres, different types of spinneret set-up and summary of the pros and cons of each spinneret.

Chapter 3 covers the details of the experimental work, including the materials and chemicals used, methods adopted in this study. It also contains the details of the measurements and characterisation that have been used in this research.

Chapter 4 investigates the approach of Electrospinning from a convex needle with multiple jets towards better controlling and enhanced production rate. The electrospinning performance including the fibre quality and production rate is discussed and explained in detail. The comparison of this method with conventional electrospinning and modelling work of convex needle are also discussed.

Chapter 5 describes the details of another electrospinning method from a tube with an embedded wire loop. The comparisons of productivity, fibre diameter, electric field intensity profiles with conventional electrospinning are discussed in detail.

Chapter 6 explores the nanofibrous coating of PVA nanofibres in combination with PDMS-TMS on cotton fabrics for versatile protection. This chapter investigates the fabrication process of nanofibrous coating with a tube embedded spiral wire loop spinneret, fibre morphology analysis, and protection and comfort properties.

Chapter 7 outlines the concluding remarks and indicates the scope and limitations of this study. A possible future direction for this research is recommended to guide further endeavour.

CHAPTER 2

LITERATURE REVIEW: EVOLVEMENT OF THE SPINNERET IN ELECTROSPINNING TOWARDS LARGE-SCALE PRODUCTION OF NANOFIBRES

2.1 Introduction

Nanofibres are fibres with a diameter less than 1 μm (1000 nm) and the fibre length to diameter ratio larger than 100:1 (Alborzi, Lim & Kakuda 2010; Supaphol, Mit- uppatham & Nithitanakul 2005). Considering the fibre diameter, the fibres are also called submicron fibres (Bellan, Coates & Craighead 2006; Givens et al. 2007). The exclusive properties of nanofibres and their application in several fields have drawn the attention from both academia and industry, and extensive research and development effort have been putting on this area since the 1990s. Nanofibres can be generated from different polymers, hence have different physical properties and application potentials, such as tissue regeneration and drug delivery (Sridhar et al. 2015), energy storage (Zhang et al. 2016), biosensor (Zhang et al. 2017), composites (Li & Xia 2004; Olson et al. 2006), biomaterials (Kwon, Kidoaki & Matsuda 2005) and wound dressing (Yang et al. 2017).

Electrospinning is a nanofabrication technology which is a versatile, simple and cost-effective method of producing continuous nanofibres (Doshi & Reneker 1995). This

technique involves stretching a polymer solution under a high electric field to form solid filaments which will be deposited on a counter electrode forming a nanofibres web (Bognitzki et al. 2001; Reneker & Chun 1996). Many specific characteristics, such as excessive surface to mass ratio, capacity to form a porous fibrous membrane, controllability in fibre diameter, surface morphology and fibrous shape and easiness of being functionalized by the usage of functional polymers or adding useful chemical compounds into polymer solutions, have diversified electrospun nanofibres with different structure and properties/performance (Srinivasan & Reneker 1995). These precise functions have privileged electrospun nanofibres with great possibilities for use in diverse fields (Fang et al. 2008).

Conventionally, needle-based nozzle was employed for nanofibres production with negligible throughput. The process is simple and easy for a demonstration of nanofibre fabrication serving perfectly for research and laboratory study. However, a high throughput is needed in nanofibre fabrication to fit the industrial scale production. Research and development in electrospinning setup has been focusing on scale up production of nanofibre in the past decades. Needleless electrospinning with a variety of spinnerets has emerged as the efficient approach for large-scale production of nanofibres. Some of them have been industrialized successfully with industrial level throughput of nanofibres. This work contributes a review of the evolvement of spinneret in electrospinning. The mechanism and the performance of different spinnerets including productivity and fibre quality will be highlighted and discussed in detail.

2.2 Brief history and principle

Nanofibre was first produced via electrospinning by an English physicist William Gilbert. He first documented the electrostatic attraction between liquids and observed a spherical water drop on a dry surface warping into a cone shape when it was held below electrically charged amber (Gilbert 1958). The first patent of electrospinning process was filed by Formhals in 1934 (Anton 1934, 1938, 1939, 1943), which is regarded as the real origin of the electrospinning. During electrospinning, the solution droplet at the needle tip is inspired by the concentrated electric charge formed between the needle and the alternative electrode, and the droplet will be forced to transform into a cone shape. In 1960, Taylor studied the shape of this cone formed by a fluid droplet under the action of electric force, and he found the conical angle of the cone was around 49.3^{o} (Taylor 1964, 1969). The cone-shaped protrusion in the electrified fluid droplet was then named as "Taylor cone". Electrospinning from polymer melts was investigated by Larrondo and Manley in 1981. In 1996, Reneker and Chun proved the probability of electrospinning using different polymer solutions (Kowalewski, Hiller & Behnia 1993; Reneker & Chun 1996). Since then, a simple electrospinning setup was established in which a needle-like device used as the spinneret.

The basic electrospinning setup consists of a high voltage power supply, a syringe pump, a needle-like device as spinneret and a counter electrode collector, as illustrated in Figure 2-1. It is a proof-of-concept setup of utilizing electric field as the driving force in wet spinning of polymer solution. Polymer solutions are pumped through the nozzle to maintain a continuous flow with a meniscus forming at the tip. When a high voltage power supply is applied to the needle, a strongly concentrated electric field will be formed on the needle (Inset of Figure 2-1). The solution will then be charged and the meniscus of solution at the tip of the needle will be converted into a Taylor cone. Jet initiation starts when the electric field is strong enough to overcome the surface tension and viscosity of the solution. The polymer jet whips around so

that the diameter of the filament of the jet is attenuated into submicron scale. Finally, the jet targets onto the collector due to the electrostatic attraction between the charged jet and the earthed collector. Solvent evaporation occurs during the traveling of polymer jet from the nozzle tip to collector, thus dry nanofibres are formed and deposited as randomly oriented nanofibres mat on the collector, as shown the morphology in Figure 2-1.

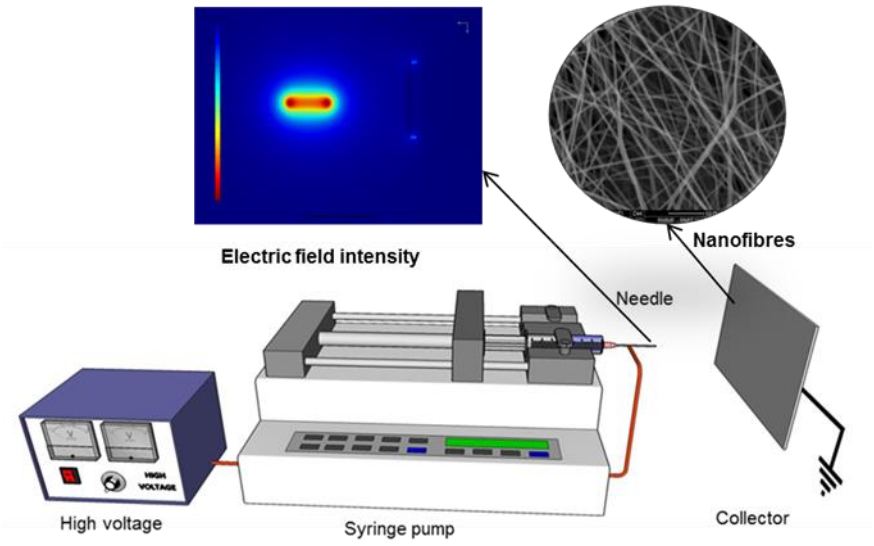

Figure 2-1: Basic setup of electrospinning.

2.3 Evolvement of the spinneret

Electrospinning is an old technique with a long history. The evolvement of spinneret in electrospinning has started around 1900s which mainly focused on the rule of mass production of nanofibres. By the time being several types of spinnerets have been developed. Enlarging the spannable area with concentrated electric field is one of the concepts to develop the spinneret efficiently. In this study, different types of spinnerets are classified for simplicity, clear understanding and comparison. Specifically, single needle, multi-needle,

needles with extra electrode, a tube with holes and porous tube are classified as dotted spinnerets; slot, slit, channels and wires are classified as linear spinneret; and roller, disc, cones and edges are classified as free surface spinnerets. For simplicity, the spinnerets are divided into 1D and 3D spinnerets.

2.3.1 1D spinnerets

The needle spinneret is simple and easy to demonstrate electrospinning, and it has been widely used especially in laboratory research. For function nanofibre development, the needle can be designed into different geometries such as core-sheath and bicomponent. In order to scale up the production rate of nanofibre from needle-based electrospinning, research effort has focused on employing numeral number of needles to electrospin simultaneously. Similarly, electrospinning from single or multiple channels (open or close) was developed to enhance the production rate. Even though the effect of scaling up production rate by increasing the number of needles/channels is evident, there are many issues before a trustable and reliable fabrication technology can be obtained.

2.3.1.1 Needle-based 1D spinnerets

The most conventional 1D setup is the single needle electrospinning. In this set-up, a single needle is used as the spinneret under the action of high electric voltage. Single needle produces only one jet which inhibits the production rate of nanofibre to 0.03-1 g/h. To increase the number of jets in electrospinning, multi-needle electrospinning had been introduced (Theron et al. 2005). A typical setup of the multi-needle spinneret is shown in Figure 2-2a, in which many needles are mounted together as the spinneret. Many polymer jets are generated so that the production rate is increased. However, the multi-needle interference each other due to the uneven distribution of electric field around the multi-needle. This repulsion between needles usually generates “corona discharge” hindering the production rate

as well as fibre quality (Yang, Shi & Xue 2010). There is another issue of clogging of needle while using multi-needle as the spinneret. An additional cleaning device is required for each needle. To solve the issue of repulsion, needles were placed in distance so that a large space was required to accommodate the needles (Theron et al. 2005; Varesano, Carletto & Mazzuchetti 2009). The large operating space and cleaning device have confined the application potential of multi-needle electrospinning.

An extra cylindrical electrode has been utilized to enclose the multi-needles (Kim, Cho & Kim 2006), as illustrated in Figure 2-2b. This external auxiliary electrode centred the fibre deposition area with enhanced fibre production rate. However, coarser fibres were observed as the auxiliary electrode shortened the chaotic motion of the multi-jet in electrospinning.

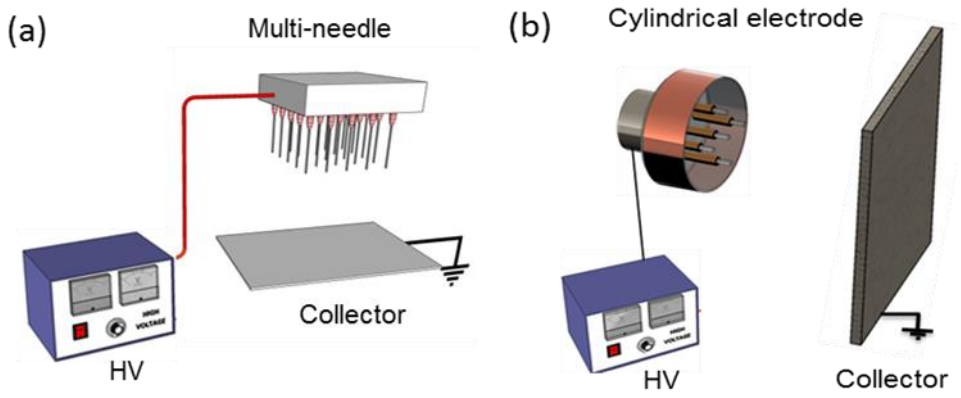

Figure 2-2: Schematics of multi-needle electrospinning set up (a) and multi-needle with an extra cylindrical electrode (b).

2.3.1.2 Channel-based 1D spinnerets

A porous hollow tube made of polytetrafluoroethylene (PTFE) was also used to generate multi-jet electrospinning (Varabhas, Chase & Reneker 2008). The tube was mounted horizontally, and holes were drilled on the tube so that polymer solution was pushed out

through the multi-hole. A wire electrode was inserted into the tube to maintain an equal electrical potential in the vicinity of each drilled holes. When the high voltage was applied, multiple polymer jets were produced simultaneously from the surface of the tube. It was reported that the 13 cm long tube with 20 holes showed 5-50 times higher production rate (0.3-0.5 g/h) than a single needle. However, the number of holes and their distribution limit the production rate. The tube with multi-hole is similar to multi-needle setup, but corona discharge can be avoided due to a better distribution of electric field on the surface of the tube.

Different channels, for instance, slot, slit, string, porous tube, etc. have been proposed as electrospinning spinneret. The schematics of these spinnerets are shown in Figure 2-3. Similar to the spinneret from a tube with holes, flat spinneret with holes (Zhou, Gong & Porat 2009, 2010) was used as electrospinning spinneret (Figure 2-3a). The holes were drilled into the flat surface of the spinneret, and polymer solution was supplied through a Teflon tube. Different number of holes (three, four and seven) was drilled into the same flat spinneret. Under the action of electric field, multiple jets were produced through these holes. Though this setup shows higher productivity compared to the needle, strong charge repulsion occurs between the jets with the number of holes increases, causing uneven distribution of fibre diameter.

Similarly, a porous polyethylene tube surrounded by a wired circular collector was used as a spinneret by Dosunmu et al. 2006. In this setup (Figure 2-3b), the tube was mounted vertically, and the polymer solution was pushed through the holes to form protrusions on the outer surface of the tube. Multiple jets were initiated sidewise from these protrusions when a high voltage was applied. The production rate was about 250 times higher than that of a

single needle, even though the obtained fibre diameter showed a greater variation. Compared with the multi-needle, porous tube occupies less space and is easier to operate, but there is also clogging problem in the holes.

Recently, A double ring slit (Figure 2-3c) spinneret comprising an inner metal ring, a Teflon inner core, an outer metal ring and a Teflon outer shell was used for electrospinning (Wei et al. 2018). The polymer solution was transported to the narrow slit between the rings, and multiple jets were produced from the top of spinneret when a high voltage was applied. The significant advantages of this spinneret are the capability of minimizing the solvent evaporation rate with improved solution utilization ratio. However, this spinneret requires a high applied voltage (50-70 kV) (Wei et al. 2018).

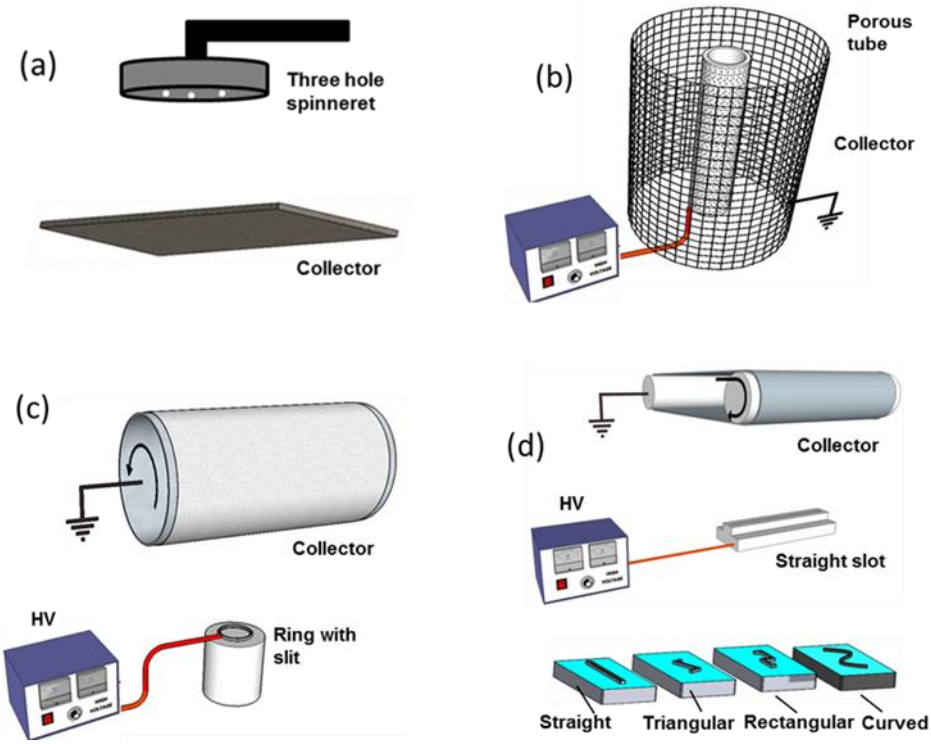

Figure 2-3: Schematic of flat spinneret with three holes (a), porous tube spinneret (b), double ring slit spinneret (c) and slot spinneret with straight, curved, rectangle and triangle profiles (d).

Another electrospinning setup with different types of slot was developed (Yan et al. 2017), as demonstrated in Figure 2-3d. Curved, straight, rectangle and triangle slots were used as spinneret, and PVA polymer solution was fed into the spinneret through a solution supplying system. The solution was fed until the liquid surface reached the top line of the slot. A high voltage was applied to the solution in the spinneret to charge the solution. Jets ejection occurred from the surface of the top slot when the applied voltage was higher than 50 kV. The distribution of electric field on the curved, rectangle and triangle slots was more uniform than the straight slot. It is evident that the curved convex slot as spinneret has a higher productivity and more uniform distribution of electric field intensity compared to other shapes of slots. It was claimed that slot spinneret combines the advantages of both needle and needleless electrospinning by providing less solvent evaporation, higher productivity, and no clogging issues. Even though the effect of slot geometry on the electrospinning process and fibre morphology has investigated, more research and innovation are required to implement the process into the mass production of nanofibres.

Currently, a metal plucked string spinneret (Chen et al. 2019b) was employed to generate multiple jets in electrospinning with a comparatively lower electric voltage. In this setup, cyclical motion of string creates vibration into the reservoir. This vibration helps the string to create droplets which are stressed under an electric field to generate multiple jets. The fine average diameter of nanofibres with a narrow distribution range of 143 ± 16 nm was obtained with a voltage of 25 kV. The production rate was 26 times higher compared to a single needle.

Table 2-1 summarizes the privileges and drawbacks of all the 1D spinnerets reviewed above.

Table 2-1: Summary of 1D spinnerets.

Spinneret	Privileges	Drawbacks
Needle	• Good fibre quality with narrow diameter distribution.	• Extremely low production rate (0.1-1g/h). • Clogging in the needle tip. • Not suitable for industrial application.
Multi-needle	• Higher production rate compared to needle.	• Clogging in the needle tip. • Corona discharge between needles. • Large operating space is required.
Multi-needle with extra electrode	• Corona discharge prevented. • Improved the fibre production rate.	• Coarser fibres. • Clogging in the needle tip.
Tube with holes	• Simple set-up and easy to operate. • Production rate is 3-50 times higher than a single needle.	• Number of holes limits the production rate.
Porous tube	• 250 times higher production rate compared to single needle.	• Wider fibre diameter distribution.
Flat electrode with holes	• Easy set-up. • Higher production rate compared to multi-needle.	• Strong charge repulsion between jets.
Slot spinneret	• Curved slot shows higher productivity. • Uniform distribution of electric field for curved slot as compared to straight, triangle, and rectangle slots.	• Higher applied voltage (above 50 kV) required.
Double ring slit	• Solvent evaporation prevented.	• High applied voltage (70 kV).
Plucked string	• 26 times higher production rate. • A lower applied voltage compared to single needle.	• Further study of string's mechanism is necessary.

2.3.2 3D spinnerets

Increasing the number of needles/channels can enhance the production rate to some extent, but the production rate is still low due to the low spannable area of the spinneret. The main concept of electrospinning is to generate the electrostatic force which exceeds the critical

value of the electrospinning solution. Ideally, spinneret with any shape/geometry can be used as long as the electrostatic force on which is high enough to overcome the surface tension and viscosity and others of the polymer solution/melt. Research effort has also been paid on the development of electrospinning from an electrified free surface of a polymer solution. Free surface electrospinning can be described as a self-initiated jet initiation system which takes place on a free liquid surface. As the spinneret in this case is not a needle or a channel, the method is also called needleless electrospinning. In needleless electrospinning, spinneret geometry plays an important role in determining the control of the spinning process, fibre morphology, and of course the production rate. The electric field is the main driving force to initiate the formation of the polymer jet in electrospinning (Niu, Wang & Lin 2012a). When a free surface of polymer solution is charged by an electric field with a higher intensity, it is possible to generate multiple polymer jet. Stronger the electric field intensity results in higher fibre production rate with narrower fibre diameter distribution. This intensity together with the distribution of the electric field around the spinneret is highly influenced by the geometric shape of the spinneret (Niu, Wang & Lin 2012b).

The first needleless electrospinning-like phenomenon was noticed by Simm in 1979, in which a fleece of polymeric fibres was electrostatically sprayed through a ring spinneret (Simm et al. 1979). Lukas et al. (Lukas, Sarkar & Pokorny 2008) investigated the self-organization of charged jets initiated from a free liquid surface in the electrospinning process, and a one-dimensional electro-hydrodynamic theory was established as the fundamentals of upward needleless electrospinning. The theory predicted critical field distance, inter-jet distance and relaxation time necessary for jetting under a high voltage. Generally, free-surface electrospinning requires a high enough voltage to overcome the surface tension and viscosity of the solution for jet initiation, although this can vary depending on the type of spinneret

used. Even the jets on a free surface are extremely difficult to control as they tend to arrange and organize randomly.

2.3.2.1 3D spinnerets with a solution bath

Loading the polymer solution onto the surface of 3D spinnerets is important as it determines the forming of the free surface of polymer solution. Some 3D spinnerets in electrospinning come with a solution bath for the purpose of solution feeding. Generally, in a 3D spinneret with solution bath a rotating spinneret is used to pick up polymer solution from the bath. The setup is composed of a 3D spinneret, a high voltage power supply, a polymer bath and a nanofibre collector. In most cases, the spinnerets are partially immersed into the polymer solution, and a motor is used to initiate active rotation to the spinnerets. Once the spinneret is rotating at a certain speed, the polymer solution will be coated onto the surface of the spinneret due to the viscous nature of the solution. Multiple polymer jet can be generated when the spinneret with polymer solution on load are subject to a high electric field. Usually the bath-based electrospinning generates jets to an upward direction so that the dropping of polymer solution to the collector due to the weight of the solution can be avoided. Differently shaped 3D configureuration, such as magnetic fluid bath, cylinder, ball, disk, ring, wheel, needle disk, probed rotating cylinder, snowflakes shaped spinnerets etc. have been developed so far.

Yarin and Zussman (Yarin & Zussman 2004) first proposed free surface electrospinning with the aid of a magnetic fluid. The setup contains two-layered system with the upper layer polymer solution and the lower layer magnetic fluid, as shown in Figure 2-4a. When a high voltage (32 kV) was applied, polymer jets (26 jets/cm^2) were generated from numerous cones/protrusions on the upper layer of polymer solution. The magnetic fluid induced a

magnetic field, resulting in the formation of spikes on the surface of polymer solution. The technology displayed a 12-times enhancement of the production rate (PEO nanofibre) as well as eliminating clogging problem compared to equivalent multiple nozzles. Conversely, this method is very complicated to establish with coarse nanofibres generated.

Lukas (Lukas, Sarkar & Pokorny 2008) illustrated an upward electrospinning setup using a linear cleft capillary, as shown in Figure 2-4b. It was proved that nanofibres can be electrospun from conductive liquids without the aid of magnetic fluid. A one-dimensional electro-hydrodynamic theory was also established to explain the fundamentals of upward needleless electrospinning. The theory predicts the critical field distance, inter-jet distance and relaxation time for jetting under a specific high voltage.

Jirsak et al. (Jirsak et al. 2009) patented a needleless electrospinning setup in which a cylindrical rotating roller as the spinneret, as shown in Figure 2-4c. The cylinder is half immersed in the polymer bath, and polymer solution will be loaded onto the upper roller surface forming wavy pattern under the action of a high voltage (Cengiz & Jirsak 2009). A large number of polymer jets were generated from the wavy surface at an upward direction. This setup was rapidly commercialized under the brand name of "Nanospider™" by Elmarco Co. (Jirsák & Dao 2009). The roller electrospinning showed a great potential as an industrially applicable device, and it reached a high spinning capacity of PVA nanofibres of 108 g/h. Likewise, Wu et al. (Wu et al. 2010) reported an upward needleless electrospinning using a metallic cylindrical-shaped electrode named "Tip-less Electrospinning" (TLES). The non-rotating cylindrical spinneret made the electrospinning process discontinuous. The polyethylene oxide (PEO) nanofibres produced with this spinneret were 260 times higher compared to the needle electrospinning. There is no way to supply the polymer solution into

the spinneret, so that the solution layer on the spinneret surface declines in thickness gradually.

Niu et al. (Niu, Lin & Wang 2009) used the finite element method (FEM) to analyse electric field intensity in needleless electrospinning and demonstrated the influence of spinneret geometry on electrospinning. Needleless electrospinning of polyvinyl alcohol (PVA) nanofibres with a rotating disc, cylinder and ball spinneret was compared. The electric field in the electrospinning zone was analysed through FEM. FEM is an efficient way to determine the electric field intensity by providing a visualize electric field interaction according to the experimental parameter (Wang, Wang & Lin 2012; Zheng & Zeng 2014). It has found that disk spinneret (Figure 2-4d) formed high electric field intensity consequently showing a higher electrospinning performance than the cylinder spinneret. The disk spinneret concentrated a high electric field on the top part of the disc, leading to highly stretched polymer jets with finer nanofibres and narrower diameter distribution than cylinder spinneret. On the contrary, cylinder spinneret showed a large surface area with electric field mostly concentrated on both ends of the cylinder. Most of polymer jets were generated from the ends of the cylinder with uneven as-spun nanofibres.

Later on, Niu et al. (Niu, Lin & Wang 2009) compared the electric field intensity of disc, cylinder and ball spinneret, and it was found that a lower electric field intensity was formed on the ball surface thus generating fewer jets (Figure 2-4e). It was also specified that applied voltage and collecting distance affects the electric field intensity. In this experiment, a higher electric voltage of 47-62 kV was used, and the electric field intensity increased with the increase of the applied voltage and decrease of collecting distance.

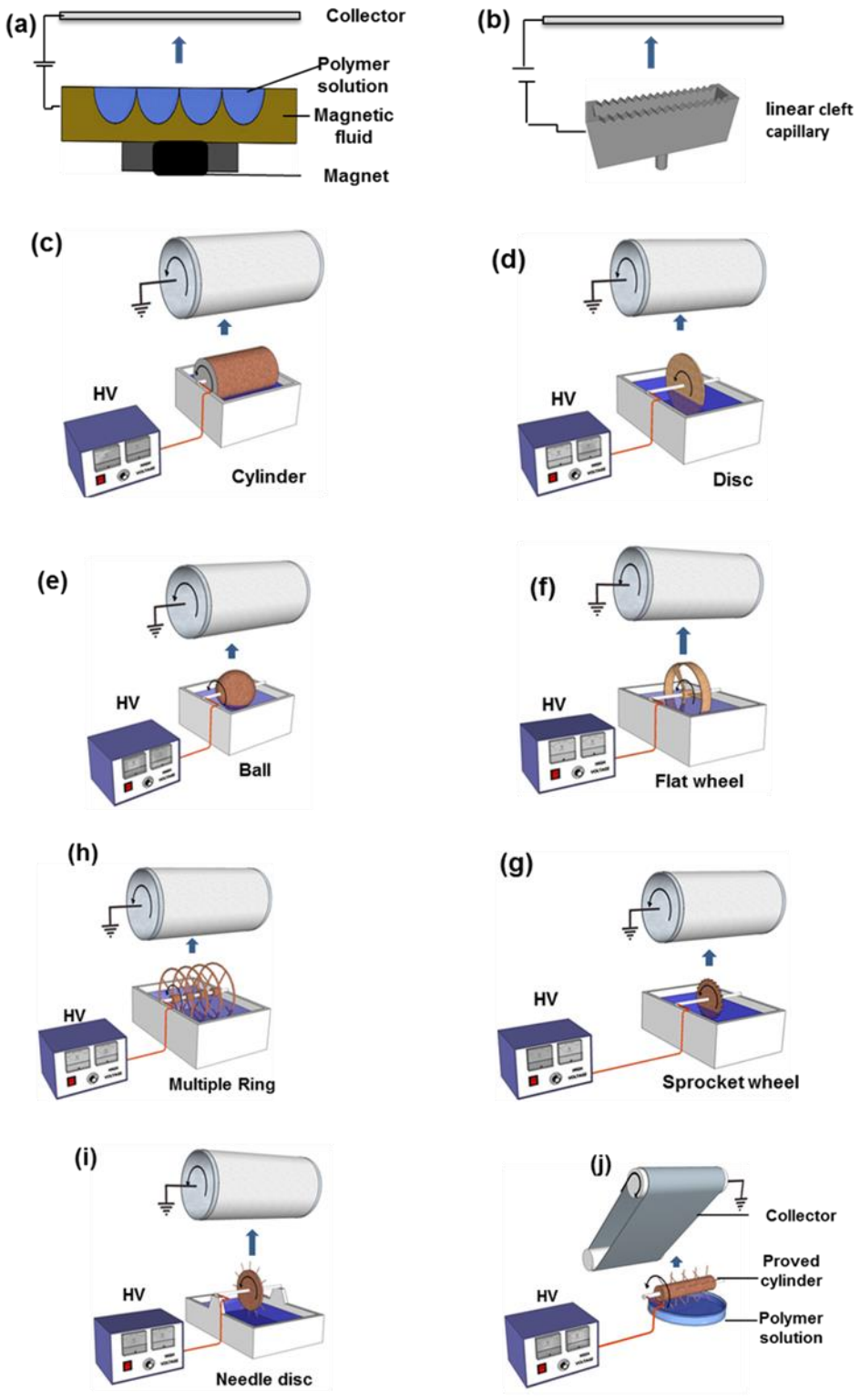

Figure 2-4: Schematics of magnetic fluid spinneret setup (a), linear cleft capillary spinneret setup (b), cylinder spinneret setup (Nanospider™) (c), disk spinneret setup (d), ball spinneret setup (e), flat wheel spinneret setup (f), sprocket wheel spinneret setup (g), multiple ring spinneret setup (h), needle-disk spinneret setup (i) and helical probed cylinder spinneret setup (j).

In addition, the production rate increased with the increase of applied voltage along with finer fibre generated. Above all, these three spinnerets showed a much higher production rate compared to conventional spinnerets. With the similar concept, a flat wheel (Figure 2-4f) (Ali et al. 2017) was proposed as spinneret, and the performance of flat wheel was between the cylinder and disk and ring spinnerets. The production rate of this spinneret was 15-40 times higher than that of the traditional electrospinning and much closer to the ring and disk. In order to produce more uniform nanofibres, sprocket wheel disk (Ali et al. 2017) was reported as spinneret, in which sprocket was added at the edge of the disk (Figure 2-4g). The electric field analysis results indicated that higher intensity of electric field was generated on the teeth of sprocket wheel.

Wang et al. used single and multiple rings as spinnerets, as shown in Figure 2-4h (Wang, Lin & Wang 2014). The production rate increased with the increase of the number of rings in the spinneret. The resulted fibres from multiple rings were coarser with a larger diameter distribution than a single ring. The electric field intensity of multiple rings was found to be much higher than that of multiple disks, and the strong electric field was formed on the top half area of each ring. Thus, the more efficient result was obtained using single ring spinneret instead of disk spinneret.

More recently, a needle-disk spinneret (Figure 2-4i) (Liu, Ang & He 2017) that is almost similar to the sprocket wheel was proposed, but the needle tips instead of sprockets were covered with polymer solution through the rotating action of the spinneret. This spinneret produced nanofibres with super high throughput of 13.5 g/h, which is 183 times higher than conventional electrospinning. Both the needle-disk and the sprocket wheel provide the

advantages of the more controlled process, more uniform nanofibres with smaller fibre diameter distributions.

Identical to the needle-disk spinneret, Moon (Moon, Gil & Lee 2017) introduced a method of needleless electrospinning using helically probed rotating cylinder as spinneret (Figure 2-4j). Needles were mounted on the rotating cylinder in a helical configureuration, and conductive silver paste (white) was used to connect the needles. The cylinder rotated with the aid of a DC power supply, and the polymer solution was positioned under the rotating cylinder. When the cylinder was rotating, polymer droplets formed at the end of each needle. Taylor cones were generated on each needle when a positive voltage was applied. The production rate of this proposed spinneret was six times higher than the conventional electrospinning, but only a low applied voltage (15 kV to 17 kV) was used and nanofibres with highly crystalline polymers could be spun.

Table 2-2: Summary of 3D spinnerets with a polymer bath.

Spinnerets	Privileges	Drawbacks
Magnetic fluid	• 12-times higher (PEO nanofibres) production rate compared to needle method.	• Complicated set-up. • Wider fibre diameter distribution.
Cylinder (Nanospider™)	• Simple and industrially applicable setup. • High production rate (108 g/h).	• Higher applied (30-70 kV) voltage. • Open set up of polymer bath causes solvent evaporation.
Disk	• Finer nanofibres than cylinder. • Higher throughput than cylinder.	• Solvent evaporation. • High applied voltage.
Ball spinneret	• Generates evenly distributed electric field intensity. • Higher production compared to needle.	• Lower electric field intensity than disk. • Solvent evaporation. • Unable to electrospin when ball diameter is below 60 mm.

		• High applied voltage.
Single and multiple ring	• Stronger electric field intensity than cylinder, disk and ball. • Finer nanofibres. • Enhanced production rate.	• Open set-up with solvent evaporation. • Lower electric field formed in the middle rings causes uneven fibres. • High applied voltage.
Flat wheel	• Higher production rate (15-40 times) than that of needle.	• Less efficiency compared to ring spinneret.
Needle-disk	• Higher electric field generated compared to disk spinneret. • High production rate (183 times) than conventional electrospinning.	• Open set-up with solvent evaporation. • High applied voltage.
Helical probed cylinder	• Higher throughput (6 times) than needle electrospinning. • Low applied voltage.	• Open set-up with solvent evaporation.

Although the rotary needleless electrospinning setups contain simpler structures, and are easy to industrialize with high throughput, the flow rate of the polymer solution cannot be controlled precisely. Besides, the polymer concentration will increase gradually due to the evaporation of solvent from the open solution bath. Unstable jets due to the unevenly concentrated electric field on the surface of spinneret are another issue. These drawbacks limit the commercialization of the technology.

A recent design of spinneret was proposed by Yang et al. (Yang et al. 2016) with the name fractal electrospinning. The shape of the spinneret was based on the Koch snowflake structure and high-intensity electric fields were concentrated on the tips of the fractal spinneret edges. This spinneret produced fine and uniform TPU nanofibres with a high productivity around 10g/h. A relatively low voltage of around 20 kV was used compared to 100-120 kV for Nanospider™. It is very evident that the shape and geometry of spinneret have direct impact on the electrospinning performance of needleless electrospinning. An ideal design of

spinneret will not only enhance the production rate with fine and uniform as-spun nanofibres, but also saves the power consumption as the electric field concentration is optimized most. Table 2-2 summarizes the privileges and drawbacks of all the above reviewed 3D spinnerets with a bath.

2.3.2.2 3D spinnerets from air/bubbles

Multiple-jet electrospinning can also be generated by the aid of air or gas, in which bubble or foam is formed instead of Taylor cone for generating multiple jets, as shown in Figure 2-5. In 2007, Liu (Liu & He 2007) proposed "bubble electrospinning", in which bubbles were produced when compressed air or nitrogen was blown into the polymer solution, and a high voltage was applied to initiate the formation of multiple jets. The number of jets produced was affected by the number of bubbles, bubble size as well as applied voltage. Although many polymers such as PEO (Liu & He 2007), PVA (Yang et al. 2009), and PLA, PAN (He et al. 2008) have been successfully electrospun with a high throughput, strip-like and sphere-like morphologies occur due to the popping of bubbles (He et al. 2012).

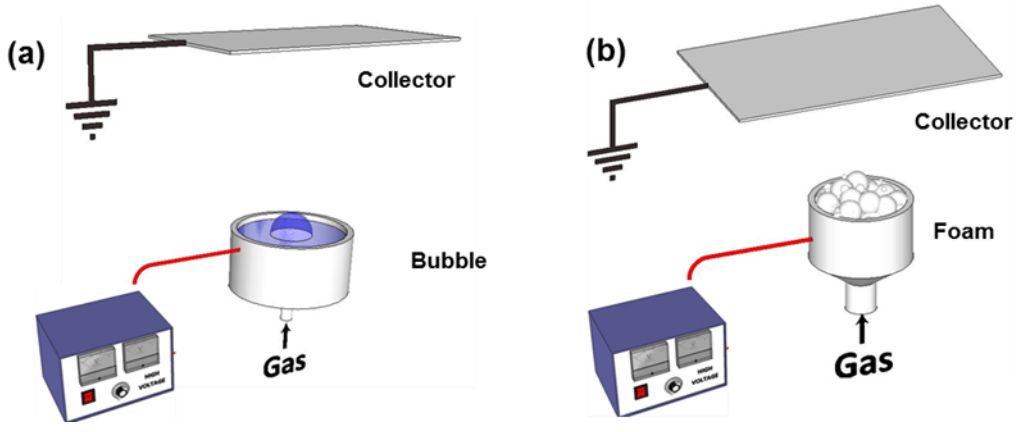

Figure 2-5: Schematics of single bubble electrospinning setup (a) and foam setup (b).

To maintain a uniform bubble, a new approach of electrospinning from a single spinning bubble with a large surface area is developed. Multiple jet initiated from the large surface of the bubble as illustrated in the Figure 2-5a. Similarly, Higham et al. proposed foam electrospinning in which foams were generated by injecting compressed carbon dioxide through a porous plate into a polymer solution (Higham et al. 2014). Bubbles of the foam were then generated and rose to the surface of the polymer solution where a high voltage was applied by immersing a copper electrode (Figure 2-5b). Several polymer jets ejected toward the collector directly above the foam. The production rate was around 300 times greater compared to single needle electrospinning under a low applied voltage (10-22 kV). Overall, bubble and foam electrospinning show a new way of developing 3D spinnerets to produce nanofibres with high throughput.

Table 2-3 summaries the privileges and drawbacks of 3D spinnerets from air/bubbles.

Table 2-3: Summary of 3D spinnerets from air/bubbles.

Spinneret	Privileges	Drawback
Bubbles	• Many polymers can be electrospun with minimal diameter.	• Broken bubbles cause strip/sphere-like morphologies.
Foam	• 300 times greater compared to single needle. Low applied voltage (10-22 kV).	• Solvent recovery problem.

2.3.2.3 3D spinnerets from edge

Another new method of electrospinning was developed by Thoppey (Thoppey 2012) with the name edge-plate electrospinning, in which single-plate, multiple-plates and aluminium bowl were used as 3D spinnerets, as illustrated in Figure 2-6. The similarity of all edge-plate spinnerets is the spinneret remains stationary and electrospinning occurs in sidewise

direction. In the setup of single-edge electrospinning, a single-plate was mounted at 40^{o} horizontal angle (Muthuraman 2012a, 2012b). Polyethylene oxide (PEO) polymer solution was provided to this edge-plate by the aid of an electrically insulated reservoir connected with one or more plastic pipettes. Polymer solution reached the plate edge due to gravitational force. When a high voltage was applied, the solution formed a neck shape and became elongated, polymer jets were then ejected. Following the same method, a complementary approach to create multiple streams was developed by overlapping multiple plates known as waterfall configuration (Thoppey et al. 2011), as illustrated in Figure 2-6a. In comparison with needle electrospinning, the production rate was five times higher even using only one plate.

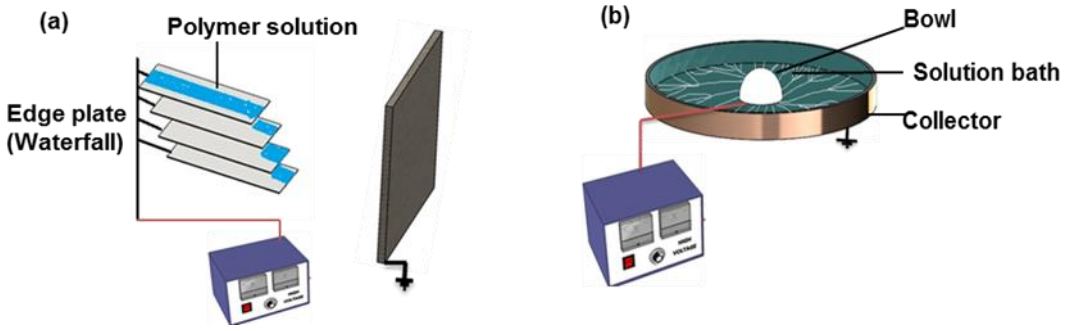

Figure 2-6: Schematics of edge plate spinneret setup (a) and bowl spinneret setup (b).

For edge-plate and waterfall configurations, the polymer flow was gravity-assisted and was dependent on the angle at which the plates were held, the volume of the solution in the reservoir, as well as the size of pipette aperture. However, the solution dropping may occur due to inappropriate plate angle and/or solution concentration. It is difficult to adjust the parameters of edge electrospinning which is a hindrance to obtain desired fibre quality. Moreover, low fibre quality was found in the case of multiple-plates compared to single plate

due to the intermittent jet formation. To stabilize and optimize the processing parameters, Thoppey et al. (Thoppey et al. 2011) reported aluminium bowl as the spinneret (Figure 2-6b). The bowl was deposited on the polymer bath and surrounded with the concentric cylindrical collector. After applying a high voltage to the solution on the bowl edge, cone shaped protrusion was created, and jet initiation started from the edge of the bowl. Collected nanofibres were similar as needle electrospinning with a narrow distribution as high electric field intensity was generated at the edge of the bowl. Production rate was 40 times higher than conventional needle electrospinning. The drawback is that this process is discontinuous as the process stops once the solution level reaches below the bowel edge.

Table 2-4 summarizes the privileges and drawbacks of 3D spinnerets from edge.

Table 2-4: Summary of 3D spinnerets from edge.

Spinneret	Privileges	Drawback
Single and multiple plate	• No clogging problem. • High throughput (5 times) than single needle.	• Difficult to adjust plate angle and setup with different polymers as well as concentrations.
Aluminium bowl	• Higher production rate (40 times) than conventional setup.	• Discontinuous process.

2.3.2.4 3D spinnerets without solution bath

In these types of electrospinning setup, solution was supplied to the spinneret through a pump, tube or centrifugal force instead of polymer solution bath. For example, splashing needleless electrospinning, rotary cone, corona electrospinning, stepped pyramid and metal dish can be used to generate electrospinning.

In 2010, Tang et al. (Tang, Zeng & Wang 2010) introduced a novel design in the solution supplying system called splashing needleless electrospinning, as shown in Figure 2-7a. In this setup, a metal roller spinneret as the positive electrode was connected to a high voltage power supply for generating an electric field. A solution distributor was located above the spinneret, and PEO solution droplets were splashed onto the surface of the spinneret, resulted in multiple polymer jet. The production rate was 24-45 times larger than that of the single needle electrospinning with the diameter range of 100-400 nm. Similarly, Lu et al. (Lu et al. 2010) described a needleless electrospinning setup using a rotating cone as the spinneret (Figure 2-7b). In this setup, polymer solution was continuously fed onto the surface of the cone through a tube. Numerous jets were generated from the rim of the cone under a high voltage.

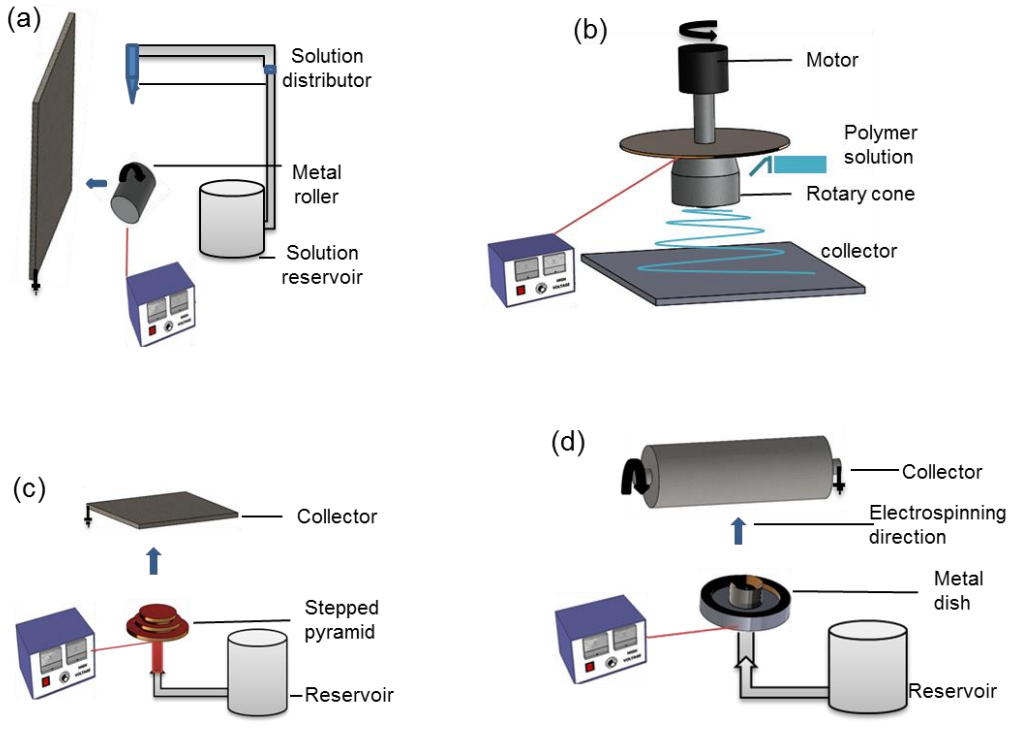

Figure 2-7: Schematics of splashing needleless electrospinning setup (a), rotating cone spinneret setup (b), stepped pyramid spinneret setup (c) and metal dish spinneret setup (d).

Poly (vinyl pyrrolidone) (PVP) nanofibres were fabricated with a production rate of about 10 g/m and with a diameter of 220–320 nm. In comparison with the single needle electrospinning, the nanofibres production rate was 950 times higher.

Recently, Molnar and Nagy (Molnar & Nagy 2016) proposed an electrospinning spinneret termed as corona electrospinning. The setup consists of a long circular channel with a sharp-edged outer metal ring electrode. The setup does not require a solution bath and the exposed surface of the solution is also kept at the minimum to reduce solvent evaporation. This ring concentrates charge and induces large local electric field strength to aid the formation of multiple Taylor cone. Finer nanofibres were observed in comparison to a single needle setup. Stepped pyramid as spinneret was proposed by Jiang et al. (Jiang, Zhang & Qin 2013), in which nanofibres were produced from the edge each pyramid without a polymer bath (Figure 2-7c). Polymer solution (PVA) was distributed to the edge of the spinneret from the reservoir. When the high voltage (55-70 kV) was applied to the spinneret, multiple jets were observed from the edge of the stepped pyramid stage. The curved edge of the spinneret become favourable sites of jet initiation due to high electric field magnitude, generating finer nanofibres at a high production rate. The spinneret was further enhanced for high throughput by utilizing micro-bubble (using Triton X-100) solution system (Jiang et al. 2015). The highest production rate was 5.7 g/h, and it was claimed that with the same production rate smaller bubble size led to smaller diameter distribution of nanofibres. Jiang and Qin (Jiang & Qin 2014) also fabricated core-sheath nanofibres through this spinneret.

Table 2-5: Summary of 3D spinnerets without solution bath.

Spinneret	Privileges	Drawback
Metal roller spinneret	• 24-45 times higher production rate than single needle. • Diameter range 100-400 nm.	• Solution supply was not consistent.
Rotating cone	• Extremely high production rate	• Solution supply was

	(nearly 950 times) than single needle. • Diameter range 220–320 nm.	not consistent.
Corona electrospinning	• Less solvent evaporation. • Finer nanofibres.	• High applied voltage 55 kV is required.
Stepped pyramid	• Finer nanofibres (PVA 142-205 nm). • Production rate of 4g/h (nearly 100 times higher than single needle).	• High applied voltage 50-70 kV. • Solvent evaporation.
Metal dish	• High production rate. • Continuous process.	• High voltage (55-75 kV) is required.

Most recently, Wei et al (Liang et al. 2018) reported a metal dish as the spinneret with high throughput. In this setup (Figure 2-7d), the metal dish spinneret was placed on a metal base which was connected to a high voltage power supply. PAN polymer solution was supplied through a control pump into the spinneret. The polymer solution was stored in the metal dish until the solution edge reached a certain radian of the dish. Multiple polymer jet occurred in the circle of the metal dish. Quality nanofibres with narrow fibre diameter distribution were prepared from applied voltage between 55 kV and 75 kV, with the production rate 0.46-3.66 g/h. Though electrospinning using metal dish showed a great potential in the production of nanofibres, a high electric potential was still required to produce narrow fibre diameter.

Overall, these 3D spinnerets without solution bath show better result to protect the polymer solution effectively from evaporation, and the flow rate of solution can be controlled precisely ensuring a stable process. Table 2-5 summarizes the privileges and drawbacks of 3D spinnerets without solution bath.

2.3.2.5 3D spinnerets from coil/wire

Wire-based spinnerets have been proven to be very promising in generating highly efficient needleless electrospinning, due to their potential in optimizing electric field distribution on the curved surface. In 2009 A conical wire coil was employed as a spinneret to prepare

nanofibres by Wang et al. (Wang et al. 2009). In this setup (Figure 2-8a), the polymer solution was conveyed to the spinneret under the movement of gravity and guided through the coil shape. When the high voltage (45-70 kV) was applied, higher electric intensity formed on the coil surface. The work showed notable production rate of nanofibres compared to disk and cylinder electrospinning. However, high consumption of electricity increases the process cost, and conical wire coil limits the amount of polymer solution that inhibits the mass production of nanofibres.

Two stainless wires were connected about 180^{o} apart with a spindle to be a spinneret, as shown in Figure 2-8b (Forward & Rutledge 2012). When the spindle rotated with the aid of a DC motor, entrainment of the fluid occurred, resulting in the formation of liquid droplets on the wire. Electrostatic jetting from each liquid droplet then occurred. Although the production rate of this spinneret is higher than the conventional electrospinning, it depends on the amount of polymer solution entrained on the wire as well as the rotation rate of the spindle.

Furthermore, Wang et al. (Wang et al. 2012) proposed tubular spiral coil as a spinneret in needleless electrospinning, as depicted in Figure 2-8c. The tubular coil allowed continuous loading of polymer solution by rotation above a polymer bath. This mechanism produced PVA and PAN nanofibres successfully with a higher production rate and finer and more uniform fibres than needle electrospinning. The analyses of electric field intensity illustrated that high electric field intensity was generated around each spiral coil (Wang et al. 2012). The strengthened electric field intensity on the coil surface led to strong electrostatic force, resulting in thin fibres and high fibres production rate.

Liu et al. (Liu et al. 2014) reported an innovative design of efficient needleless electrospinning using a circular rotary bead-wire as spinneret (Figures 2-8d). In this setup, a rotary bead-wire was driven by a DC motor used as electrode, and polymer solution was supplied through a solution brush. Under a high voltage (15-30 kV), numerous polymer jets were generated and the average diameter of the resultant polyvinyl pyrrolidone (PVP) nanofibres was around 200 nm. This method showed a big potential in enhancing the production rate as well as enhanced electric field distribution.

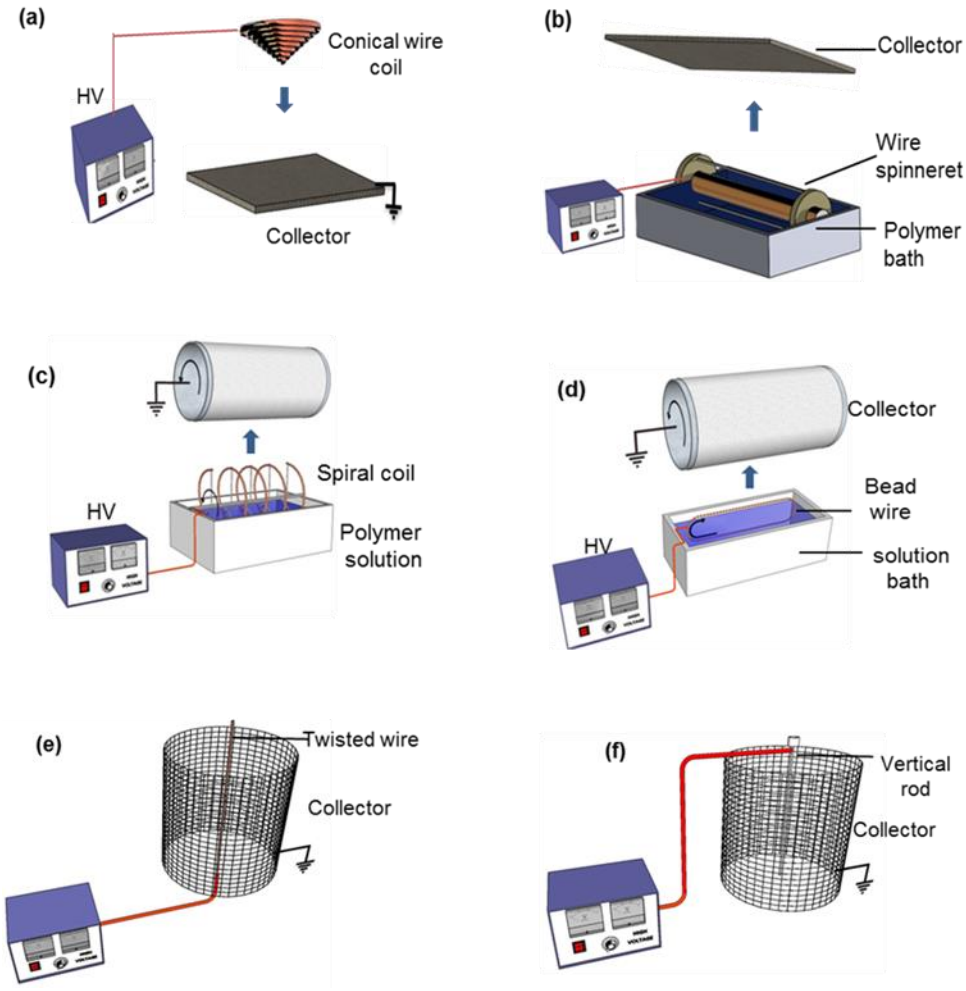

Figure 2-8: Schematics of conical wire coil spinneret setup (a), single wire spinneret setup (b), spiral wire coil spinneret setup (c), rotary bead-wire spinneret setup (d), multiple twisted wire setup (e) and vertical rod (f).

Besides, Holopainen et al. (Holopainen et al. 2014) presented multiple twisted wire electrospinning to produce nanofibres (Figure 2-8e). The twist in the wire was essential for the formation of stable polymer flow from the top of the wire towards downward direction with the aid of gravity. When a high voltage was applied, multiple Taylor cones were simultaneously self-formed on the downward flowing solution. High production rate of polyvinyl pyrrolidone (PVP) and hydroxyapatite (HA) nanofibres was achieved. However, the major limiting factor of this setup is the drying of the polymer solution on the wire during the electrospinning process, which will eventually force to interrupt the process.

A needless vertical rod electrospinning method was also proposed by Shin et al. (Shin et al. 2015). The setup (Figure 2-8f) contains vertically oriented threaded rods for holding multiple drops to launch many simultaneous jets. When a high voltage (above 35 kV) was applied, numerous Taylor cones were produced from the surface of the rods, and nanofibres were collected in the grounded circular collector sidewise. This technique showed a high production rate of PVP nanofibres of 4.5 g/h with the fibre diameter range 200-400 nm. For further development of this spinneret, different numbers of rods were used as the spinneret. However, with the increase in the number of rods, the applied voltage had to increase to facilitate the spinning process. For example, two rods required 50 kV while three rods required 70 kV and so on.

Table 2-6 summarizes the privileges and drawbacks of 3D spinnerets from coil/wire.

Table 2-6: Summary of 3D spinnerets from coil/wire.

Spinneret	Privileges	Drawback
Conical wire coil	• Higher production rate. • Narrow fibre diameter distribution.	• Limited amount of polymer solution. • Not suitable for mass

	• No corona discharge at 70 kV.	production.
Spiral wire coils	• High quality fibre. • Higher production rate.	• Solvent evaporation occurs
Rotary bead-wire	• Higher production rate (40 g/h) • Low applied voltage (30 kV).	• Wide fibre diameter distribution.
Single wire (Nanospider™)	• High production rate.	• Drying of the polymer solution. • High applied voltage.
Multiple twisted wire	• Easy and simple setup. • High production rate.	• Drying of the polymer solution on the wire surface.
Vertical rod	• Higher productivity (4.5 g/h). • Narrow diameter distribution (200-400 nm).	• High applied voltage (35-100 kV).

2.4 Protective clothing

Protective clothing refers to apparel and other fabric-related materials that have functional properties rather than aesthetic appeal. These clothing are essential to protect the wearer especially, for Military personnel and industrial worker, from potentially hazardous and toxic chemicals as well as to lower the risk of injury or illness. There are several types of methods and ways to develop protective clothing for versatile application. However, the nanofibre based protecting coating is a new approach which provides the advantages of light weight clothing materials, greater breathability along with an improved liquid and chemical protections. In this study, Chapter 6 represents a new approach of protective clothing with nanofibres.

2.5 Summary

Designing of spinneret in electrospinning is the determining factor in large-scale production of fine and uniform nanofibres. Multiple needle electrospinning can enhance the production rate to some extent, but there are many issues including clogging in needles and electric

repellency between needles with uneven nanofibres collected. Electrospinning from holes/channels has overcome the issue of clogging, but a high applied voltage must be used, and solution evaporation is another issue. Free surface electrospinning has demonstrated that multiple polymer jet can be generated from an electrified area, resulting in a big boost in production rate. But usually a polymer bath is needed to load polymer solution to spinnerets, causing solvent evaporation issue. A high applied voltage is needed again to charge the free surface, even though tailed design of spinneret can enhance the efficiency of power with a lower applied voltage used. Electrospinning from bubbles uses a low applied voltage, even though the breakage of bubbles results in coarser nanofibres. Electrospinning from edge can significantly enhance the production rate, but the setup is hard to setup and the process is usually discontinuous. Needleless electrospinning without a polymer bath overcomes the solution feeding issue, but still high applied voltage is the concern. Wire electrospinning has been proven to be highly efficient in concentrating electric field on the spinnerets. With a low applied voltage used, the as-spun nanofibres are fine and uniform but ensuring a stable and trustable process with proper controlling is still a challenge. Designing of 3D spinneret with a large spannable area and with a high capacity in concentrating electric field together with ease in polymer solution feed and process controllable is the key in further development of large-scale production of nanofibres from electrospinning.

In this study, three new spinnerets have been demonstrated. Chapter 4 describes and compares the convex needle spinneret with needle whereas chapter 5 illustrate a wire loop with tubing with enhanced throughput. These spinnerets are able to produce finer nanofibres with lower electric voltage demonstrating easy and effective method for nanofibre fabrication.

CHAPTER 3

MATERIALS, METHODOLOGY, AND MEASUREMENTS

Chapter 2 described the background and literature review on the evolvement of different types of spinnerets in electrospinning. Chapter 3 illustrates the materials, methodology, relevant measurement, and characterization techniques which were used during the investigation to follow the aim and objectives of this research.

3.1 Materials

In electrospinning, various raw materials can be used in the form of solution or melt. Different polymers are dissolved in various solvent based on the nature of the polymer. In this investigation, different raw materials are used. For electrospinning PVA, PAN etc. polymers are used along with deionised water and DMF as the solvent. For nanofibrous coating, PDMS and TMS are used as a repellent. Cotton fabrics are used as substrate material and are placed in the surface of the collector while electrospinning. Nanofibres are collected on the surface of the cotton fabric in the experiment of nanofibrous coating.

3.1.1 Fabrics

100% cotton, twill weave, and weight 250 GSM and 3x1 constructions were sourced from Bruck Textiles, Australia.

Table 3-1: Represents the polymer specifications which were used in electrospinning.

Polymer	Specification	Solvent	Supplier
PAN	85,000 g/mol.	DMF	Good Fellow Cambridge Limited (England)
PVA	100,000 g/mol.; 96% hydrolyzed	deionized water	Sigma Aldrich Pty Ltd, Australia

Table 3-2: Specifications of chemicals and suppliers.

Chemicals	Supplier
Acetic acid	Ajax Fine. Chem. PTY. Ltd Australia
Acetonitrile	BDH Limited Poole, England.
Dimethylformamide	Sigma Aldrich Pty Ltd, Australia
Isopropyl alcohol	BDH Limited Poole, England.
Methanol	Honeywell International Inc. USA
N-Heptane	RCL LAB SCAN Limited, Australia
N-hexadecane	Sigma Aldrich Pty Ltd, Australia
Sodium Hydroxide	Chem Supply Pty Ltd, Australia.
Sulphuric acid (98%)	RCL LAB SCAN Limited, Australia
Toluene	Rhone May & Baker Pronalys Chemicals Pty Ltd, Australia
Repellent:	
Xiameter (FBL-O563) PDMS-TMS	Dow Corning Pty Ltd, Australia.

3.2 Methodology

The research methodology which is used in this study is presented in the flow chart (Figure 3-1). The aim of this study is to develop linear spinnerets which will be stable, capable to produce high-quality nanofibres, as well as to provide better controlling of parameters. As

linear spinnerets geometric shape play a vital role to enhance the effectiveness and controllability, several types of linear spinnerets are tried to get the desired objectives. The experimental work of electrospinning requires high applied voltage. As a result, it is impossible to measure the effectiveness of spinnerets directly from the experimental work. For this, COMSOL Multiphysics software was used which analyse the result according to the experimental set-up.

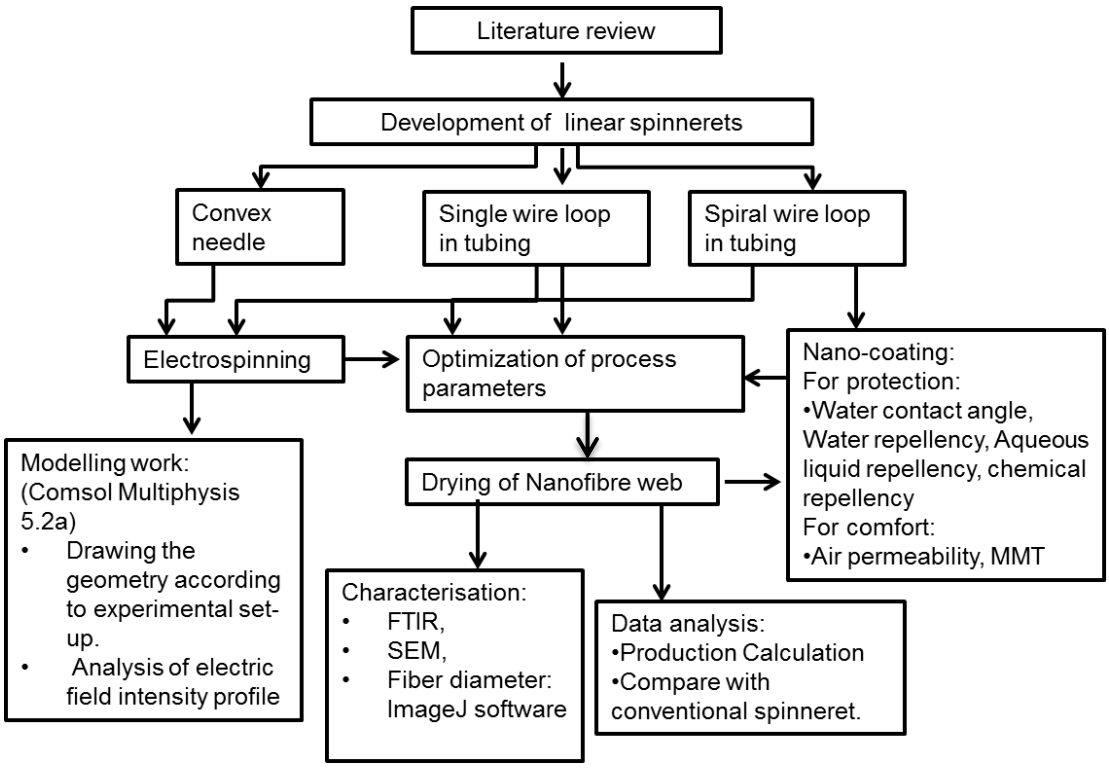

Figure: 3-1 Flowchart of methodology.

3.2.1 Development of linear spinnerets

3.2.1.1 Convex needle

The first research approach was taken using a convex channel as spinneret (tube diameter: 0.84 mm inside, 1.20mm outside diameter, wall thickness 0.18mm, 38mm length). It contained a split in the convex tip to provide a limited free surface in conventional

electrospinning set-up. This type of shape was created to facilitate solution distribution (Yan et al. 2017). The details set-up of this spinneret is mentioned in Chapter-4.

3.2.1.2 Single wire loop embedded in a tube

The second spinneret which was used in this study was a wire loop embedded at the tip of the Teflon tube and also applied in conventional electrospinning setup. The Teflon tube was 125 mm in length with its inside diameter 4.2 mm, outside diameter 6.2 mm and wall thickness 1 mm. The tube curved to an angle of 30^{o} in an upward direction. A small stainless-steel wire loop with the radius of 0.25 mm was placed inside the tip of the tube with one end of the wire penetrated out the wall for power connection.

3.2.1.3 Spiral wire loop embedded in a tube

The last linear spinneret was spiral wire loop (three turns) which is similar to the single wire electrospinning set-up except that the spiral wire loop projected in the downward direction from the tube at an angle of 30^{o}.

3.2.2 Electrospinning

Electrospinning apparatus consists of mainly four components, a syringe pump, a high voltage power supply, solution container, and a collector. In this study, a KDS 200 digital syringe pump (from KD Scientific Inc., Holliston, MA, USA) was used along with a 10 ml plastic syringe as solution container to provide a constant flow of solution supply. To generate high voltage ES30P-5W (maximum output voltage of 30 kV) was used. Two types of metallic collector with rectangular shape and circular shape were used for different experiments (Figure 3-2a-c).

3.2.2.1 Basic parameter of electrospinning

There are four basic parameters in electrospinning such as electric voltage, solution concentration, flow rate, collecting distance etc. Different types of polymer solution with varying concentrations are used in this study. The basic parameter of electrospinning is adjusted to ensure large number of jets generation through the spinneret as well as to ensure improved fibre productivity.

3.2.3 Drying of nanofibres

Drying of nanofibres web, as well as nanofibrous coated samples, were carried out in the laboratory oven at 60°C for 30 minutes. Through drying the solvent was completely evaporated from the nanofibres.

3.3 Measurements and characterisation

3.3.1 Equipment and test methods

3.3.1.1 Scanning electron microscope (SEM)

The morphology of each sample was observed by scanning electron microscopy (FEI Quanta™-200 ESEM, UK) (Figure 3-2f) after being sputter-coated (IMBROSE, Spi A20014, Australia) (Figure 3-2d). Morphology of the fabric was observed with different magnification in low vacuum mode of the instrument at voltage of ranges 15-30 keV.

3.3.1.2 Fibre diameter and production rate

The average fibre diameter will be calculated from the SEM images using image analysis software (ImageJ). The production rate of electrospun nanofibres was calculated based on the

largest flow rate of the polymer solution while no liquid dropped from the spinneret tip was maintained. It was measured based on the dry weight of the collected nanofibres.

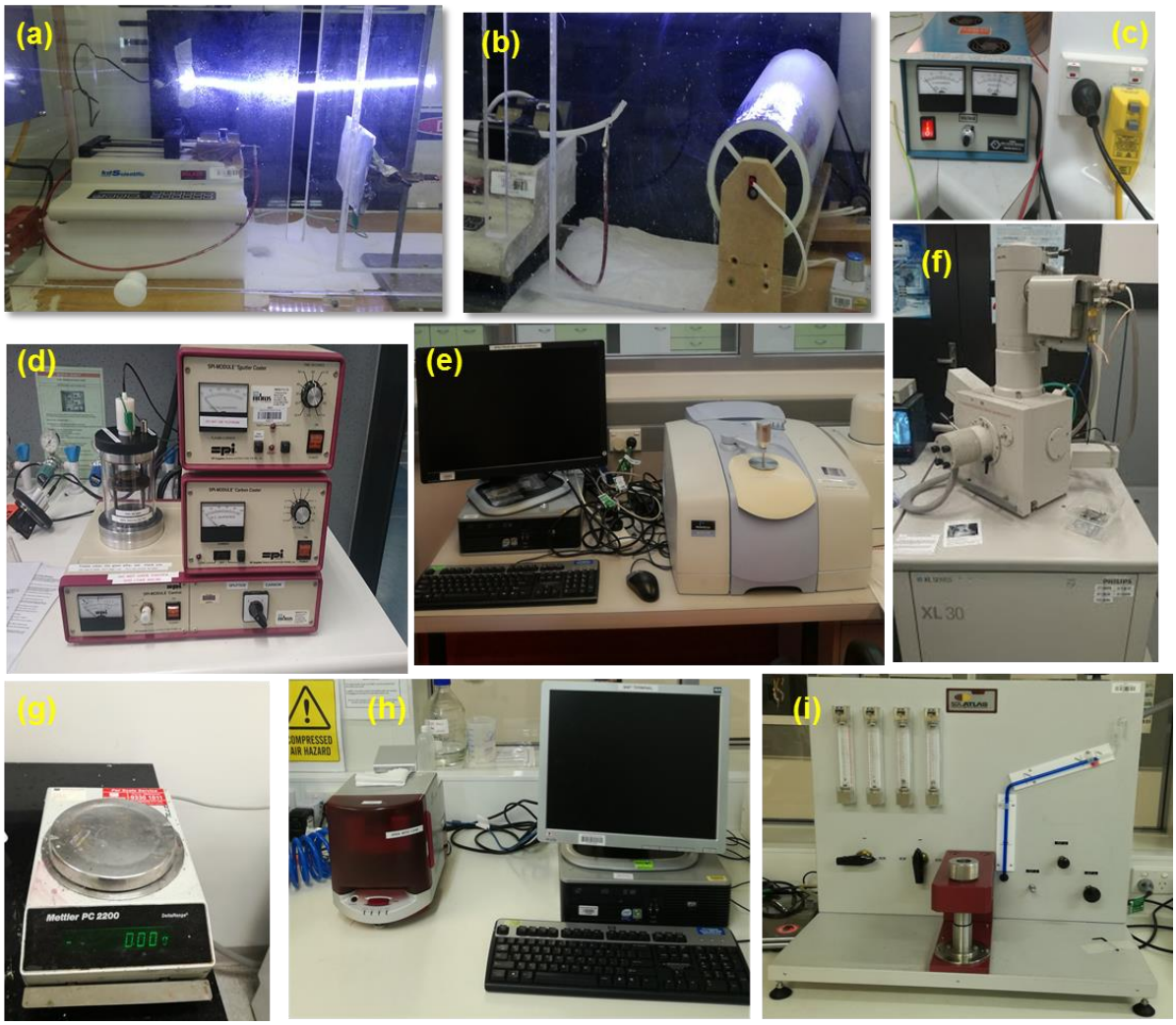

Figure 3-2: The equipment (a) electrospinning set-up with convex needle, (b)wire loop electrospinning, (c)high voltage power supply, (d) Sputter coating m/c, (e)FTIR, (f)SEM, (g) electric balance, (h)MMT tester, (i) Air permeability tester.

3.3.1.3 Water contact angle measurements

The water contact angle was calculated using a contact angle system (Data physics, CA20, Germany) at room temperature by Sessile Drop Method. An ultra-pure water droplet (4 microliter size) from a Milli-Q filtration system was used to measure the contact angle. A fabric sample 10cm x 10cm size was placed above a tilting table. A fixed needle was

mounted 10 mm above that tilting table for supplying the water droplet. A syringe was placed to hold the water and it allows the transfer of the droplet from the needle tip onto the surface of the fabric. When the water droplet falls on the fabric surface a photo was taken to calculate the contact angle by Sessile Drop Method. The contact angle values were averaged from ten readings taken at different places on the fabric surface.

3.3.1.4 FTIR spectroscopy

ATR-FTIR spectrum was reported for each of the samples using a spectrophotometer (Perkin Elmer 300, USA). A single layer of fabric was placed on the ATR crystal above a diamond crystal (Figure 3-2e). After that pressure clamp was lowered to provide good contact between the sample and diamond crystal. The FTIR spectra were obtained within the range between 4000-650 cm^{-1}.

3.3.1.5 Air permeability test

Air permeability is the volume of air in millilitres that passes through 100 mm^2 of fabric at a pressure difference of 10 mm head of water in one second. Airflow of the samples was measured with the air permeability tester (SDL Atlas Pty Ltd, England) using AS-2001.2.34:1990 (Method 2.34: Physical tests- Determination of permeability of fabric to air). During the test, the specimen was clamped over an air inlet of the apparatus and the air was passed through it by means of a pump (Figure 3-2i). The air valve was then adjusted to give a pressure drop across the fabric of 10 mm head of water and the airflow is then measured using a flow meter. Ten specimens were tested and the mean airflow in cubic centimetre per square centimetre per second was calculated from the average results.

The calculation of the air permeability of the fabric was done by using this formula:

Air permeability, $L = \frac{V}{A}$

Where

L = air permeability, in cubic centimetres per square centimetre second

V = rate of air flow, in cubic centimetres per second

A = area of fabric under test, in square centimetres

3.3.1.6 Moisture management properties (MMT)

The moisture management property of fabrics was measured on the SDL Atlas moisture management tester (MMT) (Figure 3-2h), in accordance with the standard AATCC-TM-195 (American Association of Textile Chemists and Colorists, 2017). Five specimens 8cm × 8 cm were prepared to do the test under the standard condition (ASTM D1776). In this test a saline solution was penetrating from the top side to the bottom side of the sample to measure the moisture management property. Wetting time (WT), Absorption rate (AR_T), Maximum wetted radius (MWR), Spreading speed (SS_i), One way transport capability (OWTC), Overall (liquid) moisture management capability (OMMC) were displayed on the associated computer.

Table 3-3: Summary of equipment, and test methods.

SL no.	Test and Method used		Equipment
1	Sputter coating m/c	-	IMBROSE, Spi A20014, Australia
2	SEM image	-	FESEM, Quanta™-200, UK
3	Fabric conditioning	AS 2001.1-1994	Conditioning cabinet
4	FTIR spectroscopy	-	Perkin Elmer 300, USA
5	GSM	AS-2001.2.13-1989	GSM cutter, Zweigle, Germany
6	Air permeability test	AS 2001.2. 33-1990	Air permeability tester, M021S, SDL Atlas, UK
7	Moisture management test (MMT)	AATCC TM 195-2017	Moisture Management Tester, SDL Atlas, UK
8	Water repellency (spray	AATCC 22-2014	Spray rating tester, Toyoseiki, Tokyo,

	test)		Japan
9	Contact Angle measurements	Sessile Drop Method	Contact angle system Data Physics, OCA 20, Germany
10	Aqueous liquid repellency test	AATCC 193-2012	no Equipment required
11	Chemical resistance test	-	no Equipment required

3.3.1.7 Water repellency test

The Water repellency test (Toyoseiki, Tokyo, Japan) was performed in accordance with AATCC 22: 2010 to measure the water resistance of the coated fabrics (American Association of Textile Chemists and Colorists, 2014). Before testing, samples were conditioned at 20 ± 2 °C and 64 ± 2% RH for 4 hours. The sample was cut according to the standard 180 mm × 180 mm size and placed between the test hoops inclined at an angle of 45^{o}. On the surface of the inclined sample, 240 mL of distilled water was sprayed for 30 s. Each sample was then spray rated following the instruction of the international standard chart for spray rating given in the below Table 3-4.

Table 3-4: AATCC Standard spray test ratings.

Rating	Description
100 (ISO-4)	No wetting or non-sticking of the upper surface
90 (ISO-4)	Slightly random sticking or wetting surface at sprayed points
80 (ISO-3)	Wetting of the upper surface at sprayed points
70 (ISO-2)	Partial wetting of upper surface at sprayed points
50 (ISO-1)	Completed wetting of the sprayed surface
0	Wetting of the whole upper and lower surface at sprayed points

3.3.1.8 Aqueous liquids repellency test

The test was performed in accordance with the AATCC 193: 2012 standard (American Association of Textile Chemists and Colourists, 2012a) where three specimens were cut in the size of 2 mm × 2 mm square. Then the specimens were placed in a petri dish (American

Association of Textile Chemists and Colourists, 2012a) and three droplets of the chemical (Isopropyl alcohol, 10 microliters) were placed on the specimen. The droplets on the fabric were observed after 300 s at an angle of 44°. Grading of aqueous liquids repellency was recorded if the droplets repelled, otherwise, a zero was recorded if it spread or penetrated into the fabric (illustrated in Table 3-5).

Table 3-5: AATCC Standard for aqueous liquids.

Grade number	Composition	Surface tension (dynes/cm)
0	None (fail 98% Water)	-
1	98:2 Water: Isopropyl alcohol	49.0
2	94:6 Water: Isopropyl alcohol	40.0
3	90:10 Water: Isopropyl alcohol	32.0
4	80:20 Water: Isopropyl alcohol	33.0
5	70:30 Water: Isopropyl alcohol	27.4
6	60:40 Water: Isopropyl alcohol	24.3
7	50:50 Water: Isopropyl alcohol	23.4
8	40:60 Water: Isopropyl alcohol	23.0

3.3.1.9 Chemical resistance test

American Society for Testing and Materials (ASTM) has been developed for the chemical resistance testing. The specific issue of method requirements for chemical evaluation is enlightened in ASTM F1001-99(a) for protective clothing (Forsberg 2001). The list of chemicals is followed by the standard methods and the chemical resistance was appraised using the similar method for the aqueous liquid repellency testing. Three specimens (2 mm × 2 mm) were cut and placed in a petri-dish. Three 10.0 microliter drops of the chemicals were placed on each fabric specimens. The time for chemicals to diffuse into the sample was recorded for each sample.

3.3.2 Software and its application

Table 3-6: Summary of software.

SL no.	Software name	Description
1.	COMSOL Multiphysics 5.2a	Modeling work for the geometries
2.	SOLIDWORKS software	Drawing the geometries
3.	ImageJ	To calculate the fibre diameter
4.	Origin7.0	Data analysis and representation

3.3.3 Origin7.0 software

Origin which is scientific graphing and data analysis software used in this research work. It has powerful visual representation tools with accompanying descriptive statistical parameters which helped in hypothesis testing, model development as well as data analysis.

3.3.4 SOLIDWORKS software

The SOLIDWORKS CAD software is a mechanical design automation application to produce models and detailed drawings. SOLIDWORKS models are defined by 3D design and it is based on components. The model consists of 3D geometry that defines its edges, faces, and surfaces and parts are the basic building blocks in this software. Through this software, it is easy to design models quickly and precisely.3D geometries are developed through this software and exported to COMSOL Multiphysics for modelling and simulation work.

3.3.5 Modelling work with COMSOL Multiphysics 5.2a software

Needleless electrospinning is potentially influenced by spinneret geometry (Niu, Wang & Lin 2012b). During electrospinning, when polymer solution extrudes through the spinneret, it receives surface tension, electric force, viscoelastic force, and gravitational force. When the high voltage is applied to the polymer droplet, the electric charges begin to concentrate on the outer surface of the droplet. The electrostatic repulsion counteracts the surface tension of the droplet and the droplet is stretched. At a critical point, a stream of liquid erupts from this

stretched surface forming the Taylor cone. Therefore, electric charge accumulation in the spinneret surface is the key factor for jet initiation in the electrospinning process (Niu, Wang & Lin 2012a). Direct measurement of electric field intensity is difficult as high voltage involved for electrospinning. From the literature, it is found that using the simulation software COMSOL through three-dimensional (3D) finite element methods (FEM), electric field intensity can be measured and explained very easily.

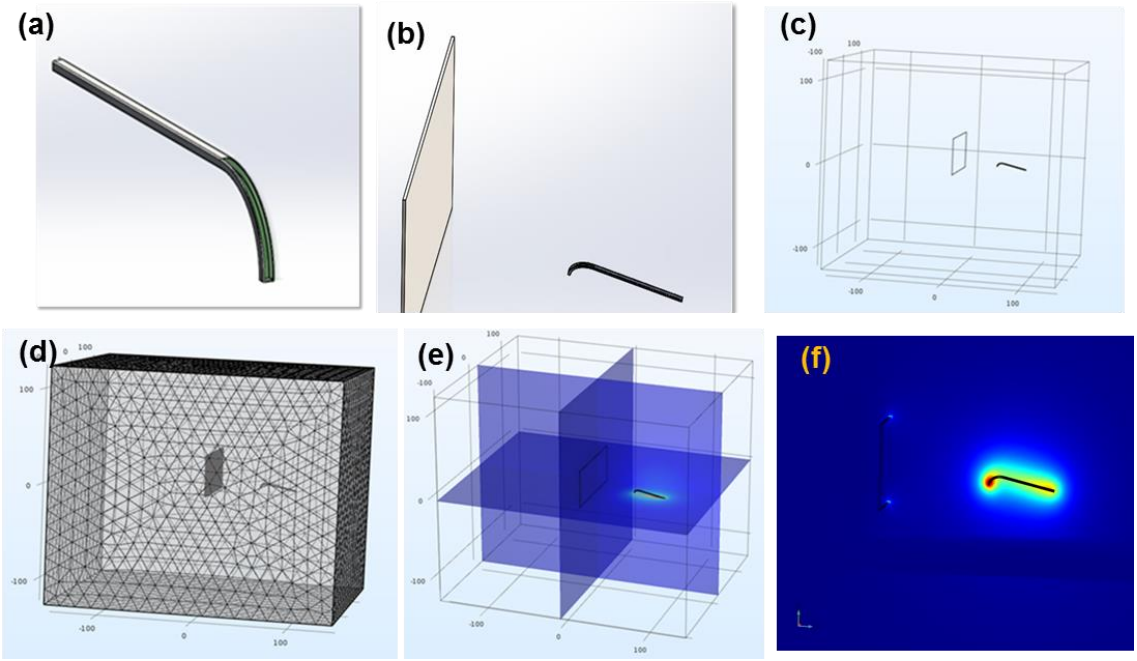

Figure 3-3: The basic steps of modelling work for convex needle, (a) convex needle drawn in SOLIDWORKS as part, (b) assembly of collector and needle in solid work, (c) imported geometry in COMSOL, (d) Mesh profile, (e)electric field analysis profile in multi-slide view, (f)side view.

FEM provides suitable methods to analyse partial differential equations (PDEs) to solve a wide variety of engineering PDEs problem. The purpose of the finite element methods is to reproduce scientifically and mathematically the behaviour of a real system framework. Besides, this model involves each component, material properties, constants, limit conditions, and different highlights that are utilized to establish the system (Wang, Wang & Lin 2012;

Zheng & Zeng 2014). As a result, it is easier to visualize and understand the electric field profile and spinneret geometry. For this study, a finite element method (FEM) program package COMSOL Multiphysics 5.2a is used.

Basic theory:

Maxwell's equations are used to solve the electromagnetic analysis under certain boundary conditions. These PDEs equations can be solved by FEM. The basic electrostatics equation is

$$-\nabla.\varepsilon_0\,\epsilon_r\,\nabla V=\rho \quad \ldots\ldots\ldots\ldots\ldots\ldots\ldots\ldots\ldots\ldots\ldots\ldots\ldots\ldots(1)$$

Where,

V =electric potential and

ρ =electric charge density.

The sub-domain settings and boundary settings are as follows.

The constitutive relationships describe the macroscopic properties of the medium. It is

$$D=\varepsilon_0\varepsilon_r E \quad \ldots\ldots\ldots\ldots\ldots\ldots\ldots\ldots\ldots\ldots\ldots\ldots\ldots\ldots\ldots(2)$$

Where,

ε_0 = permittivity of vacuum

ε_r = relative permittivity.

Boundary conditions and spinning parameter have to apply to solve the equation through FEM.

For clear understanding, the basic steps which were involved in the modelling work of convex needle are illustrated in Figure 3-3. At first, the 3D geometries had been drawn in SOLIDWORKS (Figure 3-3a-b) and imported into COMSOL interface (3-3c). In this

software AC/DC module has been chosen with electrostatic physics to perform the electric field intensity study.

Then the model parameters, materials, setting for the subdomain and boundary required to be defined. The meshing process could be performed for achieving final geometry in Figure 3-3d. When the final profile is achieved, the geometry is ready to run the simulation and analysis of the results. Finally, the electric field intensity profile was calculated as shown in Figure 3-3e as multi-slide view and side view Figure 3-3f. In this study, for each spinneret same procedure had been followed to analyse the electric field intensity profile.

CHAPTER 4

ELECTROSPINNING FROM A CONVEX NEEDLE WITH MULTIPLE JETS TOWARDS BETTER CONTROLLING AND ENHANCED PRODUCTION RATE

In this Chapter, multiple jets were successfully generated from a convex needle spinneret based on a conventional electrospinning setup. A convex channel was created in the front part of the needle to generate a limited free surface in the electrospinning process. A high flow rate was implemented with more than one polymer jet being produced, resulting in the production rate 2-3 times higher than conventional electrospinning. Finer nanofibres were produced from the convex needle when the applied voltage was 19 kV. The electric field intensity distribution of this spinneret was analysed and compared with conventional needle spinneret by Comsol Multiphysics modelling. The research work has demonstrated that scaling up the production rate of nanofibres from needle-based free surface electrospinning is possible. It will benefit further development of electrospinning with enhanced throughput and more precise controlling.

4.1 Introduction

The conventional electrospinning technique involves a single needle in producing nanofibres with negligible throughput and hassle in controlling and maintaining. Scaling up the

production rate so as to fulfil the industrial needs has been the bottleneck in commercializing electrospinning. Research efforts have been put on developing multiple needle electrospinning (Xie & Zeng 2012) and inventing needleless electrospinning (Zhang et al. 2018) towards mass production of nanofibres. Needleless electrospinning has attracted extensive attention due to its capacity in mass production. Using free surface as the spinneret, different geometric structures including cylinder (Jirsak et al. 2009), bubble (Yang et al. 2009), slit (Lukas, Sarkar & Pokorny 2008), tube (Varabhas, Chase & Reneker 2008), disc (Niu, Lin & Wang 2009) and wire (Wang et al. 2009) have been reported to generate needleless electrospinning. The technology of generating nanofibres from a series of spinnerets including roller and wire has even been commercialized by Elmarco Ltd. under the brand name Nanospider®.

Generation of multiple jets in needleless electrospinning is the result from the electrically amplified liquid waves within the free surface (Lukas, Sarkar & Pokorny 2008). Thus, concentrating electric field to a limited area with the highest electric field intensity (in kV/cm) is the incentives in this research area (Niu & Lin 2012; Niu, Lin & Wang 2009). Wire-based spinnerets have been proven to be very promising in generating highly efficient needleless electrospinning, with its potential of optimizing electric field distribution on the curved surface (Wang et al. 2012; Wang, Wang & Lin 2014). Some spinnerets have been developed with a low solvent evaporation rate and low electricity consumption. For instance, a double ring slit with the significant advantages of minimizing the solvent evaporation rate and improved solution utilization ratio was used by Wei et al. (Wei et al. 2018), but this spinneret required a higher applied voltage (50-70 kV). A metal plucked string spinneret was employed to generate multiple jet with comparatively low electric voltage (25 kV) with a narrow diameter distribution range (Chen et al. 2019a). A tube with an embedded wire loop

also was used to generate needleless electrospinning with multiple jets (Jahan, Wang & Wang 2018).

Controlling of the loading of solution to the free surface in needleless electrospinning has been the issue that affects the generation of multiple jets and the quality of the as-spun nanofibres. Ideally, a thin layer of polymer solution on the free surface with the most concentrated electric field is the best solution in generating multiple jets continuously. Too thick a layer of polymer solution usually results in a splash of solution, and coarse fibres with blocks as well as accumulation in the nanofibrous structure will be obtained. Another issue is that the solvent evaporates from either the polymer bath or those areas of the spinneret where no jets are generated. The uncontrollable evaporation of solution will result in inconsistent solution and instable spinning process with compromised fibre quality. In order to optimize the loading of polymer solution to the surface in needleless electrospinning, a convex needle was used in this work to demonstrate the possibility of controlling the loading of solution with a limited free surface. The electrospinning performance of this convex needle electrospinning was investigated and compared with needle electrospinning, and the electric field intensity profile was also analysed to understand the mechanism.

4.2 Materials and Methods

4.2.1 Materials

Polyacrylonitrile (PAN, average molecular weight 85,000) and Dimethylformamide (DMF) polymer solution was prepared by dissolving PAN into DMF with different concentrations (5%, 7%, 9% and 10%) followed by vigorous stirring using an electromagnetically driven magnet at room temperature for 24 hours.

4.2.2 Electrospinning

The convex needle electrospinning was derived from conventional needle-based electrospinning with a modification on the needle, as shown in Figure 4-1. The needle (tube diameter: 0.84 mm inside and 1.20 mm outside; length: 38 mm) was converted into a convex needle by splitting its tip to a length of 8 mm, removing one half of the split parts and curving the other half into a convex shape (1/4 circumference).

In electrospinning, a polymer solution was loaded onto the convex needle from a syringe driven by a syringe pump. A flat metal plate covered with an aluminium foil was used to collect the as-spun nanofibres.

A high-voltage power supply was connected to the convex part of the needle and the collector was earthed. For comparison, a conventional needle electrospinning was employed to spin nanofibre. An applied voltage of 15-20 kV was applied to both needles with the distance from needle to collector 13 cm under a proper flow rate.

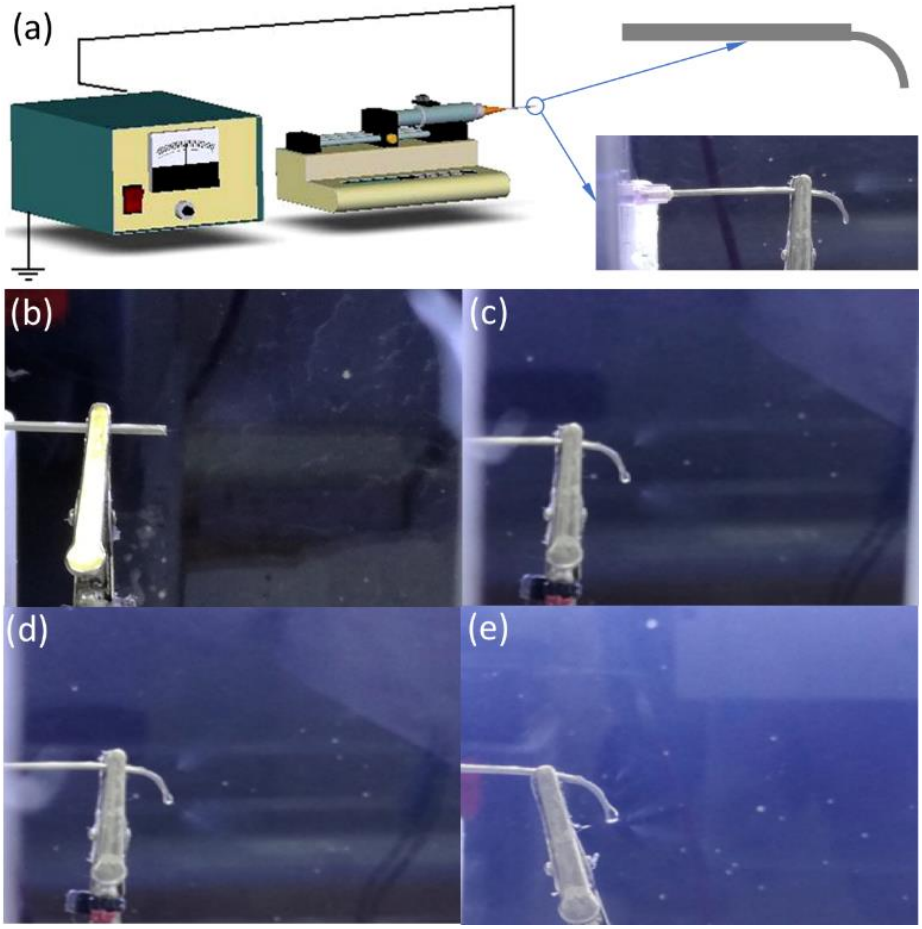

Figure 4-1: Schematics of experimental setup (a) and photos of the tip of needle in conventional electrospinning (b) and of the convex needle with multiple jets in needleless electrospinning (c-e).

4.3 Measurements and characterisation

Photos were taken using a camera to show the jets on the tip of the needle/convex needle during electrospinning. The morphology of the as-spun nanofibres was observed and fibre diameter of the nanofibres was measured from the SEM photos. Flow rate was recorded for each experiment, and production rate was measured by weighing the collected nanofibres.

4.4 Results and discussion

Precise controlling and stabilizing of the spinning process have been the issues of needleless electrospinning from free surface. Despite the facts that multiple jet with enhanced production rate are contributed, the large area of free surface in needleless electrospinning has resulted in instability of jet generation and changes in polymer solution. Especially, the polymer concentration changes greatly with time in the process of electrospinning due to the evaporation of solvent from the large free surface of polymer solution. Besides, charging a large area of free surface is not efficient and an extremely high applied voltage is required (Wang et al. 2009).

Needleless electrospinning from a wire with precise control and limited free surface would be promising. A convex at the front part of the needle in conventional needle-based electrospinning has confined the free surface to a limited area of the convex channel. As shown in Figure 4-1, polymer solution is distributed along the convex channel in the form of arc at the outer side of the quarter circumference. Due to the weight of the polymer solution, the solution flew slowly along the channel, and because of the viscose nature of the solution, dropping could be avoided if the flow rate of the syringe pump was properly selected. Selection of polymer concentration is also important to avoid dropping from the needle as an extremely low concentration (<5%) with a low viscosity will result in dropping. A proper flow rate under a specific polymer concentration to achieve the balance between the weight of solution and the viscosity of the solution will maintain the polymer solution on the convex needle without dropping. In the end, a convex surface of polymer solution was created on the curved channel of the modified needle for generation of multiple jets. The free surface of polymer solution in this design is very limited. Considering the length of the arc and the diameter of the needle are 8 mm and 0.84 mm, the surface area of the convex needle can be

calculated to be $0.5\pi 0.84\times 8=10.56$ mm^2. However, when being loaded with polymer solution, the spannable area should be $0.84\times 8=6.72$ mm^2. The surface of polymer solution in needle electrospinning can be calculated as the area of the inner circle of the needle, namely $0.25\pi 0.84^2=0.55$ mm^2. So that the free surface area of convex needle is about 12-13 times of that of conventional needle.

Figure 4-1b-e shows the photos of polymer jets during electrospinning. Only one polymer jet was observed from the tip of conventional needle (Figure 4-1b). Figure 4-1c-e shows the photos of multiple jets being generated from the curved needle during the spinning process. Obviously, many polymer jets were generated from the convex channel of the needle, and the numbers of jets were decided by the experimental parameters including applied voltage and polymer concentration. With the increase the applied voltage, more and more polymer jets were generated due to the enhanced electrostatic force to the free surface. A higher applied voltage usually means more polymer jets with a higher flow rate to accommodate the consumption of polymer solution. The polymer concentration of the solution has a direct effect on the spinning process.

Too thin and too thick polymer solution are not applicable as dropping cannot be avoided with <5% concentration and clogging always happen when the concentration is >10%. The maximum numbers of polymer jets were four as observed during experiments. The jets were usually generated from different areas and then these areas were employed as active spots for continuous jet generating. Sometimes the jets overlapped each other, and the jet might extinguish at one spot and shifted to another spot on the free surface of solution. The shifting of jets was very evident under a high applied voltage such as 19 kV. Compared with needle

electrospinning (Figure 4-1b), multiple jet was generated simultaneously from the convex (Figure 4-1c-e)

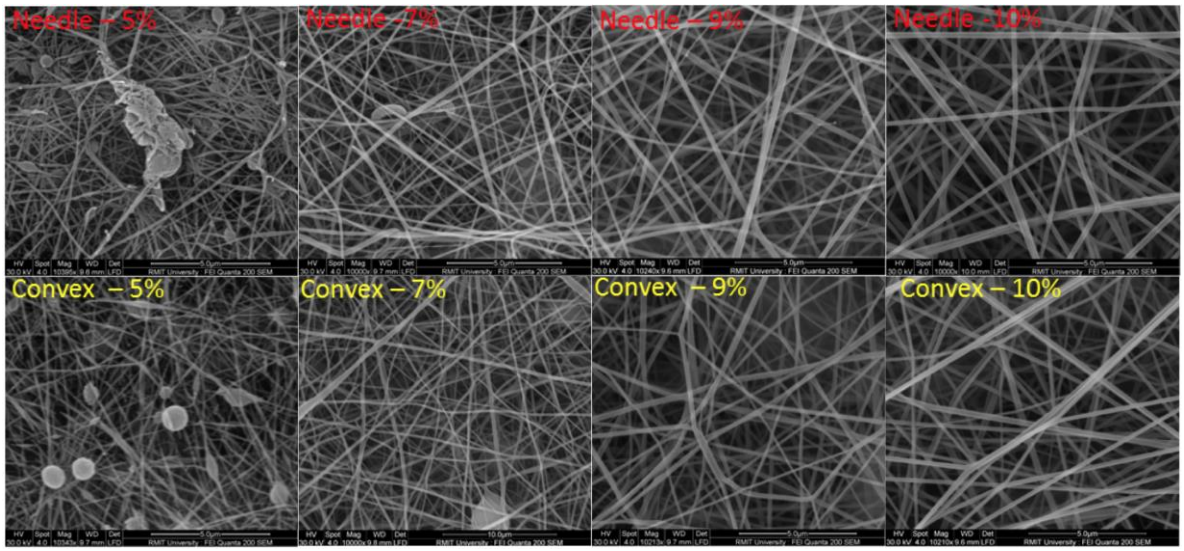

Figure 4-2: SEM photos of the as-spun nanofibres from conventional electrospinning and the modified electrospinning with the convex needle.

4.4.1 SEM photos

The as-spun nanofibres from the convex needle show porous nanofibrous structure as shown in the SEM photos in Figure 4-2. The diameter of the fibres is between 100-300 nm, and there is no evident difference between the nanofibres from needle and convex needle. Similar to the trend in conventional electrospinning of PAN, beads-on-string structure was obtained when the polymer concentration was 5% (Kalayci et al. 2005; Ma, Yang & Nie 2009). Increase of polymer concentration resulted in improved fibrous structure with fibre diameter increased slightly (He, Wan & Yu 2008).

4.4.2 Fibre diameter analysis

Figure 4-3a-b shows the calculated fibre diameter from SEM photos under different experimental parameters. Both electrospinning methods show the same trend in the change of diameter as the profiles show. The fibre diameter increases with the increase of polymer concentration, and it decreases with the increase of applied voltage. As shown in Figure 4-3b, the effect of applied voltage on fibre diameter from convex needle is more evident than that from needle, and the diameter drops quickly with the increase of applied voltage from 17 kV to 19 kV in the convex needle electrospinning.

4.4.3 Effect of applied voltage and polymer concentration

Fibre diameter from these two methods was different when specific applied voltage and polymer concentration were selected. For instance, the fibre diameter from convex needle with any polymer concentration was smaller than that from needle when the applied voltage is 19 kV (Figure 4-3c). In contrast, the fibre diameter from convex needle was larger when the applied voltage is less than 19 kV (Figure 4-3d). The larger fibre diameter and instability as shown in Figure 4-3d was probably due to the change of polymer concentration as a result of the evaporation of solvent from the larger free surface of polymer solution in convex needle. It seems that thinner fibres can be spun from convex needle when the applied voltage is high enough (such as 19 kV) (Yördem, Papila & Menceloğlu 2008).

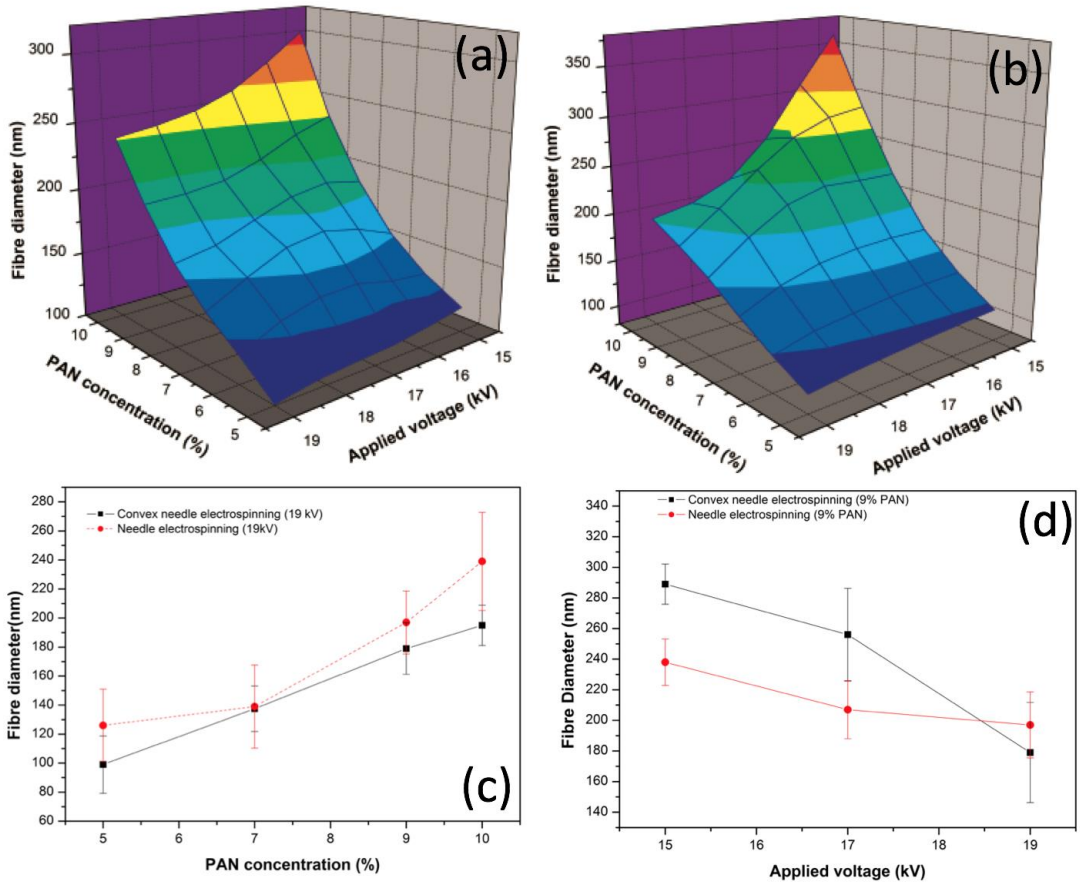

Figure 4-3: Fibre diameter analysis of conventional electrospinning (a) and convex needle electrospinning (b), and the effect of polymer concentration (c) and applied voltage (d) on the fibre diameter.

4.4.4 Comparison of flow rate and production rate

The flow rate of the syringe pump in electrospinning determines the production rate. The maximum flow rate of conventional needle electrospinning is limited to 0.5-1.5 mL/h. Too high a flow rate will result in dropping from the tip of needle and uneven nanofibres with many blocks in the fibrous structure. Figure 4-4a-b shows the maximum flow rates of syringe pump for needle and convex needle, respectively.

In general, the flow rate increases with the increase of applied voltage as the solution is exhausted more quickly under a higher electrostatic force. When the polymer concentration is

low, the flow rate must be very low to prevent dropping. With the increase of polymer concentration, the viscosity of solution increases and thus a higher flow rate can apply. However, under too high a polymer concentration, such as 10%, a slightly low flow rate must be employed as the solution does not flow quickly. Due to the generation of multiple jets, the flow rate of convex needle was 1.5-3 mL/h, which was 2-3 times higher than that of needle electrospinning.

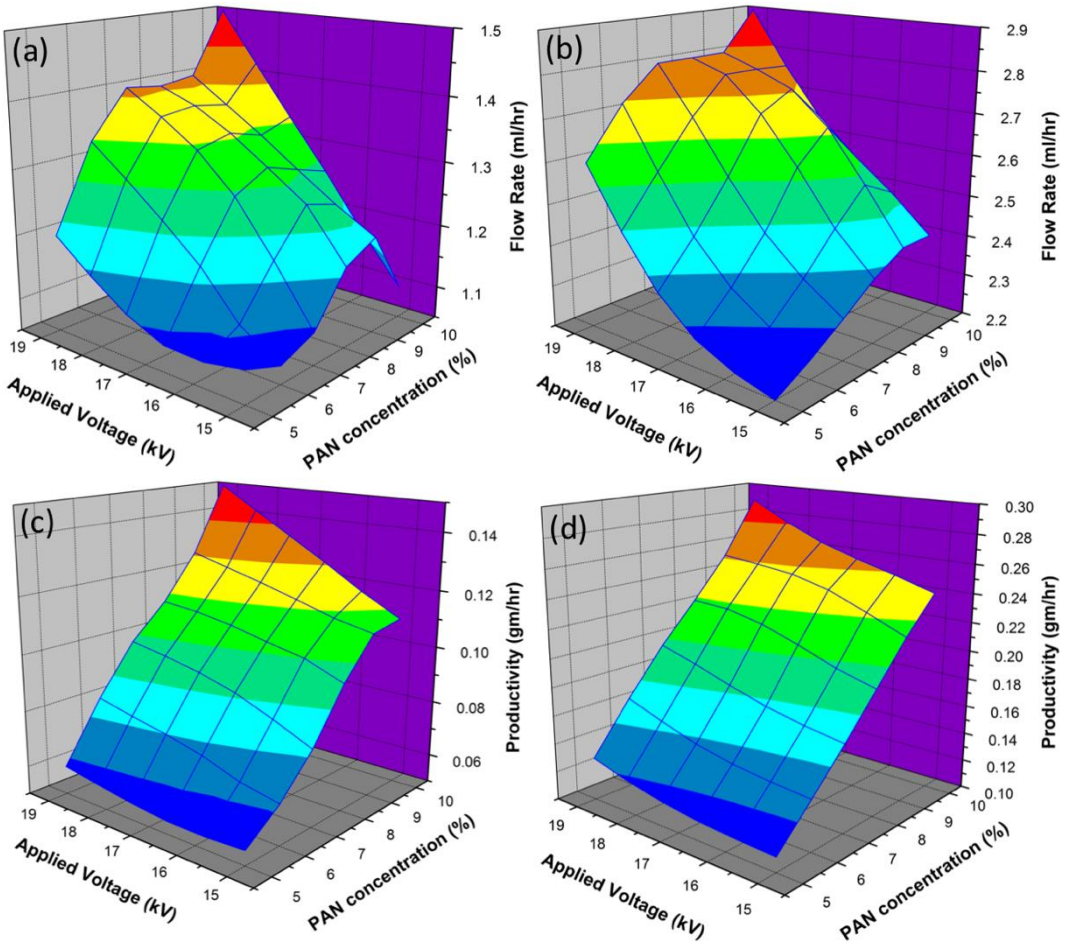

Figure 4-4: Flow rate of conventional needle electrospinning (a) and convex needle electrospinning (b), and production rate of needle electrospinning (c) and convex needle electrospinning (d).

The production rate of both electrospinning methods under different experimental parameters is shown in Figure 4-4c-d. The general trend of the production rate against applied voltage

and polymer concentration is the same, as it increases with the increase of polymer concentration or the increase of applied voltage (Deitzel et al. 2001). The production rate of convex needle electrospinning was within the range of 0.1-0.3 g/h, whereas that for needle electrospinning was 0.05-0.15 g/h. It is evident that under specific experimental parameters, the production rate of convex needle is at least two times higher than that of conventional needle. The reason is because more than two jets can be produced simultaneously for convex needle, whereas only one jet can be produced for conventional needle.

4.4.5 Electric field intensity profile

Electric field profile is the key factor in determining the electrospinning performance. The electric field intensity profiles of both the needle and convex needle were calculated from the finite element analysis with the aid of COMSOL Multiphysics 5.2a software (Niu & Lin 2012; Niu, Lin & Wang 2009; Wang Wang & Lin 2014). As shown in Figure 4-5a-b, the convex needle shows a curved path in its front arc with concentrated electric field whereas needle in Figure 4-5c-d shows concentrated electric field in its tip only. Both spinnerets show similar trend of the electric filed intensity from spinneret to the collector (Figure 4-5e). The electric field intensity of convex needle is higher as compared to the needle. Similarly, the tip of both needles exhibits the highest electric intensity and the intensity value of convex needle is a bit higher than that of needle (Figure 4-5f).

It is evident that the convex needle concentrates the electric field more efficiently than conventional needle, and the as-spun nanofibres from which are smaller. Moreover, the spannable area from convex needle is larger than that of needle, so that multiple jets can be produced with enhanced production rate. As the electric field profile of both needles is quite similar, the quality and the morphology of as-spun nanofibres from them are quite the same.

The mechanism of convex needle electrospinning can be explained as the generation of multiple jets from an enlarged spannable area with concentrated electric field on the needle.

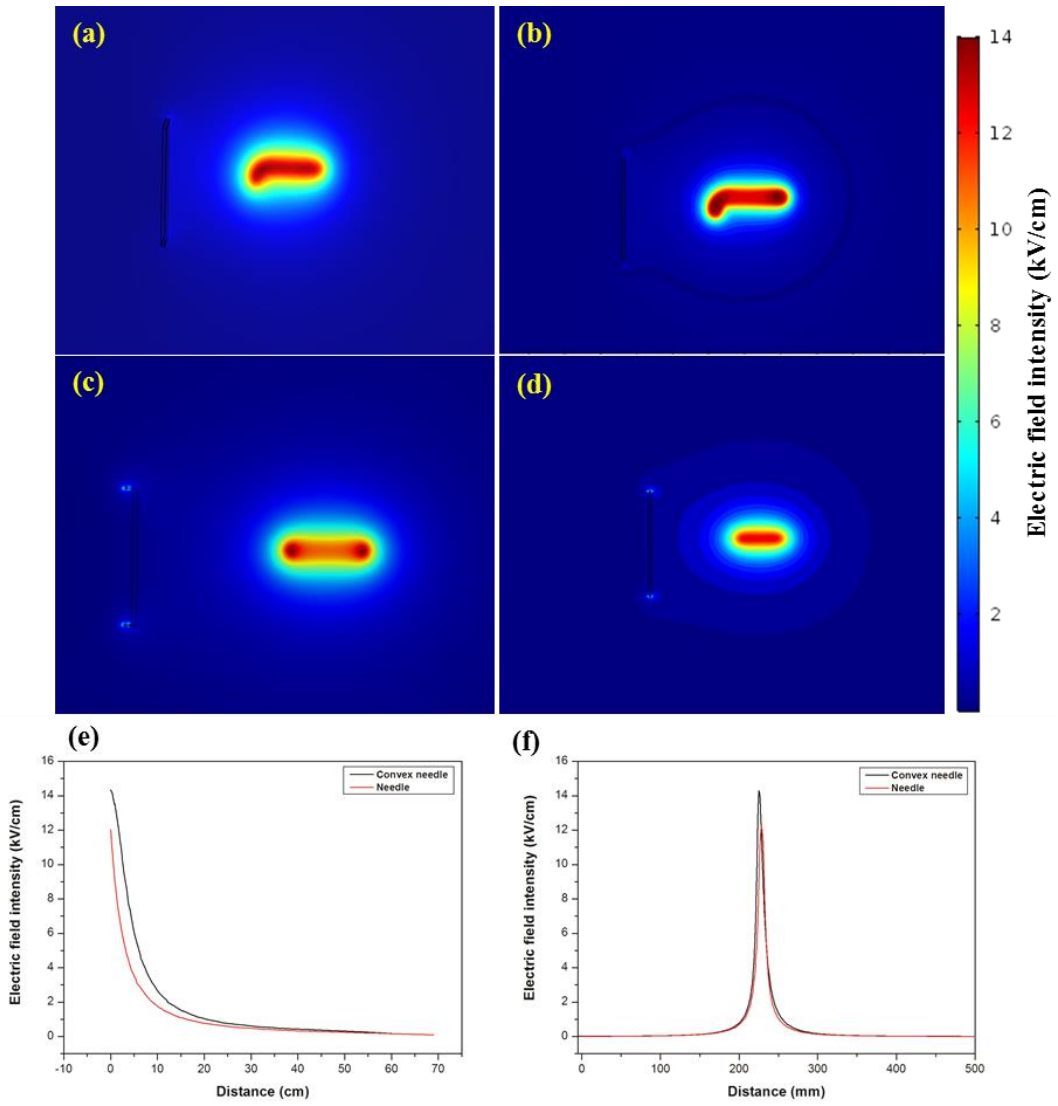

Figure 4-5: Electric field profile of convex needle (a, b) and needle electrospinning (c, d), and the distribution of electric field intensity from spinneret to collector (e) and across the tip of spinneret (f).

The curved free surface is efficient in consolidating electric field, and its relatively small free surface area contributes to the controlling the spinning process. This work demonstrated that the generation of multiple jets from modified needle was possible, and needleless electrospinning could be generated from conventional needle with a little modification. The

developed technology can scale up the production rate of nanofibres by employing a number of convex needles at the same time.The normal needleless electrospinning from a large area of free surface has difficulties in controlling the solution feeding, maintaining the concentration of solution without changing and ensuring the efficiency and safety as extremely high voltage is used. The as-developed needleless electrospinning from the convex needle has overcome all these issues, and thus it has a big potential in further commercialization of needleless electrospinning.

4.5 Summary

A convex channel in the front part of a conventional needle has shown the capacity of generating multiple jets with a limited free surface and better controlling of feeding solution. Multiple jets were observed from the created curved channel in the convex needle. The fibre diameter and production rate were greatly affected by the experimental parameters including applied voltage and polymer concentration. Thinner fibres were collected from the convex needle when the applied voltage was 19 kV. The flow rates together with the production rate of convex needle electrospinning were 2-3 times higher than that of conventional needle electrospinning. Electric field analysis revealed that the convex needle concentrated a stronger electric field on the curved area with slightly higher electric field intensity than that of conventional needle. The generation of multiple jets from the convex needle as demonstrated in this work has the potential in scaling up the production rate of nanofibre in electrospinning.

CHAPTER 5

NEEDLELESS ELECTROSPINNING FROM A TUBE WITH AN EMBEDDED WIRE LOOP

Enhancing the production rate while maintaining the controlling in electrospinning have been the challenge for years. Chapter 4 has demonstrated that multiple polymer jet can be generated from needle-based convex needle elecrospinning with enhanced controlling and solution feeding. This Chapter proposes a novel spinneret from a tube with a single wire loop embedded in its one end. With the feeding of solution precizely controlled and the spinning process stablized, multiple polymer jet can be continuously generated from the wire loop. The as-spun fibres show nanofibrous structure and its fibre diameter is greatly affected by the applied voltage and polymer concentration. As compared to needle electrospinning, the wire loop spinneret generates a stronger electric field with a larger spinnable area due to its special geometrical structure and a higher applied voltage it is connected to. Slightly coarser nanofibres are fabricated as compared to the nanofibres from needle electrospinning, and the production rate is as high as 0.48 g/h.

5.1 Introduction

Nanofibre has revealed an enormous application in diverse areas (Ahuja & Kumar 2009; Barhate & Ramakrishna 2007; Chen, Sun & Chen 2013; Huang et al. 2003; Lee & Obendorf 2007). The exclusive property of nanofibres, such as excessive surface to mass ratio, capacity to form a porous fibrous membrane, controllability in fibre diameter, surface morphology, fibrous structure and easiness of being functionalized have made electrospun nanofibre demandable from different industries. Electrospinning is the basic, versatile and cost effective method to produce nanofibres (Reneker & Chun 1996; Subbiah et al. 2005). However, several issues still need to be overcome for commercial applications, for instance, optimizing the process parameters, ensuring high fibres quality, enhancing production rate, and minimizing the process cost. Many researchers proposed many spinnerets to overcome the issues. The fibre production rate is extremely low, (usually 0.01–0.1 g/h) which hinders the application of needle electrospinning in industrial scale (Persano et al. 2013).

Many effort have been made to improve the electrospinning productivity, such as increasing the needle number which is called multineedle setup (Tian et al. 2015), using a porous hollow tube (Varabhas, Chase & Reneker 2008) and employing an extra cylindrical electrode (Yang et al. 2010). However, the needle-based large-scale setup incurs many issues like corona discharge, clogging in the needle tip, and complex in layout of needles (Theron, S et al. 2005). Needleless electrospinning has been introduced to overcome these issues (Niu & Lin 2012; Niu, Wang & Lin 2012a). Needleless electrospinning acts as an alternative method with the aim of producing high-quality nanofibres on the industrial scale. It uses free liquid surface where Taylor cones are generated randomly to produce several polymers jets.

Usually an open free surface is used in generating needleless electrospining (Niu, Wang & Lin 2012a). Solvent evapotation occures during electrospinning which leads to coarser nanofibre with decreased productivity in the case of free surface electrospinning (Thoppey et al. 2011). Another issue of needleless electrospinning is the requirement of a higher electric potential (40-70 kV) (Wang et al. 2012). Although a higher electric potential provides a much higher production rate (20-60 times) (Wang et al. 2009) than conventional electrospinning, it is an expensive procedure and a larger fibre diameter distribution is always found under increased applied voltage. Needleless electrospinning from a wire was reported to use lower electric voltages to produce nanofibres (Forward & Rutledge 2012). Thus, a free surface with a limited area would be promising to ensure little or no solvent evaporation and to concentrate electric field more efficiently, which will result in high quality nanofibres under normal applied voltage and enhanced production rate with better controlling and stability.

In this study, a Teflon tube with a wire loop embedded inside the tube were used as the spinneret to electrospin nanofibres. A small crescent free surface of polymer solution was created by feeding solution through the tube. We found that the wire loop generate multiple jet from a larger spinnable area with the applied voltage of up to 28 kV, resulted in enhanced production rate of nanofibres. The finite element analysis was used to provide a clear comparison of electric field intensity profile and electrospinning performance between wire loop spinneret and conventional needle.

5.2 Materials and Methods

5.2.1 Materials

Polyacrylonitrile (PAN) was used as the model polymer. Polymer solution was prepared by dissolving PAN into DMF using different concentrations of PAN (7, 9, 11, and 13% in w/w basis). The solution was prepared with the aid of an electromagnetically driven magnetic stirrer at room temperature for 24 hours.

5.2.2 Electrospinning

A wire loop was embedded at the tip of the Teflon tube to replace the needle in conventional electrospinning setup. The Teflon tube was 125 mm in length with its inside diameter 4.2 mm, outside diameter 6.2 mm and wall thickness 1 mm. The tube curved to an angle of 30^{o} in upward direction. A small stainless-steel wire loop (diameter 0.5 mm) was placed inside the end of the tube with other end of the wire penetrated out the tube for power connection, as shown in Figure 5-1. The wire loop, with a diameter of 4 mm, was located exactly inside the open cut of the tube and was stabilized within the tube tightly as the connecting part of the wire was immobilized by the wall of the tube (Figure 5-1).

A syringe pump was used to feed the polymer solution towards the wire loop and a small solution crescent was formed around the wire because of the viscose nature of the solution. The solution dropping was avoided by selecting a proper flow rate of the syringe pump. Experimental parameters for the wire loop electrospinning were PAN concentration 7-13wt%, applied voltage 19-28 kV and collecting distance 13 cm.

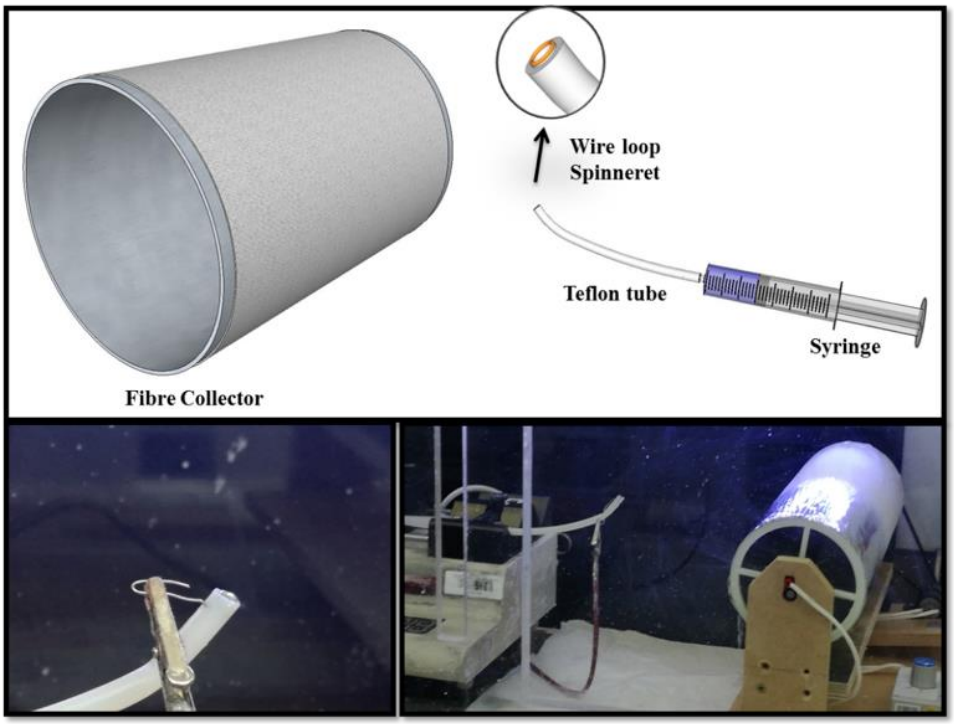

Figure 5-1: Schematics and photo of experimental setup of wire loop spinneret.

5.2.3 Measurements and characterisation

Photos of the spinneret were taken by a camera (Canon ESD 60).

The average fibre diameter was measured from the SEM images using image analysis software (ImageJ). The measurement was conducted from at least five SEM images from different areas of a sample and more than 100 fibres were employed. The flow rate was recorded as the maximum flow rate of the syringe pump without any solution dropping from the spinneret. The production rate was measured by weighing the collected nanofibres.

The electric field was calculated using finite element method-based software. The geometry was analysed and compared according to their practical dimensions, locations and relative permittivity. The wire loop was set under a given potential and the collector was set as earthed. Except the wire loop, all the side and boundaries were set as zero potential. After

meshing and computing, the electric field profile was solved by the software and the electric field intensity could be extracted for further calculation.

5.3 Results and Discussion

A loop spinneret made from a metal wire was used as the fibre generator, and a Teflon tube, in which the wire loop was embedded, was used to feed polymer solution from the reservoir (the syringe), as illustrated in Figure 5-1. When the solution reached to the end of the tube where the wire loop was embedded, a crescent surface of solution was formed due to the viscoelastic nature of the polymer solution (Figure 5-1). The polymer solution was then electrified when the wire was connected to an applied voltage.

With the increase of the applied voltage, uneven surface with some protrusions could be observed from the crescent, and a polymer jet was about to initiate when the applied voltage was increased to 12 kV. When the applied voltage was below 19 kV, one or two polymer jets were generated from the crescent. Multiple jets were generated when the applied voltage exceeded the threshold of 19 kV (Figure5-2).

In conventional electrospinning setup, a voltage up to 22 kV can be applied for electrospinning, and a further increase in the voltage usually leads to “corona discharge” between the tip of the needle and the collector. Using the Teflon tube as the feeding channel and the wire loop as the fibre generator, the applied voltage can be maximized to 28 kV without incurring “corona discharge.” The Teflon tube with the wire loop concentrate electric field to an area around the loop rather than the tip of needle in conventional electrospinning.

The large area of the concentrated electric field consumes a higher applied voltage and the distribution of the electric field helps prevent the wire loop from discharging.

Polymer jets were drawn out from either the surface of the wire or the gap between the loop and the wall of the tube. Figures 5-2a-b shows views from different angles of the loop spinneret in the middle of electrospinning process. The number of polymer jets increased with the increase of the applied voltage, and at least five jets were generated when the applied voltage was 28 kV (Figure 5-2c). The jets were usually generated from different areas of circular surface of the crescent.

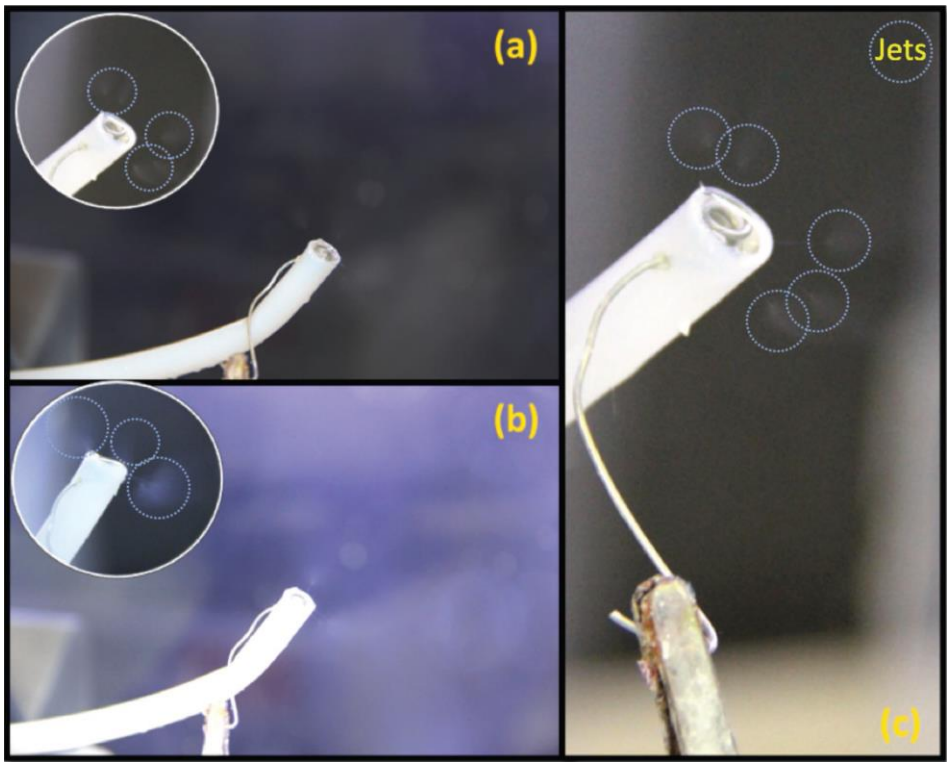

Figure 5-2: Photos of spinneret in the middle of electrospinning process (a-b) and the magnified view of multiple jet(c).

These areas were then working as active spots for continuous generation of jets. At least four or five jets were stable, and the jets were like splashing as well as overlapping each other.

Sometimes the jet extinguished at one spot and shifted to another spot on the free surface. The number of polymer jets together with the stability of the electrospinning process was decided by the experimental parameters including applied voltage and polymer concentration. The diameter of the Teflon tube has been found to be an important factor to determine the generation of multiple jets. When the diameter of the tube was too low, such as less than 1 mm, the diameter of the loop was very small and only one or two jets were generated. On the other hand, when the diameter was larger than 10 mm, a big open surface was generated, and a much higher applied voltage must be employed to electrify the solution with an unstable spinning process observed. The as-collected electrospun PAN nanofibres formed a nonwoven membrane with the colour of white on the aluminium foil (Figure 5-3a), similar to that from conventional electrospinning.

5.3.1 Morphology analysis

The morphology of the electrospun PAN shows a clearly nanofibrous structure, as shown in the SEM photos under different magnifications (Figure 5-3b–d). Nanofibres with clean surface can be observed, and all the fibres are quite even with a fibre diameter of less than 1μm. The applied voltage has a direct impact on the morphology of the as-spun nanofibre, as shown in the SEM photos in Figure 5-3e–h. Beads-on-string structure can be observed from Figure 5-3e with the applied voltage of 19 kV.

5.3.2 Effect of polymer concentration and applied voltage

With the increase of the applied voltage, the electrostatic force applied to polymer jets was higher so that the beads were further drawn into strings. As seen from Figure 5-3f–h, no beads can be observed under an applied voltage of higher than 22 kV. The surface morphology of the as-spun nanofibre is also determined by the polymer concentration (Figure

5-3i-l). When the PAN concentration was 7%, most fibres were extremely small (around 180 ± 27 nm). With the concentration increased to 13%, the as-spun fibres were bigger and the diameter was near 380 nm. There were many coarse fibres produced under the concentration of 13%, resulting in a wider diameter distribution with a bigger standard debiation of the mean diameter. It is evident the fibre diamter increases with the increase of polymer concentration because of the increase of the viscosity of the solution.

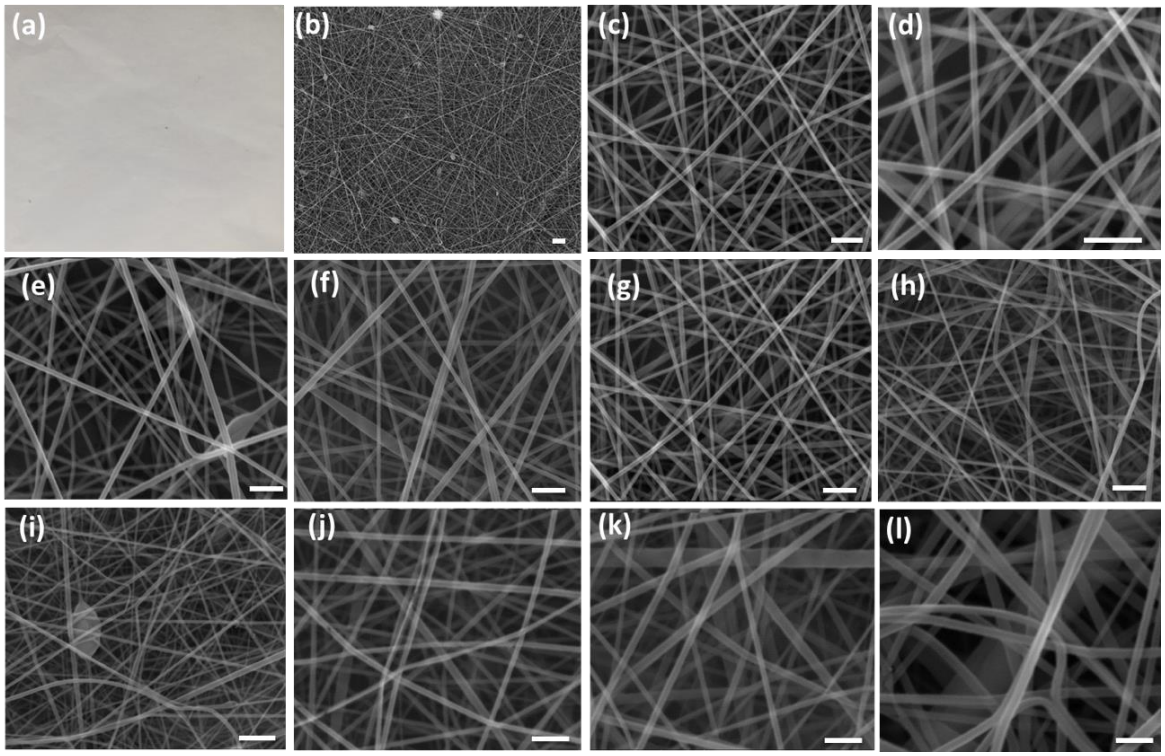

Figure 5-3: Photo of nanofibres collected on an aluminium foil (a) and SEM photos (b-d) of the as-spun nanofibres under the magnification of 1k (Bar = 100 µm), 10k (Bar = 5 µm) and 20k (Bar = 2 µm), respectively. SEM photos of nanofibres with applied voltage of 19 kV (e), 22 kV (f), 25 kV (g), and 28 kV (h) (Bar = 5 µm, PAN concentration = 11%), and with polymer concentration of 7% (i), 9% (j), 11% (k), 13% (l) (Bar = 2 µm, applied voltage = 28 kV).

Figure 5-4 shows the evolvement of fibre diameter under different experimental parameters including polymer concentration and applied voltage. With the battling between the electrostatic force and the viscosity of the solution, the fibre diameter of the as-spun

nanofibre increases evidently with the increase of the polymer concentration and with the decrease of applied voltage.

For conventional needle electrospinning, the flow rate was confined to 0.5-1.5 mL/h (Gomes et al. 2007) depending on polymer concentration and other experimental parameters. The diameter of the needle is as small as 1.0 mm, so that the flow rate is limited. Besides, only one polymer jet is generated from the tip of the needle, resulting in an extremely low associated flow rate to fit the consumption of solution. With the increase of the flow rate, polymer solution dropped from the needle tip and more beads like fibre structure formed and collected on the collector (Gomes et al. 2007).

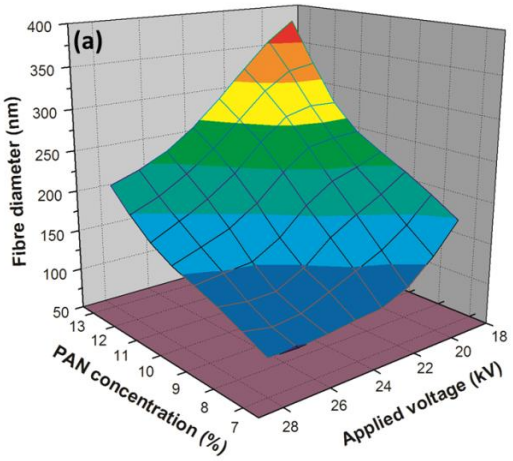

Figure 5-4: Effect of polymer concentration and applied voltage on the fibre diameter.

5.3.3 Effect of flow rate and production rate

The Teflon tube in this work, with a much bigger diameter of 4.2 mm, provides a bigger pathway for polymer solution to be fed to the spinneret. Besides, the consumption of polymer solution is higher due to the generation of multiple jets. As a result, a higher flow rate of 3-4.5 mL/h. can be utilized in this wire loop electrospinning. Depending on the specific polymer concentration and applied voltage, the maximum flow rates the spinneret can

consume change quite a lot as shown in Figure 5-5a. A lower flow rate was found when the polymer concentration was lower than 9% as too high a flow rate would result in dropping. With the increase of the polymer concentration to higher than 13%, generation of multiple jet became harder so that the flow rate was lower to accommodate the solution consumption. In the end, the flow rate shows an arc profile in Figure 5-5a with its peak at the concentration of 11%.

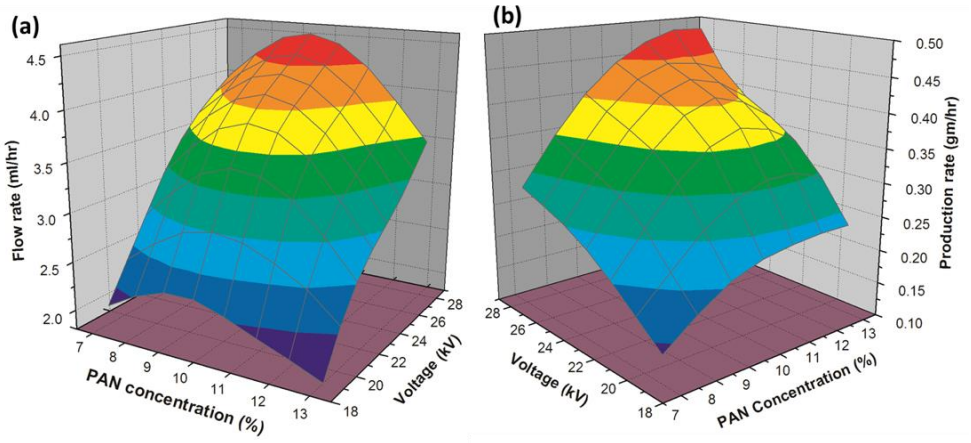

Figure 5-5: Flow rate and production rate of wire loop electrospinning under different polymer concentrations and applied voltage.

The real production rate is shown in Figure 5-5b. It is clear that under a given applied voltage, lower productivity was obtained when using relatively high polymer concentration (He, Wan & Yu 2008). And under a given polymer concentration, A high production rate was always obtained when using relatively higher applied voltage. When the applied voltage was below 19 kV, flow rate was low and it decreased with the increased of polymer concentration. The electric field intensity under a low applied voltage was low, so that the electrostatic force was not strong enough to draw many jets from the spinneret. With the increase of applied voltage, the differences in the ability to draw jets from the spinneret made the production rate change evidently under different PAN concentrations (Yu et al. 2010). It

was quite apparent in experimental work that many more jets were observed at a higher voltage of 28 kV, indicating that applied voltage had a direct effect on the production rate as shown in Figure 5-5b. In addition, when the solution concentration was too low (7%), discontinuous jets were found and jets overlapping was more prominent due to the low viscosity of the polymer solution. As a result, discontinuous process was obtained with thinner nanofibres and a low production rate. In the case of a higher concentration (13%), the viscosity of the solution was too high to facilitate jets generating, resulting in lower flow rates and production rates. To sum up, the production rate of wire loop electrospinning is 0.14-0.48 g/h under different applied voltage and different polymer concentrations.

There is a clear correlation between the production rate and fibre diameter under different experimental parameters, as shown in Figure 5-6. For a specific PAN concentration (11%), the production rate increased evidently with the increase of the applied voltage, and this was due to the enhanced electrostatic force that drew more jets from the crescent surface of solution. The average fibre diameter decreased at the same time, but the fibre diameter was not statistically different as per the standard deviation. With the increase of applied voltage, thinner fibres were fabricated due to the enhanced electrostatic force, resulting in a smaller mean diameter. With the applied voltage of 28 kV (Figure 5-6b), the average diameter increased from 110 ± 34 to 126 ± 79 nm with the increase in polymer concentration from 7 to 9%. The fibre diameter further increased with the increase of polymer concentration, with the mean diameter lower than 250 nm even at the concentration of 13% (Figure 5-6c).

Viscosity of polymer solution increased with the increase of PAN concentration, leading to less stretched jets and coarser as-spun nanofibres. The production rate increased gradually

with the increase of polymer concentration, but too high a polymer concentration (13%) led a low production rate due to the extremely high viscosity of the solution.

5.3.4 Comparison of production rate and fibre diameter with needle electrospinning

The wire loop electrospinning produced slightly coarse nanofibres with a higher production rate as compared to conventional needle electrospinning. For needle electrospinning, the fibre diameter was below 250 nm. The nanofibres under the concentration of 7–11% from both electrospinning methods were not significantly different with similar deviations, but the mean diameter from wire loop spinneret was a bit higher.

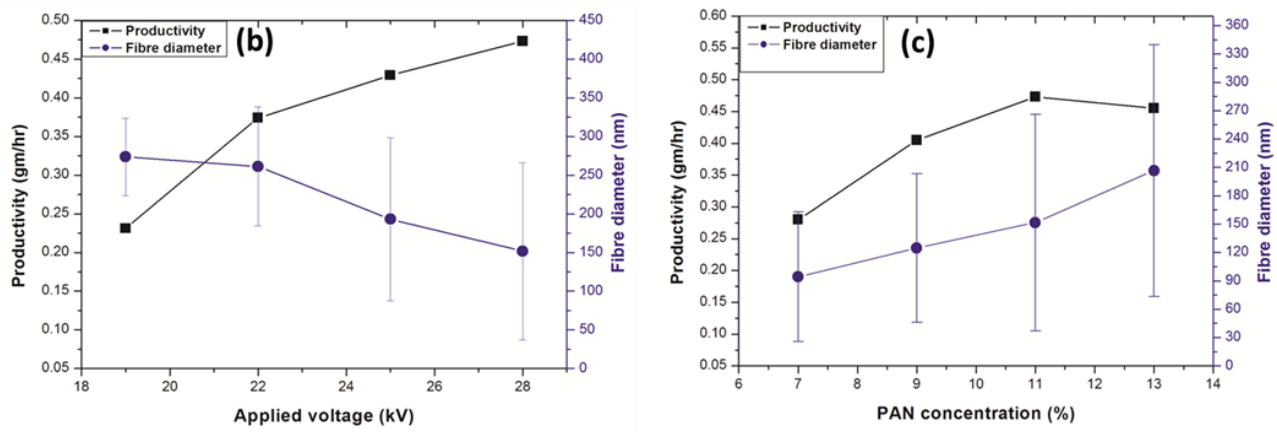

Figure 5-6: Production rate and fibre diameter with different applied voltage (b) and polymer concentration (c).

In wire loop electrospinning, the fibre diameter increased from 270.4 ± 44 to 364.8 ± 156 nm when the PAN concentration increased from 11% to 13%, as depicted in Figure 5-7a. Apparently, more coarse fibres were produced in wire loop electrospinning when the polymer concentration was 13%.

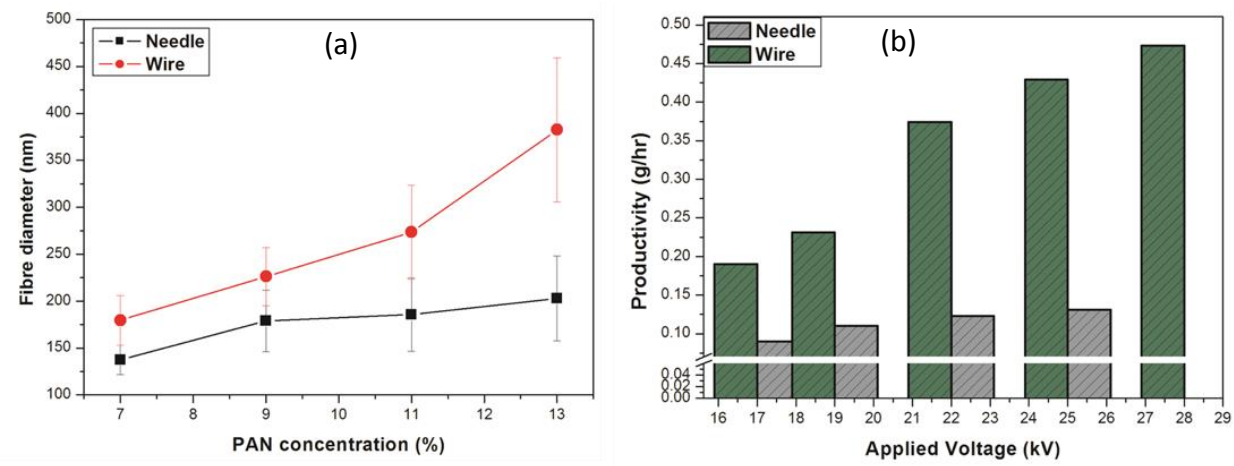

Figure 5-7: Comparison of the fibre diameter (a) and production rate (b) between needle electrospinning and wire loop electrospinning.

The production rate of needle electrospinning increased from 0.09 to 0.135 g/h when the applied voltage increased from 17 to 25 kV, whereas the production rate of wire loop electrospinning was 0.19–0.48 g/h with the applied voltage of 19–28 kV (Figure 5-7b).

In needle electrospinning, a higher applied voltage (28 kV) cannot be used as frequent corona discharge will occur. However, in wire loop electrospinning system, 28 kV can be used without discharging problem due to the electric insulation of Teflon tube. As a result, a strong electrical field was formed in the wire loop which facilitated multiple jets formation with enhanced production rate. It can be found from Figure 5-7b that the production rate of wire loop electrospinning is around four to five times higher than of needle electrospinning.

5.3.5 The analysis of electric field intensity profiles

The electric field intensity profiles of needle and wire loop were analysed and compared using the finite element analysis COMSOL Multiphysics software 5.2a. Similar to the trend of wire electrospinning, the wire loop spinneret shows a higher concentrated field on the half portion of the surface facing the collector (Figure 5-8). This is because the attractions of

positive charge in the spinneret tip from the earthed collector (Wang et al. 2009; Wang et al. 2012). Detailed views of the wire loop in Figure 5-8b-c show a large area of concentrated electric field. On the contrary, the needle nozzle shows concentrated electric field at its tip (Figure 5-8d–f). The wire loop shows higher electric field intensity than needle in both directions from the fibre generator to the collector and across the spinneret direction (Figure 5-9), and this is due to the slightly higher applied voltage and its special geometry. Therefore, a strong electric filed on the surface of a wire loop initiated the formation of multiple polymer jets. Both wire loop and needle indicated similar electric filed profiles, resulting in a similar fibre morphology and electrospinning performance. A circular free surface was created on the end of the Teflon tube to provide a large area of concentrated electric field to initiate multiple jets with enhanced production rate.

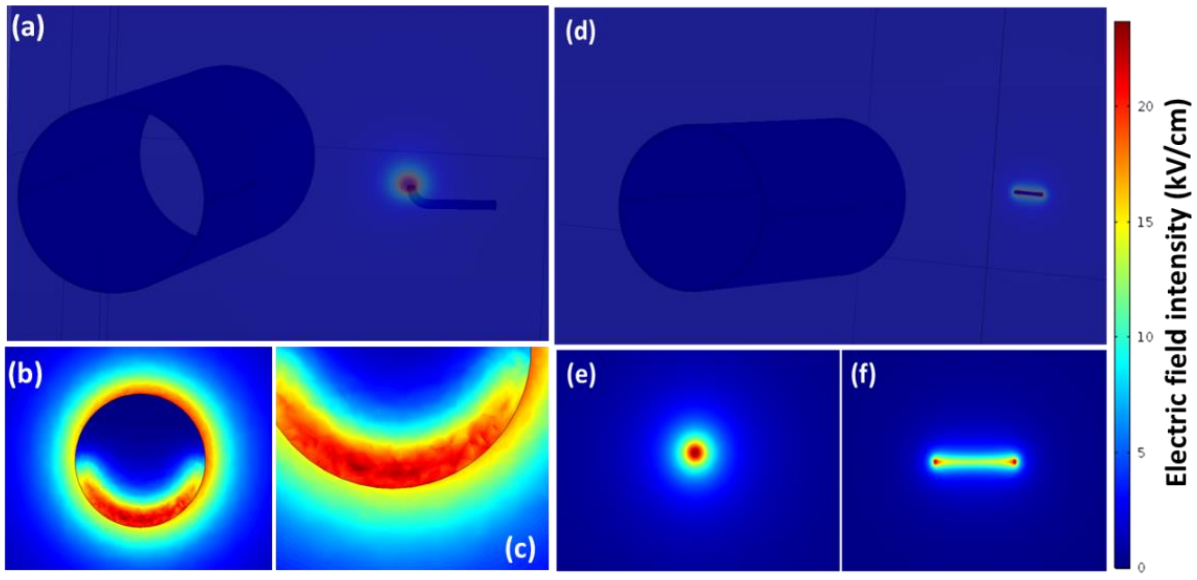

Figure 5-8: Electric field intensity profiles of wire electrospinning setup (a) with detailed views of the wire loop (b-c), and of needle electrospinning setup (d) with detailed views of the needle (e-f).

The wire embedded tube spinneret has a better controlling of the electrospinning process as the solution feeding system is more dedicated as compared to the open surface ones (Niu, Lin

& Wang 2009; Wang et al. 2009; Wang et al. 2012; Wang, Wang & Lin 2014). The flow rate can be adjusted to fit the exhausting of the solution, ensuring a crescent solution surface on the top of the loop. Dropping of solution can be avoided due to the upward direction of the tube. Besides, a stable spinning process can be expected as the polymer solution is not affected by the slight evaporation from the limited open surface of the tube.

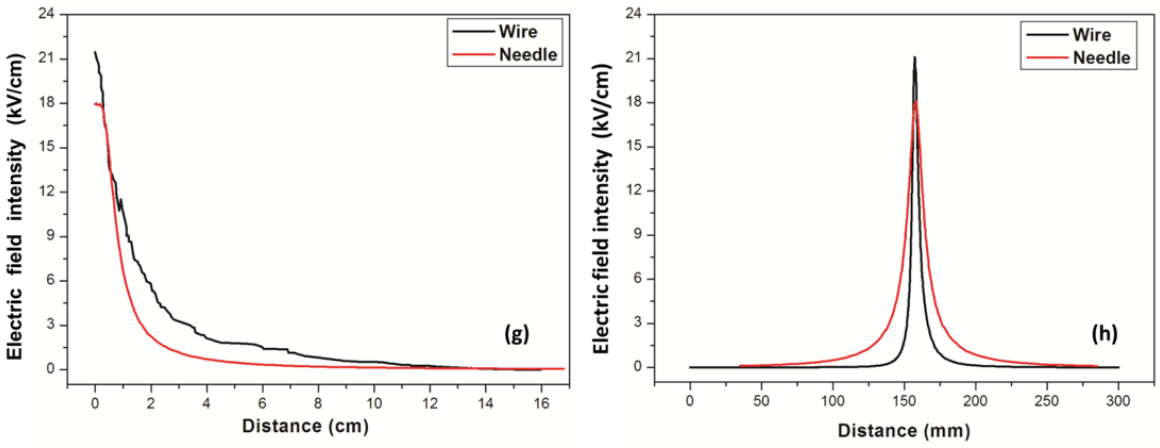

Figure 5-9: Electric field intensity distribution from fibre generator to the collector (g) and across the spinneret direction (h).

Needleless electrospinning from different open surfaces has suffered from unstable processes and uneven as-spun nanofibres due to the unavoidable evaporation of solvent from the big area of open surface. Using the tube with a wire loop embedded has limited the evaporation to a much lower level, so that the spinning process is stable and the as-spun nanofibres are quite even as seen from the SEM photos.

5.4 Summary

By embedding a wire loop into one end of a Teflon tube as the spinneret, multiple polymer jets of PAN were generated from the crescent solution surface of the spinneret. The as-spun nanofibres showed a typical nonwoven structure with fibre diameter less than 1 μm, and the

morphology of nanofibres indicated a nanofibrous structure with a clean fibre surface. The fibre diameter of as-spun nanofibre was greatly affected by the applied voltage and polymer concentration. Due to the enlarged spannable area of the wire loop spinneret, the production rate was enhanced to 0.19–0.48 g/h depending on the experimental parameters such as the applied voltage and polymer concentration. The wire loop electrospinning produced slightly coarser fibres with an enhanced production rate as compared with needle electrospinning. Electric field analysis revealed that a large area of strong electric field was formed around the wire loop with higher electric field intensity than that of a needle. This novel spinneret with enlarged spannable area can concentrate a relatively high electric field, resulting in multiple polymer jets generation and enhanced production rate. It will further benefit the development of a large-scale production of nanofibres from needleless electrospinning with better controlling and stability.

CHAPTER 6

CREATING AN INTERCONNECTED PVA NANOFIBROUS MEMBRANE ON COTTON FABRICS BY DIP COATING OF PDMS-TMS FOR VERSATILE PROTECTION WITHOUT COMPROMISING COMFORT

Performance textiles with versatile protective surface and well-preserved comfort are highly demanded but hard to achieve due to the challenge in developing functionalized surface without affecting the porous structure of textiles. Needleless electrospinning from linear spinnerets can be applied to perform nanofibrous coating on textiles. In this Chapter, nanocomposites of surface functionalized nanofibrous membrane on cotton fabrics will be developed by electrospinning PVA nanofibrous membrane on cotton fabrics using a linear spinneret followed by a PDMS-TMS (polydimethylsiloxane-trimethylated silica) dip coating. The as-fabricated nanofibrous membrane enhanced cotton fabric was characterized by SEM and FTIR spectroscopy, and its protection against water, aqueous liquids and chemicals were implemented to test the versatile protection. Besides, the air permeability and moisture management properties of the coated fabrics were tested to justify the comfort of the coated fabrics. It was found that the combination of PVA nanofibrous membrane with PDMS-TMS coating demonstrated protection against water, liquids, and chemicals without compromising comfort. The nanocomposites with the surface functionalized nanofibrous surface as the

protective layer on textiles have a big potential in developing highly versatile protective textiles with well-preserved comfort.

6.1 Introduction

Protective clothing (PC) is mandatory in specific occupations to protect personnel against external hazards such as chemical, thermal, mechanical, biological and radiation (Zhou, Reddy & Yang 2005). Chemical substances can damage the human body through its hazards affecting the respiratory system, skin, eyes, face, hands, feet, head, body and digestive system, and thus chemical protection is crucial for personnel who work in environments where they are direct exposure to chemicals and contaminants. Coating is widely used in transforming fabrics to fulfil their decorative and functional roles for diverse applications (Hertleer, Rogier & Van Langenhove 2007; Sen 2007). Applied as a thin layer on the surface of fabrics, coating brings functionality and provides versatile protection capacity to textiles. In the past years, several protective clothing has been introduced, such as flame-retardant clothing (Chen et al. 2018), self-cleaning (Wang et al. 2011; Zeng et al. 2015), cold protection (Emelyanenko et al. 2017), chemical protection (Zeng et al. 2015), oil repellency (Wang et al. 2011) and moisture management (Shin, Yoo & Son 2005) clothing.

Protective clothing has been successfully developed to serve solo functional performance. However, the outdoor wearer may face extreme threats and complexity from the environment, in which cases multiple protections is necessary for PC. Recent research and development have focused on performance textiles with versatile protections (Lu et al. 2017). Except for the excellent protection performance, PC should be light weight, air and moisture permeable to ensure comfort and wellbeing of the wearer. However, coating usually adds an

extra layer to textiles, and the breathability and thermal and moisture behaviour of this layer have greatly affected the comfort of the PC. By designing the structure of the coated layer, PC with breathability is possible. For instance, polytetrafluoroethylene (PTFE) has been used to develop protective textiles under the brand Gore-Tex® (Borisova & Reihmane 2013), bringing the properties of waterproof, breathability and windproof to serve different areas.

Maximum protection and maintaining comfort are two contradictory terms to bring together, which is the main challenge in developing PC. A balance between protection and comfort is the key to develop performance textiles. Nanofibres are extremely fine fibrous materials with the potential in protection and function. Gibson et al. (Schreuder-Gibson et al. 2003) have investigated that electrospun mat can provide protection against aerosol penetration without a significant change in moisture and air transport property. Furthermore, electrospun mat for PC has been applied as chemical warfare agent (Ramaseshan et al. 2006), PC for agriculture worker (Lee & Kay Obendorf 2006), liquid penetration barrier (Lee & Obendorf 2007), aerosol protection etc. Considering the light weight, nanoporous structure and extremely high surface area, nanofibrous membrane could be the best coating layer to bring versatile protection without compromising the comfort of textiles.

In this Chapter, cotton fabrics as a non-protective textile were used as the sample textiles and PVA nanofibrous membrane was used as the sample nanofibre, demonstrating the surface functionalization of nanofibrous membrane as the protective but breathable layer for developing cotton-based PC. Polydimethylsiloxane-Trimethylated silica (PDMS-TMS) dip coating was employed to change the hydrophilic surface of PVA nanofibres into versatile protective surface. The PDMS-TMS coating brings the repellent mechanism to withstand water, liquids, chemicals on the fabric surface (Moiz et al. 2016), while nanofibrous mat

sustains the comfort and breathability of textiles. Surface functionalized nanofibrous membrane brings together the protection and comfort as one single layer, benefiting the development of next generation PC.

6.2 Materials and methods

6.2.1 Materials

Cotton fabrics (twill 3/1) were sourced from Burke Textile Ltd. Australia. Polyvinyl alcohol (PVA, Mw=100,000; 96% hydrolysed) was purchased from Sigma-Aldrich. Polymer solution was prepared by dissolving PVA in deionized water at the concentration of 9%. The PVA powder was mixed with deionized water at 60 °C with continuous stirring with a magnetic stirrer for 96 hours to make a homogeneous solution. Xiameter FBL-0563 (A mixture of 35% polydimethylsiloxane (PDMS) and 35% Trimethylated silica (TMS)) was sourced from Dow Corning Pty Ltd., Pennant Hills, Australia. Heptane (HPLC grade) was bought from RCL LAB SCAN Limited, Australia, and Isopropyl alcohol (Ana-R) was obtained from BDH Limited, Dorset, UK. Heptane was used as the solvent to produce 3%, 5%, 7% and 9% solution of Xiameter FBL-0563.

6.2.2 Methodology

The nanofibrous coating was done by electrospinning PVA nanofibres on cotton fabrics followed by a dip coating process (Figure 6-1). A purpose-built needleless electrospinning was used to deposit nanofibres with a full coverage on the collector. The setup contains a spiral wire loop mounted in a Teflon tube as the spinneret (Inset of Figure 6-1).

The dimension of the Teflon tube is 125 mm in length, inside diameter 4.2 mm and outside diameter 6.2 mm, and wall thickness 1 mm. The front part of the tube was curved into an angle of 30^{o} in downward direction. Three spiral turns were created using a stainless-steel wire (radius 0.25 mm) according to the inner diameter of the tube. One end of spiral wire loop was placed inside the tube while the other end projecting at downward direction. Cotton fabrics were mounted on the surface of the circular rotating collector.

A high voltage power supply was used to provide 20 kV applied voltage to the wire loop spinneret. Electrospinning was run with a flow rate of 2.5 mL/h at a collecting distance of 13 cm.

After electrospinning, the cotton fabrics with nanofibres coated were dried in a dryer at 40^{o}C for 1 h. Then, the fabrics were dip coated in Xiameter FBL-0563 with different concentrations of 3%, 5%, 7%, and 9%, for 30 mins. The fabrics were then dried in the dryer at 40 ^{o}C for 2 h at 40 ^{o}C.

6.2.3 Measurements and characterisation

The morphology of cotton fabrics was observed by a scanning electron microscope (FEI Quanta™-200 ESEM, UK) after being sputter-coated (IMBROSE, Spi A20014, Australia). The observation was done at different magnifications in low vacuum mode at the voltage of 15 kV. ATR-FTIR spectrum was reported for each of the samples using a spectrophotometer (Perkin Elmer 300, USA).

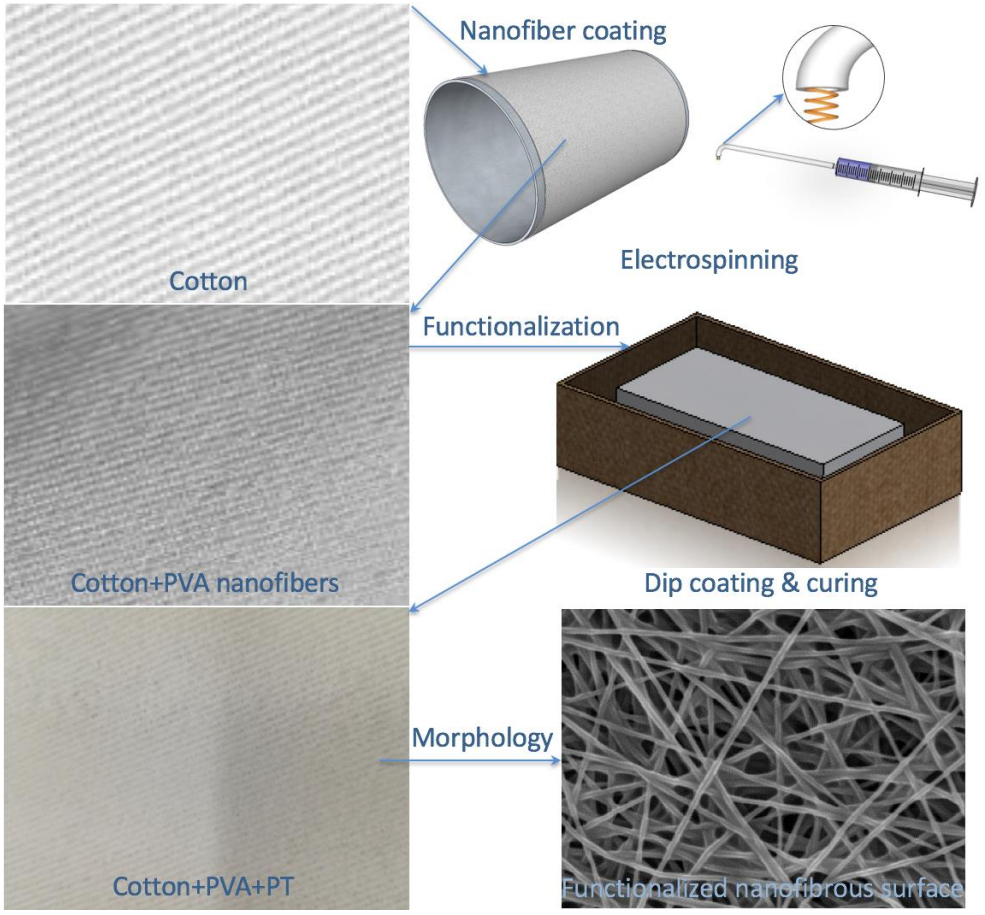

Figure 6-1: Schematics of the nanocoating process.

Aqueous liquid repellency test was performed in accordance with the AATCC 193: 2012 standard and the droplets on the fabric were observed after 300 seconds at an angle of 44°. The water contact angle was calculated using a contact angle system (Data physics, CA20, Germany) at room temperature by Sessile Drop Method. The water repellency test (Toyoseiki, Tokyo, Japan) was accomplished in accordance with AATCC 22: 2014 to measure the water resistance (American Association of Textile Chemists and Colorists, 2014). Chemical resistance was measured according to ASTM F1001-99 (a). The list of chemicals was followed by the standard methods and eleven types of chemicals were used to do the test. The time for a chemical to diffuse into the sample was recorded in seconds.

Air permeability was measured on an air permeability tester (SDL Atlas Pty Ltd, England) according to AS-2001.2.34:1990 (Method 2.34: Physical tests- Determination of permeability of fabric to air). The moisture management property of fabrics was measured on the SDL Atlas moisture management tester (MMT), in accordance with the standard AATCC-TM-195 (American Association of Textile Chemists and Colorists, 2017).

6.3 Results and discussion

6.3.1 Characterization

Deposition of PVA nanofibres on cotton fabrics has resulted in a thin layer of nanofibrous membrane on the surface, as shown the optical photo in Figure 6-1. The membrane is very thin so that the surface characteristics of fabrics with yarns and texture can be seen after deposition of nanofibres. With the porous structure of the nanofibrous membrane and the functions brought by the dip coating, a functional nanofibrous coating was generated on the surface of cotton fabrics.

Uncoated cotton fabrics show a clear cellulose fibrous structure with convolutions along the longitudinal direction (Figure 6-2a). After the 9%PT dip coating, the surface of fabrics becomes smoother as there is a thin layer of PT on fibre surface (Figure 6-2b). The electrospinning with spiral wire loop spinneret is efficient to produce high quality and uniform nanofibre mat as multiple jets can be produced simultaneously. The morphology of electrospun PVA nanofibres on cotton fabrics is shown in Figure 6-2c. A uniform and porous nanofibrous surface has been formed on the surface of cotton fabrics with nanofibres covering cotton fibres.

6.3.1.1 SEM images

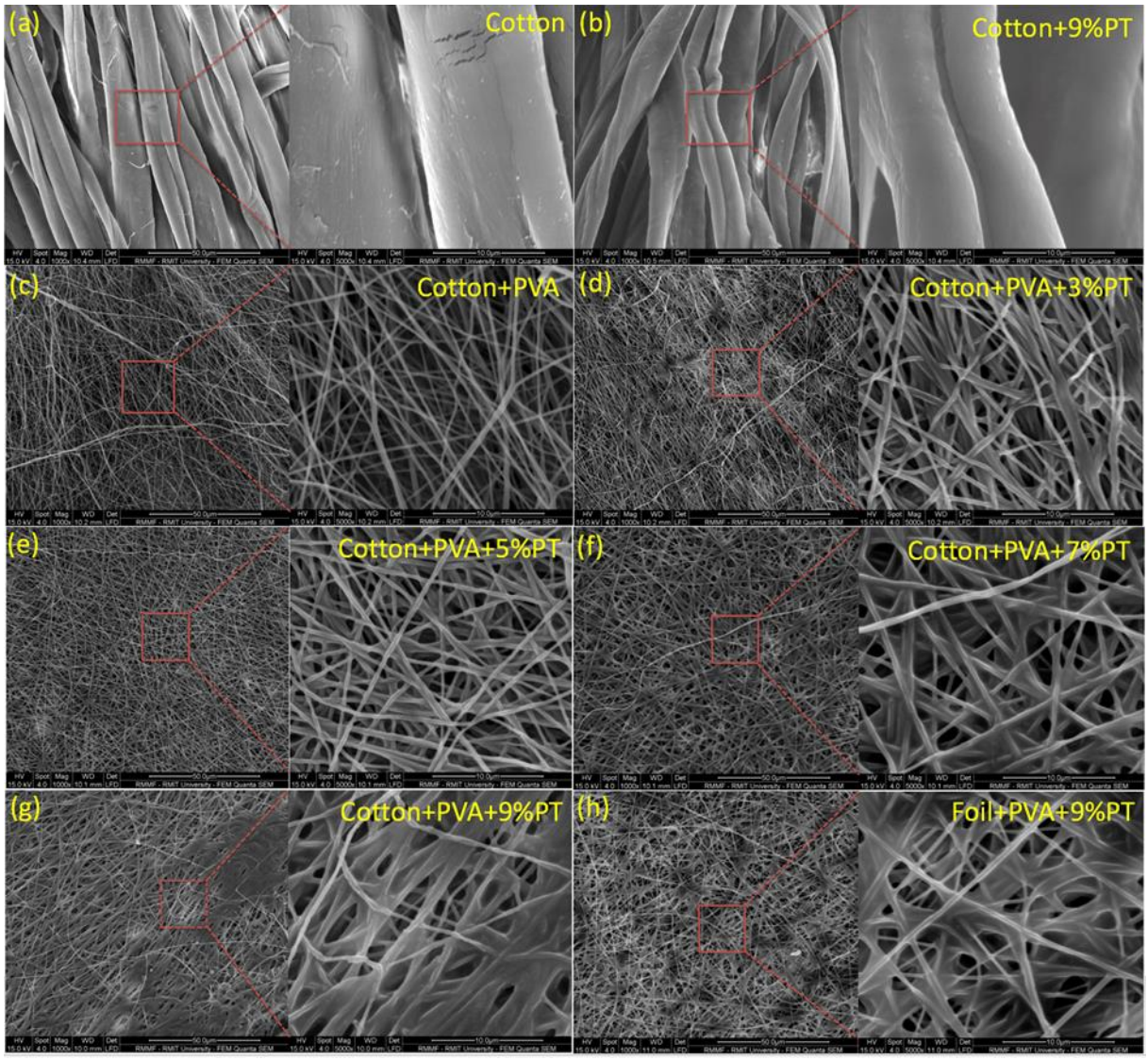

Figure 6-2: SEM photos (bar = 50 µm for 1000× and = 10 µm for 5000×) of the surface of cotton fabrics (a), cotton cured with 9%PT (b), cotton covered with PVA nanofibres (c), cotton+PVA nanofibres cured with PT with the different concentrations (d-g), and PVA nanofibres on an aluminium foil followed by dip coating with 9%PT (h).

Dip coating of PT has formed an interconnected network on the surface of the PVA nanofibrous membrane. The surface of the coated cotton fabrics shows a darker colour (Figure 6-1), but the handle of the fabrics has not affected evidently.

When the concentration of PT is low, such as 3-5%, the PVA nanofibres partly entangle with each other with the crossing points merging together (Figure 6-2d–e). When the concentration is higher than 7%, most of nanofibres bridge together forming a strongly interconnected porous layer on the surface (Figure 6-2f–g). As comparison, PVA nanofibres collected onto an aluminium foil were dip coated with PT, and the morphology of which (Figure 6-2h) is similar to that on cotton fabrics.

6.3.1.2 FTIR spectra

FTIR was employed to analyze the change of chemical components after the deposition of nanofibrous membrane and dip coating process, as shown in Figure 6-2 the FTIR spectra and Table 6-1 the detected peaks with their associated groups.

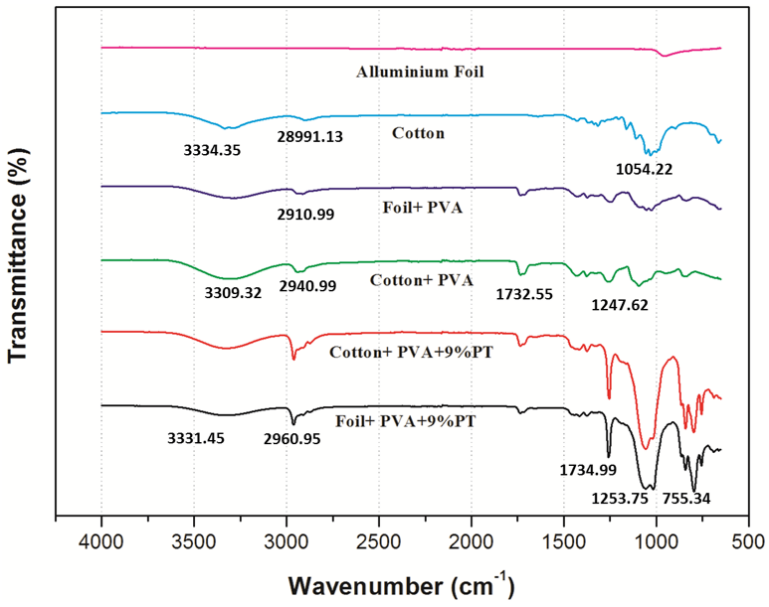

Figure 6-3: ATR-FTIR spectra of cotton fabrics coated with PVA, 9% PT, and with different concentrations of PT.

The FTIR peaks for cotton fabrics are 3334.55 cm^{-1} corresponding to O–H stretching, 2899.13 cm^{-1} region for C–H stretching, 1315.08 cm^{-1} associated with $–CH_2–$ groups, and a

peak around 1640 -1160 cm^{-1} due to the adsorption of water molecules (Murugesh Babu, Selvadass & Somashekar 2013). The FTIR spectra of cotton with PVA and foil with PVA show similar picks as the substrate materials are covered with PVA nanofibres. The prominent peaks for PVA are 3288.43 cm^{-1}, 2912.50 cm^{-1} and 1247.62 cm^{-1}, corresponding to –OH stretching, C–H stretching and C–O stretching, respectively (Jayasekara et al. 2004). The PVA nanofibres coated with 9%PT show the major peaks associated with PVA are observed, such as C–H broad alkyl stretching band 2960.94 cm^{-1} and typical strong hydroxyl bands for –OH stretching band at 3321.56 cm^{-1} (Figure 6-3). The spectrum also shows symmetric banding of TMS including the bands at 1416.17 cm^{-1} for Si–CH_3 and at 1374.47 cm^{-1} for Si–O–C. In addition, the vibration symmetric stretching bands of Si–O–Si can be observed around 1253.69 cm^{-1}, 841.20 cm^{-1}, 797.69 cm^{-1} and 755.58 cm^{-1} (Moiz, Padhye & Wang 2017). It is evident that some new peaks have been found from the FTIR spectrum after dip coating of PT.

Table 6-1: Detection of wave number and functional groups by FTIR.

Samples	**Wave number (cm^{-1})**	**Attributed to**
Cotton	3570–3200	H-bonded OH stretch
	3000–2800	C–H stretching
	1425	Bending of CH group
	1315	Asymmetric stretching of C-O-C group
	1017	Asymmetric stretching of C-O group
PVA	1420 cm^{-1}	C-H wagging
	2850–3000	C-H stretching
	3600–3650 cm^{-1}	-OH stretching
	1090–1150 cm^{-1}	C-O carboxyl stretching
PDMS-TMS	2975	Asymmetric stretching of CH_2 group
	1270–1250	Asymmetric stretching of Si-CH_3 group
	870–700	Bending stretching of Si-$(CH_3)_n$ group
	1059–1020	Asymmetric stretching of Si-O-Si group

6.3.2 Protection

Both Cotton and PVA nanofibres are highly hydrophilic without any resistance to water, liquids and chemicals. The dip coating of PT has brought excellent protection to cotton fabrics.

6.3.2.1 Water repellency

Water repellency indicates the surface wettability as a direct index of the waterproof properties of textiles. Cotton fabric is highly hydrophilic, and water can be easily absorbed into the structure of fibre and fabric. The water repellency of cotton fabric is as low as zero, and deposition of PVA nanofibres on the surface of cotton has not enhanced the water repellency as shown in Figure 6-4a. PDMS-TMS dip coating has an evident effect on enhancing hydrophobicity of cotton fabric surface due to the crosslinked network with a low surface energy they formed on the surface (Moiz et al. 2016). As shown in Figure 6-4a, the dip coating of PT has enhanced the water repellency of cotton fabrics to 90%. Besides, the PT dip coating has enhanced the water repellency of cotton+PVA to 70-90% depending on the concentration of PT. The surface of PVA nanofibres has tuned from hydrophilic to hydrophobic after PT coating. With the increase of PT concentration, the water repellency was enhanced evidently from 70% to 90%. This increase is due to the siloxane group of PT providing a low surface energy to the fabric.

6.3.2.2 Water contact angle

Both cotton and PVA nanofibres show a water contact angle of zero as they are highly hydrophilic in nature. Cotton+9%PT and cotton+PVA+9%PT, however, show a high contact angle of 135^{o} (Figure 6-4b), suggesting that PT coating provides hydrophobic and waterproof properties to the nanofibrous surface on cotton fabrics. The reason for this is that PT coating increases the surface tension of cotton+PVA to 72.8 dynes/cm, and the high contact angle of

the PT coating is due to the polydimethylsiloxane group in PT which reduces the surface energy (Chen, RS, Chang & Chang 2005). With the increase of PT concentration from 3% to 9%, the water contact angle of cotton+PVA+PT increases gradually from 120^{o} to 135^{o}, suggesting the enhancement in hydrophobicity of the coated cotton fabrics.

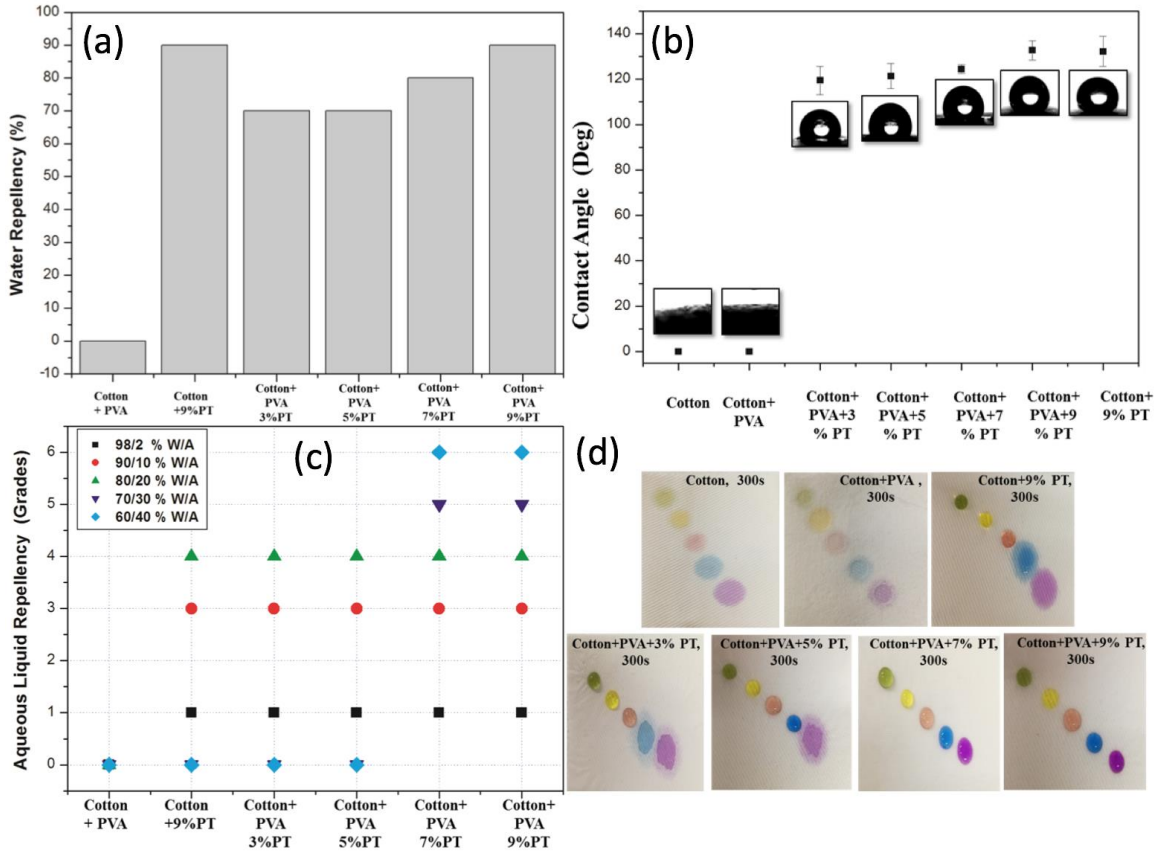

Figure 6-4: Water repellency of cotton, PVA and PT treated fabrics (a). Water contact angle of cotton, PVA and PT treated fabrics (b). Aqueous liquid repellency grades of cotton, PVA and PT treated fabrics (c), and photos of aqueous liquid repellency of cotton, PVA and PT treated fabrics (d) (green: 98/2; yellow: 90/10; orange: 80/20; blue: 70/30; purple:60/40).

6.3.2.3 Aqueous liquid repellency

Aqueous liquid repellency test determines the efficacy of the protective coating on fabrics by evaluating the resistant of fabric against wetting through a series of water/alcohol solutions of

different surface tensions. Cotton and cotton+PVA are not repellent to any aqueous liquids due to their hydrophilic nature. Cotton+9%PT show resistance to 98:2, 90:10 and 80:20 of water to isopropyl alcohol (Figure 6-4c–d).

However, it doesn't show repellency to aqueous liquids with the concentration of alcohol higher than 30%. This is because the surface of 9%PT coated cotton fabrics can only repel up to 20% alcohol with the surface tension up to 33 dynes/cm. Cotton+PVA+3-5% PT show almost equal aqueous liquid repellency performance compared to cotton+9%PT (Figure 6-4c). Cotton+PVA+PT+7-9% show excellent aqueous liquid repellency (grade 6) with the surface tension up to 24.3 dynes/cm.

It is obvious that the nanofibrous surface after PT coating provides better protection against different aqueous liquids. It also demonstrates the potential of the PT functionalized PVA nanofibrous membrane in protective clothing.

6.3.2.4 Chemical resistance

Table 6-2 lists the chemical resistance of cotton fabrics, cotton+PVA, cotton+PT and cotton+PVA+PT. As expected, cotton fabrics and cotton+PVA have no chemical resistance at all with all chemicals penetrating into the fabrics immediately. Cotton fabrics coated with 9%PT shows chemical resistance to a range of chemicals as listed in Table 6-1. The cotton+PVA+PT show much better chemical resistance than cotton+9%PT coated fabrics. Even cotton+PVA+3%PT shows better performance than that of cotton+9%PT. Cotton+PVA+9%PT shows the best chemical resistance with eight of the chemicals repelled successfully (Table 6-2). It is evident that incorporation of PVA nanofibrous membrane has greatly enhanced the PT functionalization on the surface. The chemicals take a significantly

long time to penetrate into the coated fabrics due to the presence of nanofibrous structure with a PT functionalized surface.

Table 6-2: Chemical resistance test (C: cotton; γ : surface tension).

Chemical	γ (dynes/cm)	C	C +PVA	C +9%PT	C+PVA+PT			
					3%	5%	7%	9%
Sodium hydroxide	101.0	0	0	300	300	300	300	300
Sulphuric acid	84.0	0	0	300	300	300	300	300
Dimethylformamide	36.7	0	0	10	12	25	300	300
Acetonitrile	28.7	0	0	300	300	300	300	300
Toluene	28.4	0	0	236	300	300	300	300
Acetic acid	27.0	0	0	300	300	300	300	300
n-Hexadecane	27.3	0	0	0	0	0	0	0
Paraffin oil	26.0	0	0	0	0	0	300	300
Isopropyl alcohol	23.0	0	0	0	0	0	15	35
Methanol	22.1	0	0	0	0	0	0	300
n-Heptane	19.8	0	0	0	0	0	0	0

6.3.3 Comfort

The comfort of protective clothing is always an issue as it has been sacrificed more or less due to the impermeability of the coated protective layer. The incorporation of nanofibrous membrane as the basis of functionalization has preserved the porous structure to some extent while enhancing the performance of the surface functionalization. A less amount of functional agent can be used with the same or roughly the same performance after the introduction of nanofibrous membrane.

6.3.3.1 Air permeability

Figure 6-5a shows the air permeability of all the fabrics. The air permeability of cotton fabric in this study was found to be 8.270 mL/cm^2/sec. The air permeability is greatly influenced by the pore size in the fabric structure (Fang et al. 2012; Kang et al. 2007; Zeng et al. 2015). When nanofibrous membrane was incorporated onto the surface of the cotton fabric, the air

permeability remained nearly equal due to the porous structure of the membrane (Gibson, Schreuder-Gibson & Rivin 2001).

Cotton+PT shows an evident decrease in air permeability as shown in Figure 6-5a. PT coating has evidently bridged the cotton fibres together with pore size decreased or pores being blocked. As a result, the air permeability was sacrificed evidently. The cotton+PVA+PT at 3% shows the air permeability of 7.662 mL/cm^2/sec, suggesting the air permeability of cotton fabrics has been preserved after coating. From morphology study it was evident that 3%PT coating resulted in the joint parts of PVA nanofibres merged together (Figure 6-2d), so that the pores in the nanofibrous membrane have not been blocked. With the increase of the concentration of PT, the air permeability of cotton+PVA+PT decreases gradually as shown in Figure 6-5a. The PVA nanofibres interconnected to each other with some pores being blocked as shown from the SEM photos in Figure 6-2e–g. As a result, the air permeability decreases with the increase of the concentration of PT. However, cotton fabric coated with 9%PT shows the lowest air permeability. It is evident that the presence of nanofibres on the surface of the fabric helps maintain the permeability due to their porous structure and strengthening effect in functionalization.

6.3.3.2 MMT profiles

The MMT profiles in Figure 6-5b indicate that the moisture management property of cotton fabrics has altered significantly after the deposition of PVA nanofibres and dip coating of PT. Both cotton and cotton+PVA exhibit excellent water transport capacity across the fibrous/nanofibrous structure due to their hydrophilic and wicking property (Hsieh 1995; Simončič & Rozman 2007).

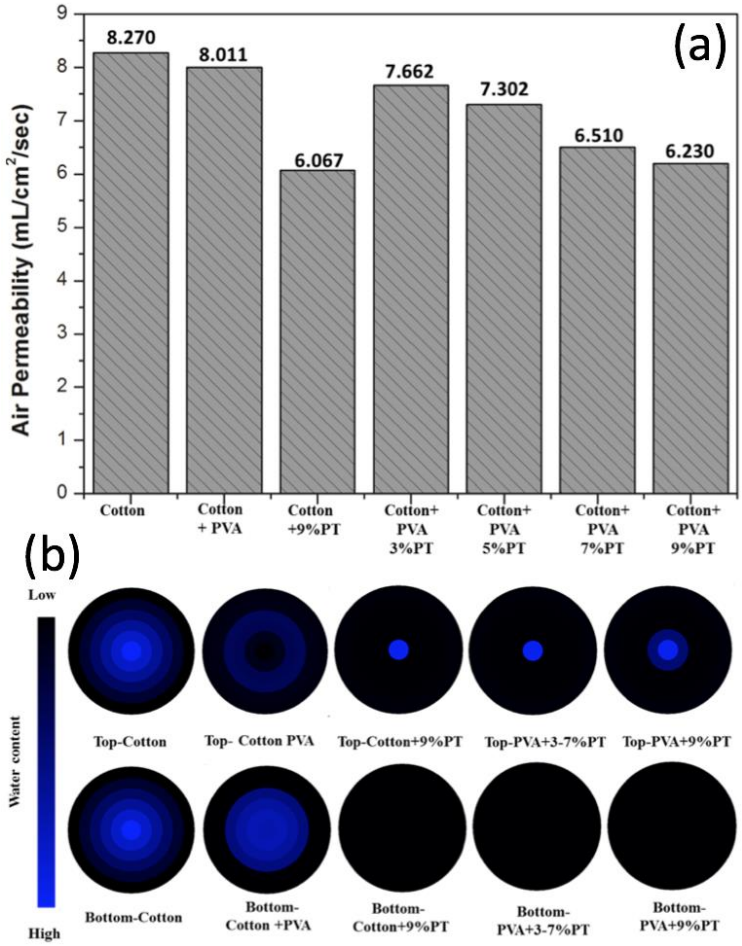

Figure 6-5: Air permeability of cotton fabrics coated with PVA, 9% PT, and with different concentrations of PT. Moisture management tester (MMT) profile of the cotton, cotton with PVA nanofibres, cotton with only PT, cotton, PVA coated with different concentrations of PT (measure time = 120 s).

PT coating has resulted in a waterproof surface without any water transported to the bottom side of fabrics, as shown the MMT profiles in Figure 6-5b. Cotton+PVA+PT with different PT concentrations shows no evident differences between the top and bottom surfaces in terms of the MMT index, as presented in Table 6-3. Generally, the moisture management capacity (OMMC) of cotton fabrics has changed from 0.46 to 0 after PVA+PT coating. Cotton+PVA+9%PT has a smoother surface than those with lower PT concentrations, so that the water spreads to a little bit larger wet area on the top side of the coated fabrics (Figure 6-

5b). However, no water can be transported to the bottom surface for all the cotton+PVA+PT fabrics, indicating that the one-way transport capability is almost zero after PT coating.

Table 6-3: MMT test results of cotton fabrics, cotton+PVA, cotton+PT and cotton+PVA+PT.

MMT Index	Cotton		Cotton +PVA		Cotton +9%PT		Cotton +PVA +3-7%PT		Cotton +PVA+9%PT	
	T	B	T	B	T	B	T	B	T	B
WT (s)	3.36	4.125	19.78	5.063	40.80	122.5	6.75-8.71	120	2.53	120
AR_T (s)	40.22	34.39	18.80	32.10	109.58	0	47.34-157.90	0	38.50	0
MWR (mm)	15	15	0	15	3.75	0	5	0	5	0
SS_i (mm/s)	2.56	2.444	0	2.13	0.337	0	0.56-0.72	0	1.77	0
OWTC	48.50		198.06		–612.65		–638.08- –717.28		–674.12	
OMMC	0.46		0.3		0.0139		0		0	

Note: Wetting time (WT), Absorption rate (AR_T), Maximum wetted radius (MWR), Spreading speed (SS_i), One-way transport capability (OWTC), Overall moisture management capability (OMMC), Top surface (T), Bottom surface (B).

6.4 Summary

PVA nanofibrous membrane was successfully functionalized by polydimethylsiloxane (PDMS)-trimethylated silica (TMS) to act as protective layer on the surface of cotton fabrics. PVA nanofibrous membrane was deposited onto cotton fabrics with the nanofibres interconnected with each other forming a cross-linked network after dip coating of PT. The chain of PDMS-TMS cross-linked and combined with the backbone chain of PVA nanofibrous membrane, converting the surface from hydrophilic to hydrophobic with a water contact angle of 135°. The PVA+PT coating enhanced the repellency and protective properties of cotton fabrics, and the coated fabrics performed excellent repellency to water,

aqueous liquid and certain chemicals. With the nanoporous structure inside PVA nanofibrous membrane and less usage of PT, the air permeability of cotton fabrics was largely maintained after coating. The cotton+PVA+PT showed a totally different MMT profile as the water droplet couldn't penetrate into the nanofibrous structure. This new method of surface functionalized nanofibrous membrane on textiles showed a potential for the further developing protective surface on textiles.

CHAPTER 7

CONCLUSION AND FURTHER RESEARCH

7.1 Conclusion

A limited free surface of polymer solution was created by modifying the front part of a needle into a half cut convex. Multiple polymer jet was successfully generated from the curved convex channel while the needle was employed to ensure good controlling of feeding solution. The flow rate of polymer solution was enhanced to 2-3 times higher than conventional needle electrospinning, resulting in a production rate of up to 0.3 g/h. An applied voltage of 19 kV was high enough to maintain the spinning process with as-spun nanofibres in a comparable quality (diameter and its distribution) to that from needle electrospinning. The electrospinning performance, the fibre diameter and production rate, of convex needle spinneret was greatly affected by the experimental parameters including solution concentration and applied voltage. Electric field analysis revealed that a strong electric field was formed on the curved convex of the modified needle with a slightly higher electric field intensity than that of conventional needle electrospinning.

A wire loop embedded in a Teflon tube was successfully used as the spinneret to generate multiple polymer jets of PAN. The Teflon tube ensured a controllable polymer solution feeding while the wire loop helped forming a crescent of polymer solution on the end of the

tube. Due to the enlarged spannable area of crescent, many polymer jets were generated at the same time and the production rate was enhanced to 0.19–0.48 g/h. Slightly coarse nanofibres were fabricated as compared with needle electrospinning, and the electrospinning performance was also dependent on the experimental parameters such as the applied voltage and polymer concentration. Electric field analysis showed a large area of strong electric field forming around the wire loop with higher electric field intensity than that of a needle.

A spiral wire inserted in a Teflon tube was successfully used to perform PVA nanofibrous coating on textiles. Multiple polymer jets were generated to coat the cotton fabrics with even PVA nanofibrous membrane. A further dip coating of polydimethylsiloxane (PDMS)-trimethylated silica (TMS) functionalized the surface of the PVA nanofibrous membrane, changing the membrane into a protective layer on the surface of cotton fabrics. The nanofibres interconnected with each other forming a cross-linked network after dip coating of PDMS-TMS, and the chain of PDMS-TMS cross-linked and combined with the backbone chain of PVA nanofibrous membrane. The functionalized PVA nanofibrous membrane on cotton fabrics showed a water contact angle of 135°, and the coated fabrics performed excellent repellency to water, aqueous liquid and certain chemicals. The cotton+PVA+PT showed a totally different MMT profile as the water droplet couldn't penetrate into the nanofibrous structure. The air permeability of cotton fabrics was largely maintained due to the nanoporous structure of the nanofibrous membrane.

These three novel linear spinnerets with enlarged spannable area can concentrate a relatively high electric field to generate multiple polymer jets with enhanced production rate. The usage of needle and tube has maintained the controlling of solution feeding and the spinning process. The novel electrospinning can be adopted to perform nanofibrous coating on textiles

towards surface functionalised textiles. This research will further benefit the development of large-scale production of nanofibres from needleless electrospinning with better controlling and stability for different applications.

7.2 Recommendation for future research work

Based on the experiment results and discussion, a number of suggestions have been identified as worthy of further research:

a. The linear spinneret can be adopted to electrospin different types of polymer materials especially focusing on the end use. For instance, these spinnerets can be used to electrospin composite materials with enhanced throughput.

b. The linear spinneret can be used for electrospraying along with electrospinning. For example, different types of particles, such as silica aerogels, activated carbon powder, carbon nanotubes and nanodiamonds, can be easily electrospun with these types of spinnerets. This will introduce a wide variety of application as nanocomposites.

c. Further modification of linear spinnerets with varying shape can be done to employ even higher electric voltages (30-40 kV). The production rate might be enhanced to be even higher than existing methods.

d. Modelling work with COMSOL Multiphysics can be further extended to analyse different polymers behaviour in contact of a high applied voltage by varying the shape of spinneret.

REFERENCES

Ahuja, T & Kumar, D 2009, 'Recent progress in the development of nano-structured conducting polymers/nanocomposites for sensor applications', *Sensors and Actuators B: Chemical*, vol. 136, no. 1, pp. 275-286.

Alborzi, S, Lim, LT & Kakuda, Y 2010, 'Electrospinning of Sodium Alginate-Pectin Ultrafine Fibres', *Journal of food science*, vol. 75, no. 1.

Ali, U, Abbass, A, Khurshid, F, Aslam, S & Waqar, A 2017, 'Needleless Electrospinning Using a Flat Wheel Spinneret', *Journal of Engineered Fabrics & Fibres (JEFF)*, vol. 12, no. 3.

Ali, U, Niu, H, Aslam, S, Jabbar, A, Rajput, AW & Lin, T 2017, 'Needleless electrospinning using sprocket wheel disk spinneret', *Journal of materials science*, vol. 52, no. 12, pp. 7567-7577.

Anton, F 1934, *Process and apparatus for preparing artificial threads*, Google Patents US1975504A.

Anton, F 1938, *Method and apparatus for the production of fibres*, Google Patents US2123992A.

Anton, F 1939, *Method and apparatus for the production of artificial fibres*, Google Patents US2158416A.

Anton, F 1943, *Production of artificial fibres from fibre forming liquids*, Google Patents US2323025A.

Barhate, RS & Ramakrishna, S 2007, 'Nanofibrous filtering media: filtration problems and solutions from tiny materials', *Journal of membrane science*, vol. 296, no. 1-2, pp. 1-8.

Bellan, LM, Coates, GW & Craighead, HG 2006, 'Poly (dicyclopentadiene) submicron fibres produced by electrospinning', *Macromolecular rapid communications*, vol. 27, no. 7, pp. 511-515.

Bognitzki, M, Czado, W, Frese, T, Schaper, A, Hellwig, M, Steinhart, M, Greiner, A & Wendorff, JH 2001, 'Nanostructured fibres via electrospinning', *Advanced Materials*, vol. 13, no. 1, pp. 70-72.

Borisova, A & Reihmane, S 2013, 'Hydrophobic treatment of blended fabric's surface', *Materials Science*, vol. 19, no. 2, pp. 169-173.

Cengiz, F & Jirsak, O 2009, 'The effect of salt on the roller electrospinning of polyurethane nanofibres', *Fibres and Polymers*, vol. 10, no. 2, pp. 177-184.

Chen, L, Wu, F, Li, Y, Wang, Y, Si, L, Lee, KI & Fei, B 2018, 'Robust and elastic superhydrophobic breathable fibrous membrane with in situ grown hierarchical structures', *Journal of membrane science*, vol. 547, pp. 93-98.

Chen, M-C, Sun, Y-C & Chen, Y-H 2013, 'Electrically conductive nanofibres with highly oriented structures and their potential application in skeletal muscle tissue engineering', *Acta biomaterialia*, vol. 9, no. 3, pp. 5562-5572.

Chen, RS, Chang, CJ & Chang, YH 2005, 'Study on siloxane-modified polyurethane dispersions from various polydimethylsiloxanes', *Journal of Polymer Science Part A: Polymer Chemistry*, vol. 43, no. 16, pp. 3482-3490.

Chen, X, Zhang, Y, He, X, Li, H, Wei, B & Yang, W 2019a, 'Electrospinning on a plucked string', *Journal of Materials Science*, vol. 54, no. 1, pp. 901-910.

Deitzel, JM, Kleinmeyer, J, Harris, D & Beck Tan, NC 2001, 'The effect of processing variables on the morphology of electrospun nanofibres and textiles', *Polymer*, vol. 42, no. 1, pp. 261-272.

Deitzel, JM, Kleinmeyer, J, Harris, D & Tan, NB 2001, 'The effect of processing variables on the morphology of electrospun nanofibres and textiles', *Polymer*, vol. 42, no. 1, pp. 261-272.

Doshi, J & Reneker, DH 1995, 'Electrospinning process and applications of electrospun fibres', *Journal of electrostatics*, vol. 35, no. 2-3, pp. 151-160.

Dosunmu, O, Chase, GG, Kataphinan, W & Reneker, D 2006, 'Electrospinning of polymer nanofibres from multiple jets on a porous tubular surface', *Nanotechnology*, vol. 17, no. 4, p. 1123.

Emelyanenko, AM, Boinovich, LB, Bezdomnikov, AA, Chulkova, EV & Emelyanenko, KA 2017, 'Reinforced superhydrophobic coating on silicone rubber for longstanding anti-icing performance in severe conditions', *ACS applied materials & interfaces*, vol. 9, no. 28, pp. 24210-24219.

Fang, J, Niu, H, Lin, T & Wang, X 2008, 'Applications of electrospun nanofibres', *Chinese science bulletin*, vol. 53, no. 15, p. 2265.

Fang, J, Wang, H, Wang, X & Lin, T 2012, 'Superhydrophobic nanofibre membranes: effects of particulate coating on hydrophobicity and surface properties', *Journal of the Textile Institute*, vol. 103, no. 9, pp. 937-944.

Forward, KM & Rutledge, GC 2012, 'Free surface electrospinning from a wire electrode', *Chemical Engineering Journal*, vol. 183, pp. 492-503.

Gibson, P, Schreuder-Gibson, H & Rivin, D 2001, 'Transport properties of porous membranes based on electrospun nanofibres', *Colloids and Surfaces A: Physicochemical and Engineering Aspects*, vol. 187, pp. 469-481.

Gilbert, W 1958, '1600. De Magnete', *London: Peter Short*.

Givens, SR, Gardner, KH, Rabolt, JF & Chase, DB 2007, 'High-temperature electrospinning of polyethylene microfibres from solution', *Macromolecules*, vol. 40, no. 3, pp. 608-610.

Gomes, DS, da Silva, AN, Morimoto, NI, Mendes, LT, Furlan, R & Ramos, I 2007, 'Characterization of an electrospinning process using different PAN/DMF concentrations', *Polímeros*, vol. 17, no. 3, pp. 206-211.

Greiner, A & Wendorff, JH 2007, 'Electrospinning: a fascinating method for the preparation of ultrathin fibres', *Angewandte Chemie International Edition*, vol. 46, no. 30, pp. 5670-5703.

He, J-H, Kong, H-Y, Yang, R-R, Dou, H, Faraz, N, Wang, L & Feng, C 2012, 'Review on fibre morphology obtained by bubble electrospinning and blown bubble spinning', *Thermal science*, vol. 16, no. 5, pp. 1263-1279.

He, J-H, Liu, Y, Xu, L, Yu, J-Y & Sun, G 2008, 'BioMimic fabrication of electrospun nanofibres with high-throughput', *Chaos, Solitons & Fractals*, vol. 37, no. 3, pp. 643-651.

He, J-H, Wan, Y-Q & Yu, J-Y 2008, 'Effect of concentration on electrospun polyacrylonitrile (PAN) nanofibres', *Fibres and Polymers*, vol. 9, no. 2, pp. 140-142.

Hertleer, C, Rogier, H & Van Langenhove, L 2007, 'A textile antenna for protective clothing'.

Higham, AK, Tang, C, Landry, AM, Pridgeon, MC, Lee, EM, Andrady, AL & Khan, SA 2014, 'Foam electrospinning: A multiple jet, needle-less process for nanofibre production', *AIChE Journal*, vol. 60, no. 4, pp. 1355-1364.

Holopainen, J, Penttinen, T, Santala, E & Ritala, M 2014, 'Needleless electrospinning with twisted wire spinneret', *Nanotechnology*, vol. 26, no. 2, p. 025301.

Hsieh, Y-L 1995, 'Liquid transport in fabric structures', *Textile Research Journal*, vol. 65, no. 5, pp. 299-307.

Hu, X, Liu, S, Zhou, G, Huang, Y, Xie, Z & Jing, X 2014, 'Electrospinning of polymeric nanofibres for drug delivery applications', *Journal of Controlled Release*, vol. 185, pp. 12-21.

Huang, Z-M, Zhang, Y-Z, Kotaki, M & Ramakrishna, S 2003, 'A review on polymer nanofibres by electrospinning and their applications in nanocomposites', *Composites science and technology*, vol. 63, no. 15, pp. 2223-2253.

Jahan, I, Wang, L & Wang, X 2018, 'Needleless Electrospinning from a Tube with an Embedded Wire Loop', *Macromolecular Materials and Engineering*, vol., p. 1800588.

Jayasekara, R, Harding, I, Bowater, I, Christie, GBY & Lonergan, GT 2004, 'Preparation, surface modification and characterisation of solution cast starch PVA blended films', *Polymer Testing*, vol. 23, no. 1, pp. 17-27.

Jiang, G & Qin, X 2014, 'An improved free surface electrospinning for high throughput manufacturing of core–shell nanofibres', *Materials Letters*, vol. 128, pp. 259-262.

Jiang, G, Zhang, S & Qin, X 2013, 'High throughput of quality nanofibres via one stepped pyramid-shaped spinneret', *Materials Letters*, vol. 106, pp. 56-58.

Jiang, G, Zhang, S, Wang, Y & Qin, X 2015, 'An improved free surface electrospinning with micro-bubble solution system for massive production of nanofibres', *Materials Letters*, vol. 144, pp. 22-25.

Jirsák, O & Dao, T 2009, 'Production, properties and end-uses of nanofibres', in *Nanotechnology in Construction 3*, Springer, pp. 95-99.

Jirsak, O, Sanetrnik, F, Lukas, D, Kotek, V, Martinova, L & Chaloupek, J 2004, *Method of nanofibres production from a polymer solution using electrostatic spinning and a device for carrying out the method*, Google Patents US20060290031A1.

Jirsak, O, Sanetrnik, F, Lukas, D, Kotek, V, Martinova, L & Chaloupek, J 2009, *Method of nanofibres production from a polymer solution using electrostatic spinning and a device for carrying out the method*, Google Patents US7585437B2.

Kalayci, VE, Patra, PK, Kim, YK, Ugbolue, SC & Warner, SB 2005, 'Charge consequences in electrospun polyacrylonitrile (PAN) nanofibres', *Polymer*, vol. 46, no. 18, pp. 7191-7200.

Kang, YK, Park, CH, Kim, J & Kang, TJ 2007, 'Application of electrospun polyurethane web to breathable water-proof fabrics', *Fibres and Polymers*, vol. 8, no. 5, pp. 564-570.

Kim, G, Cho, Y-S & Kim, WD 2006, 'Stability analysis for multi-jets electrospinning process modified with a cylindrical electrode', *European Polymer Journal*, vol. 42, no. 9, pp. 2031-2038.

Kowalewski, T, Hiller, W & Behnia, M 1993, 'An experimental study of evaporating small diameter jets', *Physics of Fluids A: Fluid Dynamics*, vol. 5, no. 8, pp. 1883-1890.

Kwon, IK, Kidoaki, S & Matsuda, T 2005, 'Electrospun nano-to microfibre fabrics made of biodegradable copolyesters: structural characteristics, mechanical properties and cell adhesion potential', *Biomaterials*, vol. 26, no. 18, pp. 3929-3939.

Lee, S & Kay Obendorf, S 2006, 'Developing protective textile materials as barriers to liquid penetration using melt-electrospinning', *Journal of applied polymer science*, vol. 102, no. 4, pp. 3430-3437.

Lee, S & Obendorf, SK 2007, 'Use of electrospun nanofibre web for protective textile materials as barriers to liquid penetration', *Textile Research Journal*, vol. 77, no. 9, pp. 696-702.

Li, D & Xia, Y 2004, 'Direct fabrication of composite and ceramic hollow nanofibres by electrospinning', *Nano letters*, vol. 4, no. 5, pp. 933-938.

Liang, W, Haonan, Y, Lin, J & Xiaohong, Q 2018, 'High-throughput nanofibre produced by needleless electrospinning using a metal dish as the spinneret', *Textile Research Journal*, vol. 88, no. 1, pp. 80-88.

Liu, S-L, Huang, Y-Y, Zhang, H-D, Sun, B, Zhang, J-C & Long, Y-Z 2014, 'Needleless electrospinning for large scale production of ultrathin polymer fibres', *Materials Research Innovations*, vol. 18, no. sup4, pp. S4-833-S834-837.

Liu, Y & He, J-H 2007, 'Bubble electrospinning for mass production of nanofibres', *International Journal of Nonlinear Sciences and Numerical Simulation*, vol. 8, no. 3, pp. 393-396.

Liu, Z, Ang, KKJ & He, J 2017, 'Needle-disk electrospinning inspired by natural point discharge', *Journal of Materials Science*, vol. 52, no. 4, pp. 1823-1830.

Lu, B, Wang, Y, Liu, Y, Duan, H, Zhou, J, Zhang, Z, Wang, Y, Li, X, Wang, W & Lan, W 2010, 'Superhigh-throughput needleless electrospinning using a rotary cone as spinneret', *small*, vol. 6, no. 15, pp. 1612-1616.

Lu, X, Sun, Y, Chen, Z & Gao, Y 2017, 'A multi-functional textile that combines self-cleaning, water-proofing and VO2-based temperature-responsive thermoregulating', *Solar Energy Materials and Solar Cells*, vol. 159, pp. 102-111.

Lukas, D, Sarkar, A & Pokorny, P 2008, 'Self-organization of jets in electrospinning from free liquid surface: A generalized approach', *Journal of Applied Physics*, vol. 103, no. 8, p. 084309.

Ma, G, Yang, D & Nie, J 2009, 'Preparation of porous ultrafine polyacrylonitrile (PAN) fibres by electrospinning', *Polymers for Advanced Technologies*, vol. 20, no. 2, pp. 147-150.

Moiz, A, Padhye, R & Wang, X 2017, 'Coating of TPU-PDMS-TMS on polycotton fabrics for versatile protection', *Polymers*, vol. 9, no. 12, p. 660.

Moiz, A, Vijayan, A, Padhye, R & Wang, X 2016, 'Chemical and water protective surface on cotton fabric by pad-knife-pad coating of WPU-PDMS-TMS', *Cellulose*, vol. 23, no. 5, pp. 3377-3388.

Molnar, K & Nagy, ZK 2016, 'Corona-electrospinning: needleless method for high-throughput continuous nanofibre production', *European polymer journal*, vol. 74, pp. 279-286.

Moon, S, Gil, M & Lee, KJ 2017, 'Syringeless electrospinning toward versatile fabrication of nanofibre web', *Scientific reports*, vol. 7, p. 41424.

Murugesh Babu, K, Selvadass, M & Somashekar, R 2013, 'Characterization of the conventional and organic cotton fibres', *The Journal of The Textile Institute*, vol. 104, no. 10, pp. 1101-1112.

Muthuraman, NT 2012a, *Development and optimization of an alternative electrospinning process for high throughput*, North Carolina State University.

Muthuraman, NT 2012b, Edge electrospinning for high throughput production of nanofibres, thesis, North Carolina State University.

Niu, H & Lin, T 2012, 'Fibre generators in needleless electrospinning', *Journal of Nanomaterials*, vol. 2012, p. 12.

Niu, H, Lin, T & Wang, X 2009, 'Needleless electrospinning. I. A comparison of cylinder and disk nozzles', *Journal of applied polymer science*, vol. 114, no. 6, pp. 3524-3530.

Niu, H, Wang, X & Lin, T 2012a, 'Needleless electrospinning: influences of fibre generator geometry', *Journal of the Textile Institute*, vol. 103, no. 7, pp. 787-794.

Niu, H, Wang, X & Lin, T 2012b, 'Upward needleless electrospinning of nanofibres', *Journal of engineered fibres and fabrics*, vol. 7, no. 3, pp. 17-22.

Olson, DC, Piris, J, Collins, RT, Shaheen, SE & Ginley, DS 2006, 'Hybrid photovoltaic devices of polymer and ZnO nanofibre composites', *Thin solid films*, vol. 496, no. 1, pp. 26-29.

Persano, L, Camposeo, A, Tekmen, C & Pisignano, D 2013, 'Industrial upscaling of electrospinning and applications of polymer nanofibres: a review', *Macromolecular Materials and Engineering*, vol. 298, no. 5, pp. 504-520.

Pham, QP, Sharma, U & Mikos, AG 2006, 'Electrospinning of polymeric nanofibres for tissue engineering applications: a review', *Tissue engineering*, vol. 12, no. 5, pp. 1197-1211.

Ramaseshan, R, Sundarrajan, S, Liu, Y, Barhate, R, Lala, NL & Ramakrishna, S 2006, 'Functionalized polymer nanofibre membranes for protection from chemical warfare stimulants', *Nanotechnology*, vol. 17, no. 12, p. 2947.

Reneker, DH & Chun, I 1996, 'Nanometre diameter fibres of polymer, produced by electrospinning', *Nanotechnology*, vol. 7, no. 3, p. 216.

Schreuder-Gibson, HL, Truong, Q, Walker, JE, Owens, JR, Wander, JD & Jones, WE 2003, 'Chemical and biological protection and detection in fabrics for protective clothing', *MRS bulletin*, vol. 28, no. 8, pp. 574-578.

Sen, AK 2007, *Coated textiles: principles and applications*, CRC Press.

Shin, HU, Li, Y, Paynter, A, Nartetamrongsutt, K & Chase, GG 2015, 'Vertical rod method for electrospinning polymer fibres', *Polymer*, vol. 65, pp. 26-33.

Shin, Y, Yoo, DI & Son, K 2005, 'Development of thermoregulating textile materials with microencapsulated phase change materials (PCM). IV. Performance properties and hand of fabrics treated with PCM microcapsules', *Journal of applied polymer science*, vol. 97, no. 3, pp. 910-915.

Simm, W, Gosling, C, Bonart, R & VON Falkai, B 1979, *Fibre fleece of electrostatically spun fibres and methods of making same*, Google Patents,US4143196.

Simončič, B & Rozman, V 2007, 'Wettability of cotton fabric by aqueous solutions of surfactants with different structures', *Colloids and Surfaces A: Physicochemical and Engineering Aspects*, vol. 292, no. 2-3, pp. 236-245.

Sridhar, R, Lakshminarayanan, R, Madhaiyan, K, Barathi, VA, Lim, KHC & Ramakrishna, S 2015, 'Electrosprayed nanoparticles and electrospun nanofibres based on natural materials: applications in tissue regeneration, drug delivery and pharmaceuticals', *Chemical Society Reviews*, vol. 44, no. 3, pp. 790-814.

Srinivasan, G & Reneker, DH 1995, 'Structure and morphology of small diameter electrospun aramid fibres', *Polymer international*, vol. 36, no. 2, pp. 195-201.

Su, Z, Li, J, Li, Q, Ni, T & Wei, G 2012, 'Chain conformation, crystallization behavior, electrical and mechanical properties of electrospun polymer-carbon nanotube hybrid nanofibres with different orientations', *Carbon*, vol. 50, no. 15, pp. 5605-5617.

Subbiah, T, Bhat, G, Tock, R, Parameswaran, S & Ramkumar, S 2005, 'Electrospinning of nanofibres', *Journal of applied polymer science*, vol. 96, no. 2, pp. 557-569.

Supaphol, P, Mit-uppatham, C & Nithitanakul, M 2005, 'Ultrafine Electrospun Polyamide-6 Fibres: Effects of Solvent System and Emitting Electrode Polarity on Morphology and Average Fibre Diameter', *Macromolecular Materials and Engineering*, vol. 290, no. 9, pp. 933-942.

Tang, S, Zeng, Y & Wang, X 2010, 'Splashing needleless electrospinning of nanofibres', *Polymer Engineering & Science*, vol. 50, no. 11, pp. 2252-2257.

Taylor, G 1964, 'Disintegration of water drops in an electric field', The Royal Society, pp. 383-397.

Taylor, G 1969, 'Electrically driven jets', *Proc. R. Soc. London, Ser. A*, vol. 313, no. 1515, pp. 453-475.

Theron, S, Yarin, A, Zussman, E & Kroll, E 2005, 'Multiple jets in electrospinning: experiment and modeling', *Polymer*, vol. 46, no. 9, pp. 2889-2899.

Theron, S, Zussman, E & Yarin, A 2004, 'Experimental investigation of the governing parameters in the electrospinning of polymer solutions', *Polymer*, vol. 45, no. 6, pp. 2017-2030.

Theron, SA, Yarin, AL, Zussman, E & Kroll, E 2005, 'Multiple jets in electrospinning: experiment and modeling', *Polymer*, vol. 46, no. 9, pp. 2889-2899.

Thompson, C, Chase, GG, Yarin, A & Reneker, D 2007, 'Effects of parameters on nanofibre diameter determined from electrospinning model', *Polymer*, vol. 48, no. 23, pp. 6913-6922.

Thoppey Muthuraman, N 2012, Development and Optimization of an Alternative Electrospinning Process for High Throughput, 3538493 thesis, North Carolina State University.

Thoppey, N, Bochinski, J, Clarke, L & Gorga, R 2011, 'Edge electrospinning for high throughput production of quality nanofibres', *Nanotechnology*, vol. 22, no. 34, p. 345301.

Tian, L, Zhao, C, Li, J & Pan, Z 2015, 'Multi-needle, electrospun, nanofibre filaments: effects of the needle arrangement on the nanofibre alignment degree and electrostatic field distribution', *Textile Research Journal*, vol. 85, no. 6, pp. 621-631.

Varabhas, J, Chase, GG & Reneker, D 2008, 'Electrospun nanofibres from a porous hollow tube', *Polymer*, vol. 49, no. 19, pp. 4226-4229.

Varesano, A, Carletto, RA & Mazzuchetti, G 2009, 'Experimental investigations on the multi-jet electrospinning process', *Journal of Materials Processing Technology*, vol. 209, no. 11, pp. 5178-5185.

Wang, D, Liu, N, Xu, W & Sun, G 2011, 'Layer-by-layer structured nanofibre membranes with photoinduced self-cleaning functions', *The Journal of Physical Chemistry C*, vol. 115, no. 14, pp. 6825-6832.

Wang, H, Xue, Y, Ding, J, Feng, L, Wang, X & Lin, T 2011, 'Durable, self-healing superhydrophobic and superoleophobic surfaces from fluorinated-decyl polyhedral oligomeric silsesquioxane and hydrolyzed fluorinated alkyl silane', *Angewandte Chemie International Edition*, vol. 50, no. 48, pp. 11433-11436.

Wang, J, Chen, N, Ramakrishna, S, Tian, L & Mo, X 2017, 'The Effect of Plasma Treated PLGA/MWCNTs-COOH Composite Nanofibres on Nerve Cell Behavior', *Polymers*, vol. 9, no. 12, p. 713.

Wang, X, Lin, T & Wang, X 2014, 'Scaling up the production rate of nanofibres by needleless electrospinning from multiple ring', *Fibres and Polymers*, vol. 15, no. 5, pp. 961-965.

Wang, X, Niu, H, Lin, T & Wang, X 2009, 'Needleless electrospinning of nanofibres with a conical wire coil', *Polymer Engineering & Science*, vol. 49, no. 8, pp. 1582-1586.

Wang, X, Niu, H, Wang, X & Lin, T 2012, 'Needleless electrospinning of uniform nanofibres using spiral coil spinnerets', *Journal of Nanomaterials*, vol. 2012, p. 3.

Wang, X, Wang, X & Lin, T 2012, 'Electric field analysis of spinneret design for needleless electrospinning of nanofibres', *Journal of Materials Research*, vol. 27, no. 23, pp. 3013-3019.

Wang, X, Wang, X & Lin, T 2014, '3D electric field analysis of needleless electrospinning from a ring coil', *Journal of industrial textiles*, vol. 44, no. 3, pp. 463-476.

Wei, L, Qiu, Q, Wang, R & Qin, X 2018, 'Influence of the processing parameters on needleless electrospinning from double ring slits spinneret using response surface methodology', *Journal of applied polymer science*, vol. 135, no. 27, p. 46407.

Wei, L, Yu, H, Jia, L & Qin, X 2018, 'High-throughput nanofibre produced by needleless electrospinning using a metal dish as the spinneret', *Textile Research Journal*, vol. 88, no. 1, pp. 80-88.

Wu, D, Huang, X, Lai, X, Sun, D & Lin, L 2010, 'High throughput tip-less electrospinning via a circular cylindrical electrode', *Journal of Nanoscience and nanotechnology*, vol. 10, no. 7, pp. 4221-4226.

Xie, S & Zeng, Y 2012, 'Effects of electric field on multineedle electrospinning: experiment and simulation study', *Industrial & Engineering Chemistry Research*, vol. 51, no. 14, pp. 5336-5345.

Yan, G, Niu, H, Shao, H, Zhao, X, Zhou, H & Lin, T 2017, 'Curved convex slot: an effective needleless electrospinning spinneret', *Journal of Materials Science*, vol. 52, no. 19, pp. 11749-11758.

Yan, X, Marini, J, Mulligan, R, Deleault, A, Sharma, U, Brenner, MP, Rutledge, GC, Freyman, T & Pham, QP 2015, 'Slit-surface electrospinning: a novel process developed for high-throughput fabrication of core-sheath fibres', *PloS one*, vol. 10, no. 5, p. e0125407.

Yang, E, Shi, J & Xue, Y 2010, 'Influence of electric field interference on double nozzles electrospinning', *Journal of Applied Polymer Science*, vol. 116, no. 6, pp. 3688-3692.

Yang, R, He, J, Xu, L & Yu, J 2009, 'Bubble-electrospinning for fabricating nanofibres', *Polymer*, vol. 50, no. 24, pp. 5846-5850.

Yang, S, Han, X, Jia, Y, Zhang, H & Tang, T 2017, 'Hydroxypropyltrimethyl Ammonium Chloride Chitosan Functionalized-PLGA Electrospun Fibrous Membranes as Antibacterial Wound Dressing: In Vitro and In Vivo Evaluation', *Polymers*, vol. 9, no. 12, p. 697.

Yang, W, Liu, Y, Zhang, L, Cao, H, Wang, Y & Yao, J 2016, 'Optimal spinneret layout in Von Koch curves of fractal theory based needleless electrospinning process', *AIP Advances*, vol. 6, no. 6, p. 065223.

Yang, Y, Jia, Z, Li, Q, Hou, L, Liu, J, Wang, L, Guan, Z & Zahn, M 2010, 'A shield ring enhanced equilateral hexagon distributed multi-needle electrospinning spinneret', *IEEE Transactions on Dielectrics and Electrical Insulation*, vol. 17, no. 5.

Yarin, A & Zussman, E 2004, 'Upward needleless electrospinning of multiple nanofibres', *Polymer*, vol. 45, no. 9, pp. 2977-2980.

Yördem, O, Papila, M & Menceloğlu, YZ 2008, 'Effects of electrospinning parameters on polyacrylonitrile nanofibre diameter: An investigation by response surface methodology', *Materials & design*, vol. 29, no. 1, pp. 34-44.

Yu, X, Xiang, H, Long, Y, Zhao, N, Zhang, X & Xu, J 2010, 'Preparation of porous polyacrylonitrile fibres by electrospinning a ternary system of PAN/DMF/H_2O', *Materials Letters*, vol. 64, no. 22, pp. 2407-2409.

Zeng, C, Wang, H, Zhou, H & Lin, T 2015, 'Self-cleaning, superhydrophobic cotton fabrics with excellent washing durability, solvent resistance and chemical stability prepared from an SU-8 derived surface coating', *RSC advances*, vol. 5, no. 75, pp. 61044-61050.

Zhang, B, Kang, F, Tarascon, J-M & Kim, J-K 2016, 'Recent advances in electrospun carbon nanofibres and their application in electrochemical energy storage', *Progress in Materials Science*, vol. 76, pp. 319-380.

Zhang, M, Zhao, X, Zhang, G, Wei, G & Su, Z 2017, 'Electrospinning design of functional nanostructures for biosensor applications', *Journal of Materials Chemistry B*, vol. 5, no. 9, pp. 1699-1711.

Zhang, Y, Cheng, Z, Han, Z, Zhao, S, Zhao, X & Kang, L 2018, 'Stable multi-jet electrospinning with high throughput using the bead structure nozzle', *RSC advances*, vol. 8, no. 11, pp. 6069-6074.

Zheng, Y & Zeng, Y 2014, 'Electric field analysis of spinneret design for multihole electrospinning system', *Journal of materials science*, vol. 49, no. 5, pp. 1964-1972.

Zhou, FL, Gong, RH & Porat, I 2009, 'Polymeric nanofibres via flat spinneret electrospinning', *Polymer Engineering & Science*, vol. 49, no. 12, pp. 2475-2481.

Zhou, FL, Gong, RH & Porat, I 2010, 'Needle and needleless electrospinning for nanofibres', *Journal of applied polymer science*, vol. 115, no. 5, pp. 2591-2598.

Zhou, W, Reddy, N & Yang, Y 2005, 'Overview of protective clothing', *Textiles for protection*, pp. 3-30.

APPENDIX

Introduction

This appendix has been divided into three segments (A, B, and C) where segment A contains the analysis procedure of electric filed intensity profile for needle electrospinning which is a Supporting documents for Chapter 4. Segment B contains the SEM photos for different concentration of PAN nanofibres along with applied voltage. The segment C provides the SEM photos of coated surface of PVA nanofibres with PDMS and TMS.

A. Supporting documents for Chapter 4

Electric filed intensity profile: The electric field is the main driving force to initiate the formation of a polymer jet in electrospinning (Niu, Wang & Lin 2012a). When a polymer solution is charged by an electric field of higher intensity, it is easier to generate more jets. Stronger the electric field intensity results in a higher fibre production with narrower fibre diameter. This intensity is highly influenced by the spinneret geometric shape (Niu, Wang & Lin 2012b). FEM is an efficient way to determine the electric field intensity by providing a visualize electric field interaction according to the experimental parameters (Wang, X, Wang & Lin 2012; Zheng & Zeng 2014). Figure A-1 illustrates the analysis process of an electric field intensity profile for needle electrospinning. The geometry of needle along with collector has been drawn in SOLIDWORKS and transferred to the COMSOL interface (Figure A-1a).

After defining the materials, and setting all boundary conditions, the geometry could be run to achieve final profile of electric field intensity as Figure A-1b.

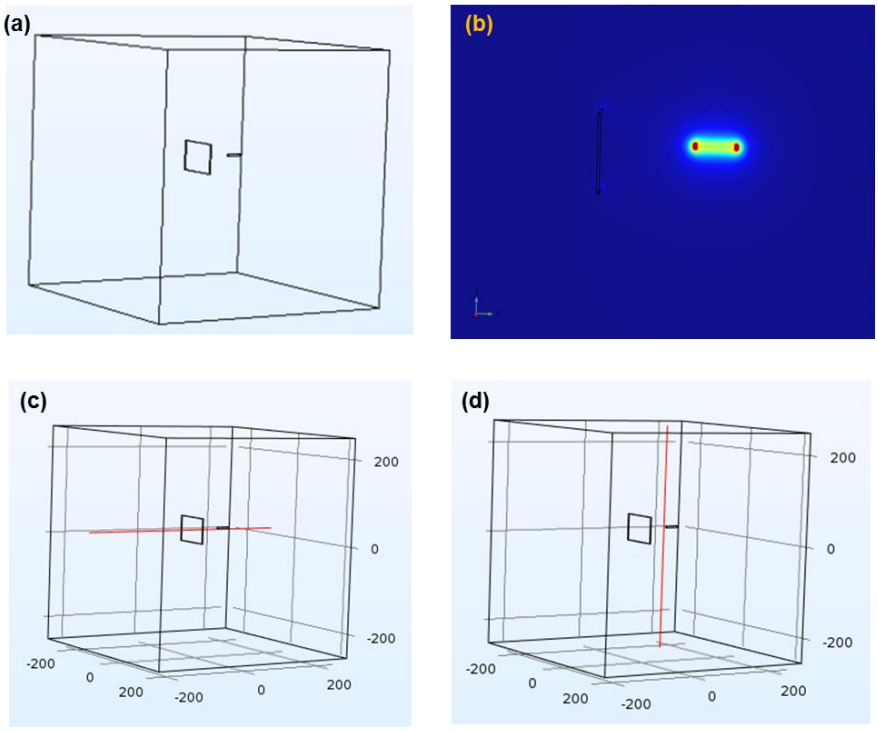

Figure: A-1 Analysis of electric field intensity profile for needle electrospinning

The resultant profile can be obtained from both directions, the needle tip to collector in spinning direction (Figure A-1c), and the intensity in needle tip in axial direction (Figure A-1d). The obtained results can be further analysed through 1D plot graph, 2D plot graph, streamlines, and multi-slides.

B. Supporting documents for Chapter 5

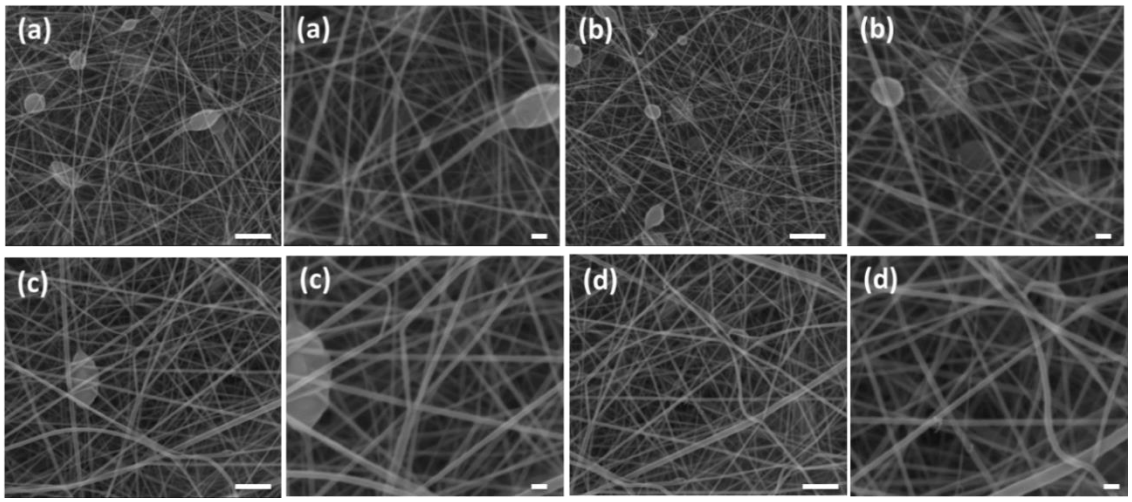

Figure B-1: PAN 7% (a) 19 kV, (b) 22 kV, (c) 25kV, (d) 28 kV. Bar= 5µm and 2µm

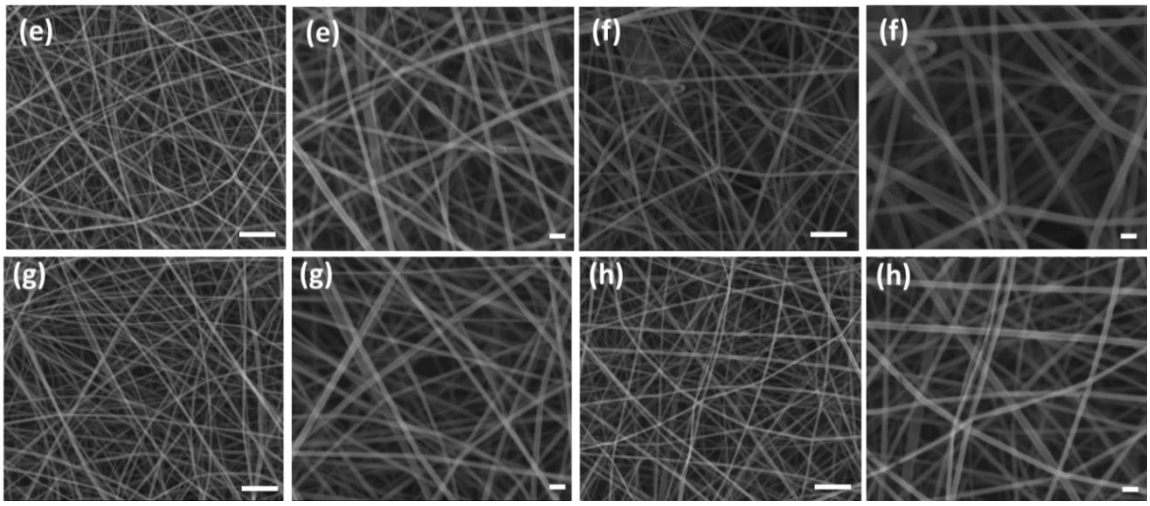

Figure B-2: PAN 9% (e) 19 kV, (f) 22 kV, (g) 25kV, (h)28 kV . Bar= 5µm and 2µm

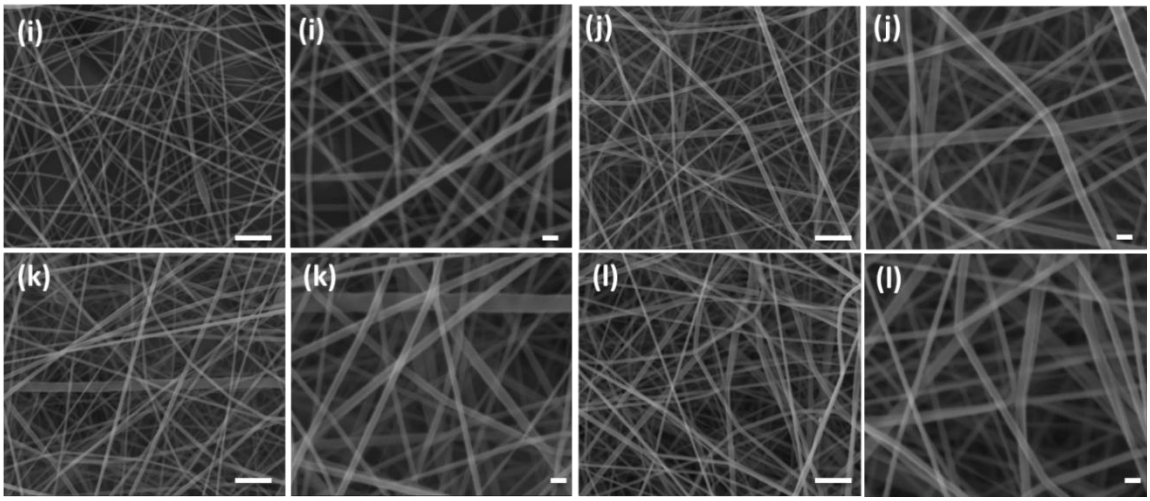

Figure B-3: PAN 11% (i) 19 kV, (j) 22 kV, (k) 25kV, (l) 28 kV. Bar= 5µm and 2µm

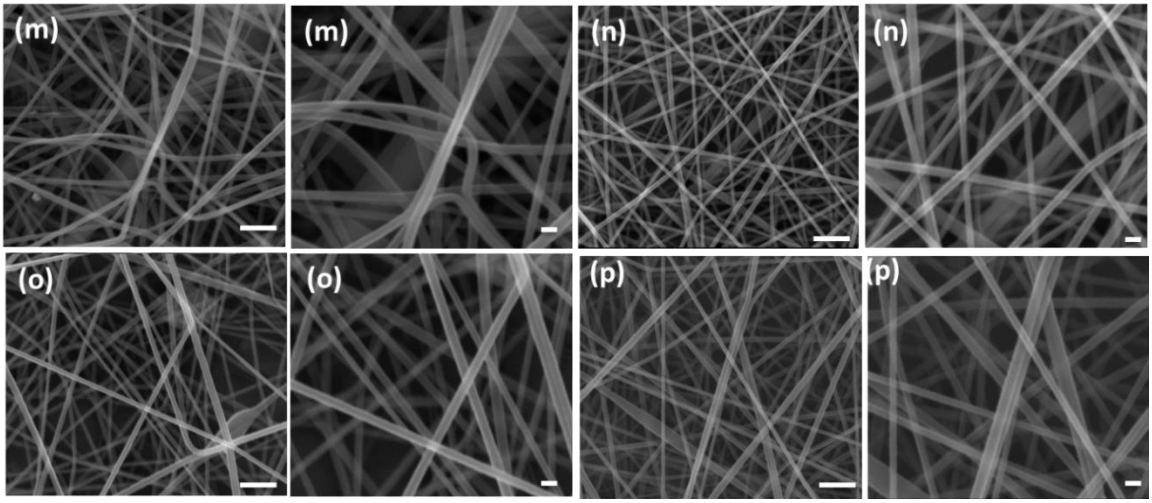

Figure B-4: PAN 13% (m) 19 kV, (n) 22 kV, (o) 25kV, (p) 28 kV. Bar= 5µm and 2µm

C. Supporting documents for Chapter 6

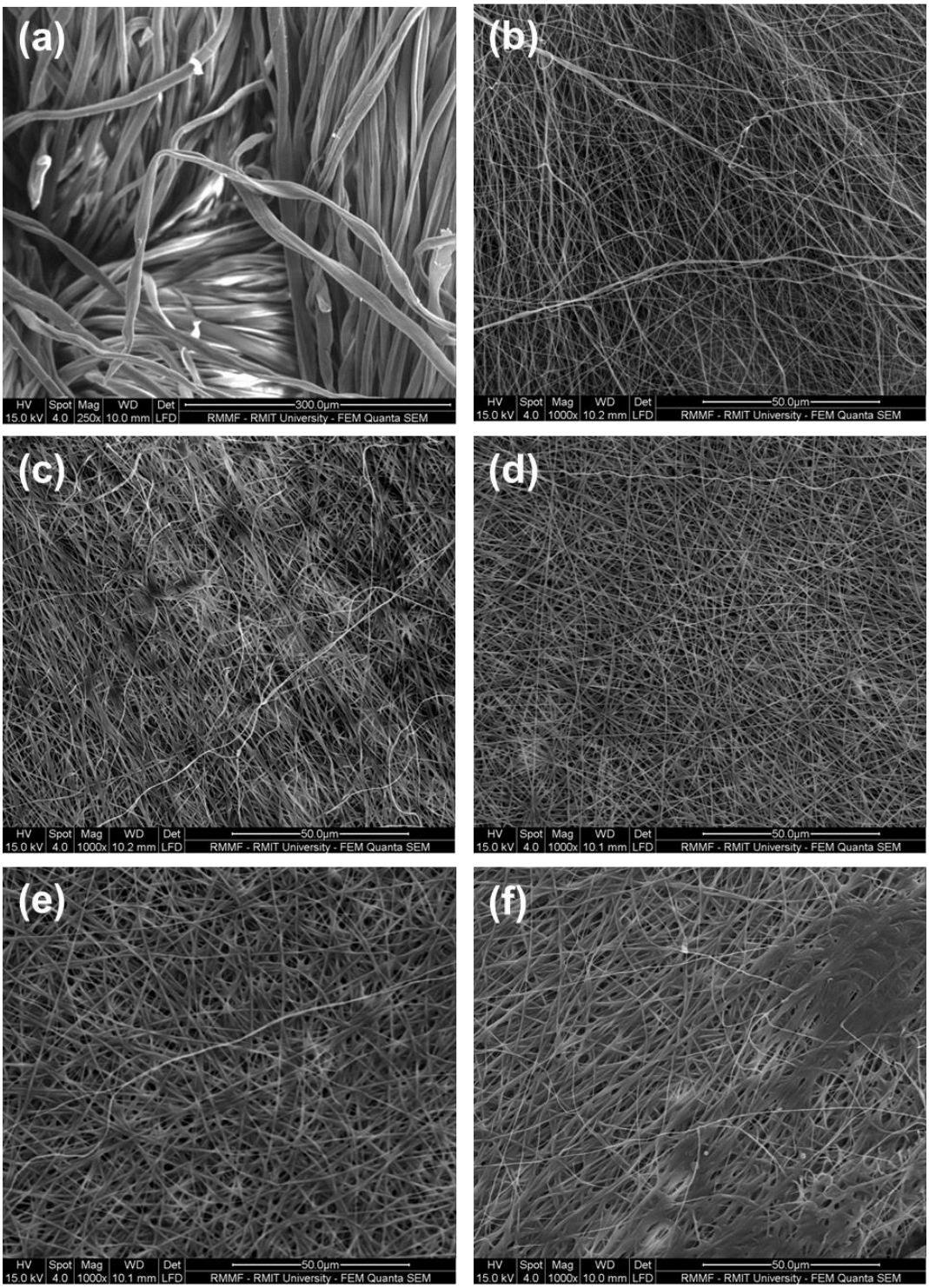

Figure C-1: SEM photos illustrate the morphology of cotton fabrics coated with PVA nanofibres, 9% PT, and with different concentrations of PT%. (a) cotton, Bar= 300µm, (b) PVA nanofibre, (c) PVA with 3% PT, (d) PVA with 5% PT, (e) PVA with 7% PT and (f) PVA with 9% PT. Bar= 50µm.